

Aus dem Institut für Physik der Universität Potsdam

Scaling and Synchronization in Deterministic and Stochastic Nonlinear Dynamical Systems

Dissertation

zur Erlangung des akademischen Grades

Doktor der Naturwissenschaften (Dr. rer. nat.)

in der Wissenschaftsdisziplin Theoretische Physik

eingereicht an der

Mathematisch-Naturwissenschaftlichen Fakultät

der Universität Potsdam

von

VOLKER AHLERS

geboren am 27. September 1971 in Bremen

Potsdam, im Juni 2001

Abstract

Subject of this work is the investigation of universal scaling laws which are observed in coupled chaotic systems. Progress is made by replacing the chaotic fluctuations in the perturbation dynamics by stochastic processes.

First, a continuous-time stochastic model for weakly coupled chaotic systems is introduced to study the scaling of the Lyapunov exponents with the coupling strength (coupling sensitivity of chaos). By means of the the Fokker-Planck equation scaling relations are derived, which are confirmed by results of numerical simulations.

Next, the new effect of avoided crossing of Lyapunov exponents of weakly coupled disordered chaotic systems is described, which is qualitatively similar to the energy level repulsion in quantum systems. Using the scaling relations obtained for the coupling sensitivity of chaos, an asymptotic expression for the distribution function of small spacings between Lyapunov exponents is derived and compared with results of numerical simulations.

Finally, the synchronization transition in strongly coupled spatially extended chaotic systems is shown to resemble a continuous phase transition, with the coupling strength and the synchronization error as control and order parameter, respectively. Using results of numerical simulations and theoretical considerations in terms of a multiplicative noise partial differential equation, the universality classes of the observed two types of transition are determined (Kardar-Parisi-Zhang equation with saturating term, directed percolation).

Kurzfassung

Gegenstand dieser Arbeit ist die Untersuchung universeller Skalengesetze, die in gekoppelten chaotischen Systemen beobachtet werden. Ergebnisse werden erzielt durch das Ersetzen der chaotischen Fluktuationen in der Störungsdynamik durch stochastische Prozesse.

Zunächst wird ein zeitkontinuierliches stochastisches Modell für schwach gekoppelte chaotische Systeme eingeführt, um die Skalierung der Lyapunov-Exponenten mit der Kopplungsstärke (*coupling sensitivity of chaos*) zu untersuchen. Mit Hilfe der Fokker-Planck-Gleichung werden Skalengesetze hergeleitet, die von Ergebnissen numerischer Simulationen bestätigt werden.

Anschließend wird der neuartige Effekt der vermiedenen Kreuzung von Lyapunov-Exponenten schwach gekoppelter ungeordneter chaotischer Systeme beschrieben, der qualitativ der Abstoßung zwischen Energieniveaus in Quantensystemen ähnelt. Unter Benutzung der für die *coupling sensitivity of chaos* gewonnenen Skalengesetze wird ein asymptotischer Ausdruck für die Verteilungsfunktion kleiner Abstände zwischen Lyapunov-Exponenten hergeleitet und mit Ergebnissen numerischer Simulationen verglichen.

Schließlich wird gezeigt, dass der Synchronisationsübergang in stark gekoppelten räumlich ausgedehnten chaotischen Systemen einem kontinuierlichen Phasenübergang entspricht, mit der Kopplungsstärke und dem Synchronisationsfehler als Kontroll- beziehungsweise Ordnungsparameter. Unter Benutzung von Ergebnissen numerischer Simulationen sowie theoretischen Überlegungen anhand einer partiellen Differentialgleichung mit multiplikativem Rauschen werden die Universalitätsklassen der zwei beobachteten Übergangsarten bestimmt (Kardar-Parisi-Zhang-Gleichung mit Sättigungsterm, gerichtete Perkolation).

Contents

1	Introduction	1
2	Nonlinear Dynamics and Stochastic Models	3
2.1	Dynamical Systems	3
2.1.1	Differential Equations and Maps	3
2.1.2	Lyapunov Exponents	4
2.1.3	Example: Skew Bernoulli and Skew Tent Maps	6
2.2	Spatially Extended Dynamical Systems	7
2.3	Synchronization Phenomena	10
2.3.1	Coupled Dynamical Systems	10
2.3.2	Example: Coupled Skew Tent Maps and Lorenz Equations	12
2.4	Stochastic Modelling of Chaotic Fluctuations	14
2.4.1	Zero-Dimensional Systems	14
2.4.2	Spatially Extended Systems	16
3	Scaling of Lyapunov Exponents	19
3.1	Coupling Sensitivity of Chaos	19
3.1.1	The Effect	19
3.1.2	Previous Theoretical Results	21
3.2	Analytical Approach	22
3.2.1	Stochastic Model	22
3.2.2	Fokker-Planck Treatment	23
3.2.3	The Second Lyapunov Exponent	27
3.2.4	Generalized Lyapunov Exponents	27
3.2.5	Asymmetrical Coupling	28
3.3	Small Noise Expansion	29
3.4	Numerical Simulations	30
3.4.1	Discrete Maps	31
3.4.2	Delay Differential Equations	35
3.5	Random Walk Picture	37
3.6	Summary and Perspectives	38

4	Avoided Crossing of Lyapunov Exponents	41
4.1	Lyapunov Exponents and Energy Levels	41
4.1.1	Numerical Evidence for Avoided Crossing	41
4.1.2	Energy Levels in Quantum Systems	43
4.1.3	Distribution of Lyapunov Exponent Spacings	45
4.1.4	Relation to Random Matrix Theory	46
4.2	Theoretical Approach	47
4.2.1	Hyperbolic Approximation of Coupling Sensitivity	47
4.2.2	Distribution Functions for Special Cases	49
4.3	Summary and Perspectives	51
5	Synchronization of Extended Systems	53
5.1	General Framework	54
5.1.1	Coupled Spatially Extended Systems	54
5.1.2	Stochastic Model	55
5.1.3	Critical Exponents and Universality Classes	58
5.1.4	Previous Results	61
5.2	Two Types of Synchronization Transition	61
5.2.1	Continuous and Discontinuous Maps	61
5.2.2	Spatiotemporal Dynamics	64
5.3	Numerical Results for Coupled Map Lattices	65
5.3.1	Continuous Maps	65
5.3.2	Discontinuous Maps	67
5.4	Numerical Results for Discrete Growth Models	68
5.4.1	Single Step Model with Lower Wall	68
5.4.2	Single Step Model with Attractive Lower Wall	72
5.5	Summary and Perspectives	75
6	Conclusion	77
6.1	Discussion of Main Results	77
6.2	Open Questions and Perspectives	79
A	Appendix	81
A.1	Numerical Calculation of Lyapunov Exponents	81
A.1.1	Discrete Maps	81
A.1.2	Differential Equations	82
A.1.3	Spatially Extended Systems	82
A.1.4	Generalized Lyapunov Exponents	83
A.2	Stochastic Differential Equations	84
A.2.1	Langevin Equation	84

A.2.2 Fokker-Planck Equation	85
A.2.3 Furutsu-Novikov Relation	86
Notation	87
References	89
Acknowledgements	99

The first questions are always to be asked, and the wisest doctor is gravelled by the inquisitiveness of a child.

RALPH WALDO EMERSON, *Intellect*, in *Essays* (1841).

1 Introduction

Natural systems that vary with time are mathematically described by dynamical systems, which can be deterministic or stochastic. While linear deterministic dynamical systems are well understood, their stochastic and nonlinear deterministic counterparts still provide many challenges. One facet of nonlinear deterministic dynamical systems that has attracted much interest since POINCARÉ's pioneering work in the 1890s is the possibility of chaotic solutions [84]. Chaos in this sense is characterized by a sensitive dependence of the system dynamics on the initial conditions. Many aspects of a dynamical system, including its stability with respect to small perturbations, are characterized by the Lyapunov exponents. These indicators that measure the exponential growth or decay of linearized perturbations play an important role throughout this work. In the last five decades much progress in the investigation of chaotic systems has been made with the aid of computer simulations. During the last ten years the focus of interest has shifted from low- to high-dimensional dynamical systems, in particular to spatially extended systems that abound in nature and display a variety of interesting phenomena, ranging from pattern formation to turbulence [17].

A very active field of research is the synchronization of coupled chaotic systems. The effect of synchronization of periodic oscillators has already been studied by HUYGENS in the seventeenth century [94]. Synchronization of chaotic systems, however, refers to coupled subsystems that are chaotic by themselves, but show a certain degree of correlation between each other, e. g., have identical amplitudes at a given time. This counterintuitive effect has only been discovered in the 1980s by FUJISAKA and YAMADA [33, 110] as well as PIKOVSKY [88], but is now reasonably well understood for low-dimensional systems [94]. The situation is again different for high-dimensional systems, as there are many open questions. One of them is the synchronization transition which is studied in this work.

For some phenomena in chaotic dynamics, universal scaling relations exist that are valid for a wide range of different specific systems. A prominent example is the sequence of period doubling bifurcations characterized by the universal Feigenbaum constant [84]. Two further examples, that are studied in this work, are the scaling of the Lyapunov exponents of weakly coupled chaotic systems and the scaling of the synchronization error of strongly coupled spatially extended chaotic systems. For these phenomena the role of chaos is to provide temporal or spatiotemporal fluctuations in the linearized dynamics. It has been found

that in several cases it is possible to model the chaotic fluctuations by random variables, which explains the universality of the observed phenomena and often allows an analytic treatment [25]. This approach is to some extent comparable with the methods of statistical mechanics. At the moment, however, there exists no general formalism for the stochastic modelling of chaotic fluctuations.

In this work we apply the method of stochastic modelling to coupled chaotic systems. The remaining chapters are organized as follows.

In chapter 2 a brief review of dynamical systems and chaos is given. The main focus is on concepts that are used in this work, i. e., Lyapunov exponents, spatially extended systems, and synchronization. Furthermore, the idea of stochastic modelling of chaotic fluctuations is reviewed and references to the literature of stochastic dynamics are given.

In chapter 3 we study the strong dependence of the Lyapunov exponents of weakly coupled chaotic systems on the coupling strength. DAIDO coined the notion “coupling sensitivity of chaos” for this behaviour which he first observed in 1984 [26]. Although some theoretical explanations of this effect have been given since, we gain further insight by using a very simple stochastic model that includes the key ingredients of the dynamics: fluctuations and coupling. We then compare the theoretical predictions of our model with results of numerical simulations.

Chapter 4 is concerned with a consequence of the coupling sensitivity of chaos that we call “avoided crossing of Lyapunov exponents”. This effect, which to our knowledge has not been reported before, appears as a strong repulsion between the Lyapunov exponents of weakly coupled disordered chaotic systems. This behaviour is qualitatively reminiscent of the energy level repulsion in nonintegrable quantum systems and can be related to random matrix theory [77]. Using the results of chapter 3, we derive an approximate distribution function for the spacings between the Lyapunov exponents and compare it with results of numerical simulations.

In chapter 5 we turn our attention to spatially extended dynamical systems and study their synchronization properties. Results of numerical simulations indicate the existence of two different types of the synchronization transition. In both cases we find a continuous phase transition between the synchronized and the nonsynchronized state. By means of stochastic models [91, 48], the universality classes of these transitions are determined via the estimation of some of the critical exponents.

Chapter 6 gives a summary of our main results and shows directions for further research. In addition, each of the chapters 3, 4, and 5 closes with a brief summary. The possible experimental relevance of our theoretical results is discussed in some detail in these summaries.

Finally, the two appendices A.1 and A.2 review some basic methods for the numerical calculation of Lyapunov exponents and for the treatment of stochastic differential equations. On page 87 an overview of the notation used in this work can be found.

2 Nonlinear Dynamics and Stochastic Models

This chapter first gives a brief review of some of the main concepts of nonlinear dynamics. In view of the following results, particular attention is paid to the Lyapunov exponents as a measure of the stability of dynamical systems. For more details and proofs the reader is referred to Refs. [52, 84]. More specialized sections treat spatially extended dynamical systems, synchronization phenomena, and stochastic models of chaotic systems.

2.1 Dynamical Systems

2.1.1 Differential Equations and Maps

A dynamical system describes the temporal evolution of the state of a system, which is characterized by a number of variables. Typical examples are angles and velocities for mechanical systems or voltages and currents for electrical ones. The d variables form a state vector $\mathbf{u} \in \mathbf{M} \subset \mathbf{C}^d$ that describes the system. Each possible state of the system corresponds to a point in the d -dimensional phase space, the temporal evolution of a state is described by a trajectory $\mathbf{u}(t)$ in this phase space. In a deterministic dynamical system the state of the system unequivocally determines its future evolution. This means that trajectories cannot cross each other. The temporal evolution is typically either described by a set of ordinary differential equations (ODEs) or by a discrete map acting on the state vector. There are, however, other forms of description, e. g., delay differential equations or partial differential equations.

In the case of ordinary differential equations we first note that it is sufficient to consider sets of first order ODEs,

$$\frac{d\mathbf{u}(t)}{dt} = \mathbf{f}(\mathbf{u}(t)), \quad (2.1)$$

where $t \in \mathbf{R}$ is the continuous time and $\mathbf{f} : \mathbf{M} \rightarrow \mathbf{C}^d$ is a function that is in general nonlinear. Equations including higher order derivatives or explicit time dependences can be transformed into this form by adding further state variables. Given an initial condition $\mathbf{u}(0)$, the temporal evolution of $\mathbf{u}(t)$ for $t > 0$ can in principle be calculated unequivocally, provided that \mathbf{f} locally satisfies a Lipschitz condition [52].

If we look at the system at discrete time instants, we can describe the temporal evolution by a map,

$$\mathbf{u}(t+1) = \mathbf{f}(\mathbf{u}(t)), \quad (2.2)$$

where $t \in \mathbf{Z}$ is the discrete time and $f : \mathbf{M} \rightarrow \mathbf{M}$ is again a function that is in general nonlinear. Given an initial condition $\mathbf{u}(0)$, it is clear that the temporal evolution of $\mathbf{u}(t)$ for $t > 0$ is determined unequivocally. A discrete map can be attributed to a continuous-time dynamical system via the Poincaré surface of section (see, e. g., Ref. [84]).

2.1.2 Lyapunov Exponents

The asymptotic stability of a trajectory can be studied by linearizing the evolution equations. A trajectory $\mathbf{u}(t)$ is called asymptotically stable if there exists a phase space volume around it such that trajectories $\mathbf{u}'(t)$ in this volume approach $\mathbf{u}(t)$ in the long time limit,

$$\lim_{t \rightarrow \infty} \|\mathbf{u}(t) - \mathbf{u}'(t)\| = 0.$$

We first limit our attention to differential equations of the form (2.1). We consider a reference trajectory $\mathbf{u}(t)$ and a second trajectory $\mathbf{u}(t) + \mathbf{w}(t)$, where $\mathbf{w}(t)$ is a small perturbation. By means of the Taylor expansion

$$f(\mathbf{u} + \mathbf{w}) = f(\mathbf{u}) + \mathbf{J}(\mathbf{u})\mathbf{w} + O(\|\mathbf{w}\|^2)$$

(where \mathbf{J} is the Jacobian of f) we can study the time evolution of the perturbation vector in linear approximation,¹

$$\frac{d\mathbf{w}(t)}{dt} = \mathbf{J}(\mathbf{u}(t))\mathbf{w}(t).$$

Note that the Jacobian $\mathbf{J}(\mathbf{u}(t))$ is in general time-dependent. If the reference trajectory consists of a fixed point, $\mathbf{u}(t) = \mathbf{u}_0$, its stability depends on the real parts of the eigenvalues γ_i ($i = 1, \dots, d$) of the constant Jacobian $\mathbf{J}(\mathbf{u}_0)$:

$$\max_i \{\text{Re } \gamma_i\} \begin{cases} < 0: & \text{asymptotically stable,} \\ = 0: & \text{marginally stable,} \\ > 0: & \text{unstable.} \end{cases}$$

In the case of marginal stability one has to consider higher order terms in the Taylor expansion of $f(\mathbf{u} + \mathbf{w})$ to decide about the stability of the fixed point.

In the case of discrete maps of the form (2.2), we can also use the Taylor expansion of $f(\mathbf{u} + \mathbf{w})$ and obtain in linear approximation

$$\mathbf{w}(t+1) = \mathbf{J}(\mathbf{u}(t))\mathbf{w}(t).$$

If the reference trajectory consists of a fixed point \mathbf{u}_0 , the stability again depends on the eigenvalues γ_i ($i = 1, \dots, d$) of the constant Jacobian $\mathbf{J}(\mathbf{u}_0)$. Here, however, the logarithms

¹We write an equal sign here and understand $\mathbf{w}(t)$ as a “linear perturbation”.

of the absolute eigenvalues are of interest:

$$\max_i \{ \ln |\gamma_i| \} \begin{cases} < 0 : & \text{asymptotically stable,} \\ = 0 : & \text{marginally stable,} \\ > 0 : & \text{unstable.} \end{cases}$$

If the reference trajectory is not a fixed point, its stability is measured by the Lyapunov exponents. We first concentrate on discrete maps of the form (2.2). Given the initial conditions $\mathbf{u}_0 = \mathbf{u}(0)$ and $\mathbf{w}_0 = \mathbf{w}(0)$ (with $\|\mathbf{w}_0\| = 1$), we define the local (or finite-time) Lyapunov exponents as

$$\lambda(t, \mathbf{u}_0) = \frac{1}{t} \ln \|\mathbf{w}(t)\| = \frac{1}{t} \ln \|\mathbf{P}(t, \mathbf{u}_0) \mathbf{w}_0\| = \frac{1}{2t} \ln(\mathbf{w}_0^T \mathbf{P}^T(t, \mathbf{u}_0) \mathbf{P}(t, \mathbf{u}_0) \mathbf{w}_0),$$

where the upper index T denotes the transpose and

$$\mathbf{P}(t, \mathbf{u}_0) = \prod_{\tau=0}^{t-1} \mathbf{J}(\mathbf{u}(\tau)).$$

The real nonnegative symmetric matrix $\mathbf{P}^T \mathbf{P}$ has real nonnegative eigenvalues $\gamma_i(t, \mathbf{u}_0)$ ($i = 1, \dots, d$) and eigenvectors which are orthogonal to each other. Choosing \mathbf{w}_0 in the direction of the eigenvector corresponding to the eigenvalue $\gamma_i(t, \mathbf{u}_0)$, we have

$$\lambda_i(t, \mathbf{u}_0) = \frac{1}{2t} \ln(\mathbf{w}_0^T \gamma_i(t, \mathbf{u}_0) \mathbf{w}_0) = \frac{1}{2t} \ln \gamma_i(t, \mathbf{u}_0).$$

In the long-time limit we obtain the Lyapunov exponents

$$\lambda_i = \lim_{t \rightarrow \infty} \lambda_i(t, \mathbf{u}_0)$$

which are according to Oseledec's multiplicative ergodic theorem independent of \mathbf{u}_0 for almost all \mathbf{u}_0 (see, e. g., Ref. [52]). Due to ergodicity, we also obtain the Lyapunov exponents by means of averaging their finite-time values with respect to the invariant measure of \mathbf{u} ,

$$\lambda_i = \langle \lambda_i(t, \mathbf{u}_0) \rangle. \quad (2.3)$$

We sort the Lyapunov exponents with decreasing magnitude, $\lambda_1 \geq \lambda_2 \geq \dots \geq \lambda_d$. A generic perturbation \mathbf{w}_0 will have components in the directions of all eigenvectors and thus rapidly align in the direction of fastest growth. A numerical method for the calculation of Lyapunov exponents is given in App. A.1.

In the case of differential equations of the form (2.1) Lyapunov exponents are defined in nearly the same way. The only difference is that $\mathbf{P}(t, \mathbf{u}_0)$ has to be replaced by $\mathbf{O}(t, \mathbf{u}_0)$, which is the matrix solution of the differential equation

$$\frac{d\mathbf{O}(t, \mathbf{u}_0)}{dt} = \mathbf{J}(\mathbf{u}(t)) \mathbf{O}(t, \mathbf{u}_0)$$

with the initial condition $\mathbf{O}(0, \mathbf{u}_0) = \mathbf{I}$ (where \mathbf{I} is the unit matrix). For trajectories of continuous-time systems one Lyapunov exponent is always zero (except for trajectories that consist of single fixed points); this accounts for the phase space motion along the trajectory.

The concept of Lyapunov exponents is one of the most important tools to characterize dynamical systems. Although the Lyapunov exponents themselves have no physical meaning, many physically relevant quantities, such as the correlation time and the entropy, depend on them (see, e.g., Ref. [25]). Furthermore, the Lyapunov exponents are used to classify dynamical systems with respect to their stability properties in the following way. After a transient time a system typically settles on an attractor. Without going into mathematical details, an attractor can be seen as a set of phase space points that is approached by all trajectories starting from a surrounding phase space volume (the basin of attraction). The Lyapunov exponents are average quantities that describe the stretching and shrinking of phase space volumes in different directions. For dissipative systems the sum of Lyapunov exponents is negative, while it is zero for conservative systems. The Lyapunov exponents provide a criterion to decide about the nature of an attractor. As chaos is characterized by a sensitive dependence of the system behaviour on initial conditions, it can be associated with a positive largest Lyapunov exponent λ_1 . For continuous-time systems we have the following classification:

$$\begin{aligned} \lambda_1 < 0 &: \text{attractive fixed point,} \\ \lambda_1 = 0, \lambda_2 < 0 &: \text{attractive limit cycle,} \\ \lambda_1 = \lambda_2 = 0 &: \text{quasiperiodic attractor,} \\ \lambda_1 > 0 &: \text{chaotic attractor.} \end{aligned}$$

Finally we remark that the Lyapunov exponents play a crucial role in the context of synchronization, see Sec. 2.3 below.

The estimation of Lyapunov exponents from time series of experimental systems is very difficult, although some methods exist for the estimation of at least the largest Lyapunov exponent [65]. Therefore, the Lyapunov exponents are most useful for systems which mathematical models are known for.

2.1.3 Example: Skew Bernoulli and Skew Tent Maps

Simple examples which allow analytical calculations of Lyapunov exponents are given by the one-dimensional skew Bernoulli map (see Fig. 2.1(a))

$$f : [0, 1] \rightarrow [0, 1], \quad u \mapsto \begin{cases} u/a & \text{if } u \leq a, \\ (u-a)/(1-a) & \text{if } u > a, \end{cases} \quad (2.4)$$

and the skew tent map (see Fig. 2.1(b))

$$f : [0, 1] \rightarrow [0, 1], \quad u \mapsto \begin{cases} u/a & \text{if } u \leq a, \\ (1-u)/(1-a) & \text{if } u > a. \end{cases} \quad (2.5)$$

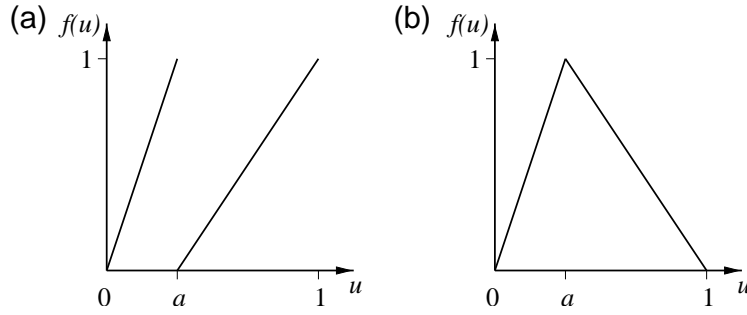


Figure 2.1: The skew Bernoulli (a) and skew tent (b) maps.

Both maps depend on a parameter $a \in (0, 1)$. Due to the uniform invariant measures of the maps, the absolute derivatives are for both maps given by

$$|f'(u)| = \begin{cases} 1/a & \text{with probability } a, \\ 1/(1-a) & \text{with probability } 1-a. \end{cases}$$

The Lyapunov exponent has the same value for both maps and is easily calculated by averaging the one step (finite-time) Lyapunov exponent according to Eq. (2.3),

$$\lambda = \langle \lambda(1, u_0) \rangle = \langle \ln |f'(u_0)| \rangle = -a \ln a - (1-a) \ln(1-a).$$

The Lyapunov exponent is positive for all values of $a \in (0, 1)$ and has a maximum at $a = 1/2$. The variance of the one step Lyapunov exponent can also be calculated,

$$2\sigma^2 = \langle [\lambda(1, u_0) - \lambda]^2 \rangle = a(1-a) \left(\ln \frac{a}{1-a} \right)^2.$$

The variance is zero only for $a = 1/2$ and has maxima at $a \approx 1/2 \pm 0.417$.

2.2 Spatially Extended Dynamical Systems

Extended dynamical systems depend on both space and time. Typically they show local dynamics and spatial coupling, often in the form of diffusion. Examples can be found in the forms of fluids, semiconductors, broad-area lasers, chemical reactors, etc. There are several approaches to describe turbulence by means of spatially extended dynamical systems [17].

Of the rich variety of phenomena that are observed in such systems, we mention space-time intermittency, moving fronts, and self-organized spatial structures. By space-time chaos a dynamical regime is denoted which is characterized by both chaotic time series at each spatial site and irregular spatial profiles at a given time.

The mathematical models that are closest to most physical extended systems are partial differential equations (PDEs). Widely studied examples are reaction diffusion systems of the form [17]

$$\frac{\partial \mathbf{u}(x,t)}{\partial t} = \mathbf{f}(\mathbf{u}(x,t)) + \varepsilon \Delta \mathbf{u}(x,t), \quad (2.6)$$

where the components of the state vector $\mathbf{u} \in \mathbf{R}^d$ are the concentrations of chemical species, $x \in [0, L]$ denotes space (with the system length $L \in \mathbf{R}^+$), and $t \in \mathbf{R}$ denotes time. The nonlinear function $\mathbf{f}(\mathbf{u})$ describes the local chemical reaction, and the term $\Delta \mathbf{u}$ (where the Laplacian acts componentwise) accounts for diffusion of molecules or atoms. Prominent other PDEs are the complex Ginzburg-Landau equation for a complex state variable $u(x,t) \in \mathbf{C}$ and the Kuramoto-Sivashinsky equation for a real scalar state variable $u(x,t) \in \mathbf{R}$, which includes nonlinear and higher order spatial coupling [17].

Especially for numerical simulations other levels of description than PDEs can be more appropriate. The first simplification of a PDE consists of the discretization of space, leading to coupled oscillators. By discretizing time as well, one arrives at so-called coupled map lattices (CMLs) [64]. In one spatial dimension a CML has the form

$$\mathbf{u}(x, t+1) = \mathbf{f}(\mathbf{u}(x, t)) + \varepsilon [\mathbf{f}(\mathbf{u}(x+1, t)) - 2\mathbf{f}(\mathbf{u}(x, t)) + \mathbf{f}(\mathbf{u}(x-1, t))], \quad (2.7)$$

where $x \in \{0, \dots, L-1\}$ denotes space (with the system length $L \in \mathbf{N}$), $t \in \mathbf{Z}$ denotes time, $\mathbf{u}(x, t) \in \mathbf{M} \subset \mathbf{C}^d$ is the state vector at the spatial site x , and $\mathbf{f} : \mathbf{M} \rightarrow \mathbf{M}$ is a nonlinear function describing the local dynamics. Often the local state vector is a real scalar $u(x, t) \in \mathbf{M} \subset \mathbf{R}$. Note that we first apply the map \mathbf{f} to \mathbf{u} and then the coupling to $\mathbf{f}(\mathbf{u})$. This ensures that the state variables stay in the interval \mathbf{M} . The coupling is a discrete diffusion operator. Generalizations to higher spatial dimensions are straightforward; in this work, however, we

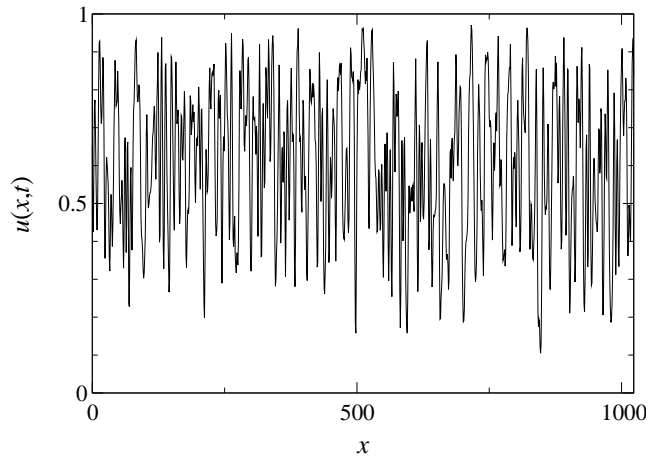


Figure 2.2: Snapshot of the state variable $u(x,t)$ of a tent map CML at a fixed time ($L = 1024$).

limit ourselves to one spatial dimension. In Fig. 2.2 a snapshot of the state variable $u(x, t)$ of a CML consisting of $L = 1024$ tent maps (i. e., skew tent maps (2.5) with $a = 1/2$)

$$f : [0, 1] \rightarrow [0, 1], \quad u \mapsto 1 - 2|u - 1/2|$$

is shown as an example; to ensure translational invariance, periodic boundary conditions $u(x + L, t) = u(x, t)$ have been used. Most phenomena that are found in spatially extended dynamical systems can also be found in CMLs. There are other forms of coupling than the diffusive one used in Eq. (2.7). In Ch. 4, for instance, global coupling will be used.

Lyapunov exponents of spatially extended systems are calculated as described for low-dimensional systems from the linearizations of Eqs. (2.6) and (2.7), respectively. The growth rates of perturbations $\mathbf{w} = (w^{(1)}, \dots, w^{(d)})^T$ are calculated with respect to the q -norm

$$\|\mathbf{w}\|_q(t) = \left[\frac{1}{L} \int_0^L \sum_{j=1}^d |w^{(j)}(x, t)|^q dx \right]^{1/q},$$

where the integral is replaced by a sum for spatially discrete systems. In spatially extended dynamical systems there are two limits that have to be taken to calculate the Lyapunov exponent: the usual limit $t \rightarrow \infty$ and the thermodynamic limit $L \rightarrow \infty$. The combination of both limits, however, induces a problem: it is not a priori clear that the perturbation vector \mathbf{w} remains normalizable. It turns out that the perturbation vector is highly localized at small spatial regions [42, 24, 91], and that finite-size and finite-time scaling relations for the Lyapunov exponent can be derived [93]. Moreover, the Lyapunov exponents of spatially extended systems have been found to be norm-independent, but to exhibit self-averaging with the system size L only if the 0-norm is used [93] (see also App. A.1). In the thermodynamic limit $L \rightarrow \infty$ the normalized spectrum of Lyapunov exponents $\lambda_i(i/L)$ (with $\lambda_1 \geq \lambda_2 \geq \dots \geq \lambda_L$) approaches a characteristic density [74]. Furthermore, the dimension and the Kolmogorov-Sinai entropy of spatially extended systems are proportional to the system size L [17].

In all of the above considerations we implicitly assumed a spatially homogeneous perturbation vector and studied the temporal evolution of its spatial average. We can, however, also start with a localized perturbation and follow its evolution in space and time. The stability of such perturbations can be characterized by velocity-dependent [30] or local [90] Lyapunov exponents.

Another peculiarity of certain spatially extended systems is known as stable chaos [95]. This notion refers to the instability with respect to finite perturbations of systems with a negative largest Lyapunov exponent. Systems exhibiting such behaviour are characterized by a very strong nonlinearity in the local dynamics, e. g., a discontinuity of the local map. An indicator for the stability of such systems is given by the velocity v_F of nonlinear information propagation that is calculated as follows. Two replicas $u_1(x, t)$ and $u_2(x, t)$ of the system are initially prepared to be in identical states everywhere except for a small spatial

region, where they have a finite difference. The systems are then let evolve independently, and v_F is calculated as the average propagation velocity of the front of the perturbation. Systems exhibiting stable chaos are characterized by a positive velocity $v_F > 0$ and a negative largest Lyapunov exponent $\lambda < 0$, whereas stable systems have $v_F = 0$ and $\lambda < 0$. The mechanism responsible for stable chaos is still under investigation [45]. In continuous-time systems stable chaos has been found in a chain of periodically kicked oscillators [19]. So far, stable chaos has not been observed in PDEs [46] and may therefore be regarded as an effect which is not typical for physical systems.

2.3 Synchronization Phenomena

2.3.1 Coupled Dynamical Systems

The phenomenon of synchronization of coupled periodic oscillators is known for a long time. Only recently, however, it has been found that also coupled chaotic systems are able to synchronize [33, 110, 88, 87]. The basic mechanism can be described as follows. Consider two coupled nonlinear maps,

$$\begin{aligned} u_1(t+1) &= f(u_1(t)) + \varepsilon_1[f(u_2(t)) - f(u_1(t))], \\ u_2(t+1) &= f(u_2(t)) + \varepsilon_2[f(u_1(t)) - f(u_2(t))], \end{aligned} \quad (2.8)$$

where $\varepsilon_{1,2}$ are the coupling parameters which may be different. The scheme is sketched in Fig. 2.3. Two frequently studied special cases are bidirectional ($\varepsilon_1 = \varepsilon_2 = \varepsilon$) and unidirectional ($\varepsilon_1 = 0, \varepsilon_2 = \varepsilon$) coupling. The systems are synchronized if the difference $w = u_1 - u_2$ vanishes.

The asymptotic stability of the synchronized state can be studied by considering a small perturbation $w(t)$ of the synchronized state. The dynamical evolution of $w(t)$ is in first order given by (see Sec. 2.1.2)

$$w(t+1) = (1 - \varepsilon_1 - \varepsilon_2)f'(u_1(t))w(t),$$

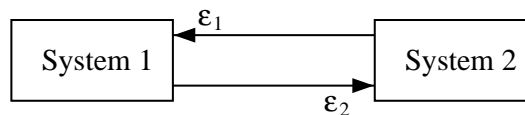


Figure 2.3: Sketch of the synchronization scheme.

where f' is the derivative of f . For the absolute value $|w|$ we obtain

$$\begin{aligned} |w(t)| &= (1 - \varepsilon_1 - \varepsilon_2)^t |w(0)| \prod_{\tau=0}^{t-1} |f'(u_1(\tau))| \\ &= |w(0)| \exp \left\{ \left[\ln(1 - \varepsilon_1 - \varepsilon_2) + \frac{1}{t} \sum_{\tau=0}^{t-1} \ln |f'(u_1)| \right] t \right\}. \end{aligned}$$

The synchronized state is asymptotically stable if the transverse (or conditional) Lyapunov exponent

$$\lambda_{\perp} = \langle \ln |f'(u_1)| \rangle + \ln(1 - \varepsilon_1 - \varepsilon_2)$$

is negative (due to ergodicity the average is over the phase space according to the natural measure of u_1). For small perturbations of the synchronized state we have $u_1 \approx u_2$, such that the coupling has negligible influence on the evolution (and thus the natural measure) of u_1 . This enables us to replace the average of $\ln |f'(u_1)|$ by the Lyapunov exponent Λ of the uncoupled map and to obtain from $\lambda_{\perp} < 0$ the synchronization condition [88]

$$\varepsilon_1 + \varepsilon_2 > 1 - e^{-\Lambda}. \quad (2.9)$$

In the case of bidirectional coupling ($\varepsilon_1 = \varepsilon_2 = \varepsilon$) we thus have the critical coupling parameter

$$\varepsilon_c = \frac{1}{2} (1 - e^{-\Lambda}).$$

These relations also hold for higher-dimensional maps.

For coupled systems of ODEs (with the coupling matrix \mathbf{C} equal to the unit matrix \mathbf{I})

$$\begin{aligned} \frac{d\mathbf{u}_1(t)}{dt} &= \mathbf{f}(\mathbf{u}_1(t)) + \varepsilon_1 \mathbf{C}[\mathbf{u}_2(t) - \mathbf{u}_1(t)], \\ \frac{d\mathbf{u}_2(t)}{dt} &= \mathbf{f}(\mathbf{u}_2(t)) + \varepsilon_2 \mathbf{C}[\mathbf{u}_1(t) - \mathbf{u}_2(t)], \end{aligned} \quad (2.10)$$

similar considerations lead to the synchronization condition [33, 88]

$$\varepsilon_1 + \varepsilon_2 > \Lambda. \quad (2.11)$$

If the coupling matrix \mathbf{C} is not the unit matrix (e.g., if the systems of ODEs are coupled only in one vector component), the synchronization condition (2.11) does not hold. Instead, one has to calculate the transverse Lyapunov exponent λ_{\perp} from the linearized equations for a perturbation \mathbf{w} of the synchronized state and check for which ε it is negative.

The synchronization conditions (2.9) and (2.11) can be used in experiments to measure the largest Lyapunov exponent Λ , which is very difficult to estimate from time series. There are other mechanisms besides diffusive coupling that lead to the synchronization of chaotic

systems; a general framework is given by the active-passive decomposition [68]. Furthermore, there are other forms of synchronization like phase synchronization and generalized synchronization [106, 94]. If the coupled systems are not identical (as it is inevitably the case in experiments), the existence of unstable periodic orbits close to the attractor can lead to temporary desynchronization events even if the conditions (2.9) or (2.11) are fulfilled [89]. The synchronization of spatially extended systems is treated in detail in Ch. 5.

2.3.2 Example: Coupled Skew Tent Maps and Lorenz Equations

As examples for the synchronization of chaotic systems we now consider skew tent maps (2.5) with parameter $a = 1/3$ and the Lorenz differential equations (see, e.g., Ref. [52])

$$\frac{d}{dt} \begin{pmatrix} x \\ y \\ z \end{pmatrix} = \begin{pmatrix} \sigma(y-x) \\ \rho x - y - xz \\ -\beta z + xy \end{pmatrix} \quad (2.12)$$

with parameters $\sigma = 10$, $\rho = 28$, and $\beta = 8/3$. The maps are coupled according to Eq. (2.8), the Lorenz equations are coupled according to Eq. (2.10) with $\mathbf{u}_i = (x_i, y_i, z_i)^T$ and the cou-

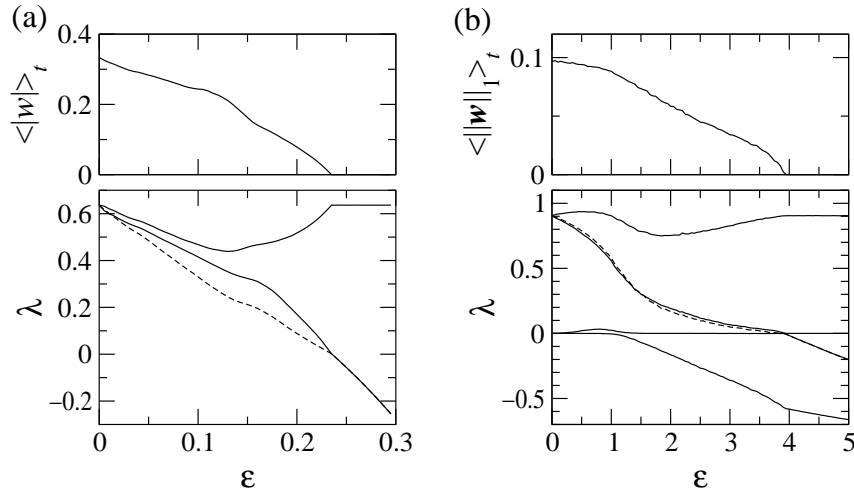


Figure 2.4: The synchronization transition of coupled (a) skew tent maps and (b) Lorenz equations. In the upper panels the average synchronization error $\langle \|\mathbf{w}\|_1 \rangle_t$ (time-averaged after some transient phase) is shown. In the lower panels the Lyapunov exponents λ_i (solid lines, $i = 1, 2$ for the maps and $i = 1, 2, 3, 4$ for the ODEs) as well as the transverse Lyapunov exponent λ_\perp (dashed lines) are shown.

pling matrix

$$\mathbf{C} = \begin{pmatrix} 1 & 0 & 0 \\ 0 & 0 & 0 \\ 0 & 0 & 0 \end{pmatrix},$$

corresponding to coupling via the x -component. In both cases we apply bidirectional coupling, $\varepsilon_1 = \varepsilon_2 = \varepsilon$.

In Fig. 2.4 the coupling dependences of the average synchronization error $\langle \|\mathbf{w}\|_1 \rangle_t = \langle \|\mathbf{u}_1 - \mathbf{u}_2\|_1 \rangle_t$, the Lyapunov exponents λ_i , and the transverse Lyapunov exponent λ_\perp are shown (for the Lorenz equations only the four largest Lyapunov exponents are of interest here). The first observation is that both λ_\perp and λ_2 become zero at the critical coupling parameter ε_c . For the coupled maps, $\varepsilon_c \approx 0.235$ in agreement with the synchronization condition (2.9). The second observation is that the largest Lyapunov exponent λ_1 has the same value for $\varepsilon > \varepsilon_c$ as without coupling. This happens because the coupling term vanishes in the case of synchronization ($\mathbf{u}_1 = \mathbf{u}_2$). We further observe that the largest Lyapunov exponent λ_1 of the coupled Lorenz equations increases for small values of ε (for the coupled tent maps this happens only for very small values of ε that are not resolved in Fig. 2.4(a)). This effect is known as coupling sensitivity of chaos and is studied in Ch. 3. Finally we note that the fourth Lyapunov exponent λ_4 of the coupled Lorenz equations becomes negative for some $\varepsilon < \varepsilon_c$. This corresponds to phase synchronization (see Refs. [106, 94] for details). In Fig. 2.5 the temporal evolution of the variables x_1 and x_2 of the Lorenz systems with and

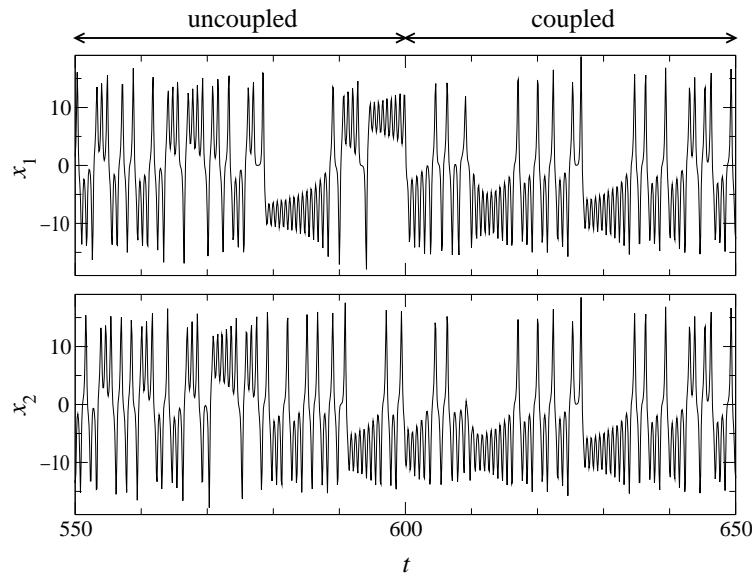


Figure 2.5: Synchronization of two identical Lorenz systems; shown are the first components $x_{1,2}$. When the coupling ($\varepsilon = 5$) is switched on at $t = 600$, both systems synchronize after a short transient.

without coupling is shown. Both Figs. 2.4 and 2.5 show that the synchronization transition is a transition between two different chaotic states, as opposed to the transition from regular to chaotic motion.

2.4 Stochastic Modelling of Chaotic Fluctuations

The phenomena described in the following chapters of this work are found for many different chaotic maps or differential equations. Rather than studying special systems, it seems thus natural to look for common characteristics. All systems considered in this work share the properties of fluctuations due to their chaotic nature and coupling between subsystems. In recent years it turned out that for several problems it is possible to model the chaotic fluctuations by random variables [88, 13, 85, 111, 34] (for an introduction see Ref. [25]). The phenomena studied in this work are found in the perturbation dynamics of coupled systems (Lyapunov exponents, synchronization error) rather than in the dynamics of their state variables. We therefore aim at stochastic models of the perturbation dynamics of coupled chaotic systems. Lyapunov exponents are widely used in the context of random dynamical systems [25, 7].

In this section we give a first overview and show relations to other work on stochastic dynamics. The particular models used to study the phenomena of coupling sensitivity of chaos and the synchronization transition in extended systems are introduced in Chs. 3 and 5, respectively. To be able to make use of the Fokker-Planck equation, we choose continuous-time models with Gaussian white noise. This choice is motivated by the observation that the effects we study are found for discrete-time as well as continuous-time systems and do not seem to depend on the distribution of fluctuations of particular systems. For low-dimensional systems very simple stochastic models can already be sufficient. In Ch. 3 a system of two stochastic differential equations is used to model the dynamics of the perturbation vectors of two weakly coupled chaotic systems. In high-dimensional systems spatial diffusion often plays an important role. In Ch. 5 a stochastic partial differential equation provides an adequate model for the synchronization transition of coupled spatially extended systems.

Problems are encountered for systems with long temporal correlations, in which white noise is not able to replace the fluctuations. Some examples are presented in the following chapters. Most chaotic systems, however, show a rapid decay of temporal correlations.

2.4.1 Zero-Dimensional Systems

Stochastic differential equations (zero spatial dimension) have been studied extensively, mostly in the contexts of fluctuating control parameters as well as internal and external noise [58, 103]. Unexpected effects like noise-induced transitions and ordering by noise have been reported. In this work, we want to model the long time behaviour of perturbations

(with the Lyapunov exponent λ),

$$w(t) \rightarrow w(0)e^{\lambda t} \quad \text{for } t \rightarrow \infty,$$

but also allow for finite-time fluctuations. Our first ansatz is the simple linear Stratonovich stochastic differential equation (see App. A.2 and Ref. [103])

$$\frac{dw(t)}{dt} = [\lambda + \xi(t)]w(t), \quad (2.13)$$

where $\xi(t)$ is a Gaussian stochastic process with

$$\langle \xi(t) \rangle = 0, \quad \langle \xi(t)\xi(t') \rangle = 2\sigma^2\delta(t-t')$$

(the averages are over different realizations of the noise process). We notice that $w(t)$ stays positive if $w(0) > 0$. The solution is simply given by

$$w(t) = w(0) \exp\left(\lambda t + \int_0^t \xi(\tilde{t}) d\tilde{t}\right) = w(0) \exp\left(\lambda t + \sqrt{2\sigma^2}W(t)\right), \quad (2.14)$$

where $W(t)$ is a Wiener process (see App. A.2). Since $W(t)/t \rightarrow 0$ for $t \rightarrow \infty$ with probability one, we have

$$w(t) \rightarrow w(0)e^{\lambda t} \quad \text{for } t \rightarrow \infty$$

with probability one. We find a transition between exponential growth and decay at $\lambda = 0$. From Eq. (2.14) we obtain the finite-time Lyapunov exponent

$$\lambda(t) = \lambda + \frac{\sqrt{2\sigma^2}}{t}W(t).$$

Its average and variance are given by (with $\langle [W(t)]^2 \rangle = t$, see App. A.2)

$$\langle \lambda(t) \rangle = \lambda, \quad \langle [\lambda(t) - \lambda]^2 \rangle = \frac{2\sigma^2}{t}.$$

The simple ansatz (2.13) is sufficient to understand the origin of the coupling sensitivity of chaos, see Ch. 3.

For the moments $\langle w^q \rangle$ we have

$$\begin{aligned} \frac{d}{dt} \langle w^q(t) \rangle &= q\lambda \langle w^q(t) \rangle + q \langle \xi(t)w^q(t) \rangle \\ &= (q\lambda + q^2\sigma^2) \langle w^q(t) \rangle, \end{aligned}$$

where we have used the Furutsu-Novikov relation [35, 83] for the second average (see also App. A.2). The solution of the last equation is given by

$$\langle w^q(t) \rangle = \langle w^q(0) \rangle e^{(q\lambda + q^2\sigma^2)t}.$$

We thus find a transition at $\lambda = -q\sigma^2$, which seems to be in contradiction to our previous result indicating a transition at $\lambda = 0$.

A closer look reveals that the moments are dominated by rare, but large finite-time fluctuations, which is not the case if we add a nonlinear damping term to Eq. (2.13),

$$\frac{dw(t)}{dt} = \{\lambda + \xi(t) - [w(t)]^v\}w(t), \quad w(0) > 0, \quad (2.15)$$

where v is positive. Again $w(t)$ stays positive if $w(0) > 0$. For this equation all moments show the same transition at $\lambda = 0$ [104, 47]. From the stationary solution of the Fokker-Planck equation or by means of embedding methods it can be shown that for $t \rightarrow \infty$ we have [104, 47]

$$\langle w^q \rangle = (v\sigma^2)^{q/v} \frac{\Gamma\left(\frac{\lambda}{v\sigma^2} + \frac{q}{v}\right)}{\Gamma\left(\frac{\lambda}{v\sigma^2}\right)}. \quad (2.16)$$

For a quadratic nonlinearity ($v = 1$) the expression for the first moment reduces to $\langle w \rangle = \lambda$.

The connection with the synchronization of coupled low-dimensional chaotic systems is as follows. If we interpret $\lambda = \lambda_\perp$ as the transverse Lyapunov exponent and $w = \|\mathbf{u}_1 - \mathbf{u}_2\|$ as the absolute synchronization error, the damping ensures that the latter stays limited if $\lambda_\perp > 0$. The result (2.16) describes the dependence of the average absolute synchronization error on the transverse Lyapunov exponent, which for $\mathbf{u}_1 \approx \mathbf{u}_2$ is approximately proportional to the difference $\varepsilon_c - \varepsilon$ between the coupling parameter and its critical value (see Sec. 2.3).

2.4.2 Spatially Extended Systems

In this work we limit ourselves to one spatial dimension. Generalizations of the concepts to higher dimensions are straightforward. Here we only give a brief introduction to the stochastic modelling of the perturbation dynamics of spatially extended systems; details can be found in Refs. [91, 93] and Ch. 5. We start by adding a diffusion term to the linear multiplicative noise equation (2.13) of the previous section,

$$\frac{\partial w(x,t)}{\partial t} = [c + \xi(x,t)]w(x,t) + \varepsilon \Delta w(x,t), \quad (2.17)$$

where c is a constant that will turn out to be related to the Lyapunov exponent λ , and ε is the diffusion constant. The sign of $w(x,t)$ may vary in space. Note, however, that $w(x,t)$ stays positive if the initial state $w(x,0)$ is positive at all x . The Gaussian stochastic process $\xi(x,t)$ has the properties

$$\langle \xi(x,t) \rangle = 0, \quad \langle \xi(x,t) \xi(x',t') \rangle = 2\sigma^2 \delta(t-t') f(x-x').$$

We are particularly interested in the theoretical limit $f(x-x') \rightarrow \delta(x-x')$, that induces the practical problem that w becomes discontinuous with respect to x . Small spatial correlations, however, are not expected to change the critical properties of the model (see Ref. [55] for

a discussion of correlated noise in the closely related KPZ equation, which is described in the following paragraph).

By application of the Hopf-Cole transformation $h = \ln |w|$, Eq. (2.17) is transformed into [91]

$$\frac{\partial h(x,t)}{\partial t} = c + \xi(x,t) + \varepsilon \Delta h(x,t) + \varepsilon [\nabla h(x,t)]^2.$$

This is the Kardar-Parisi-Zhang (KPZ) equation for growing and roughening interfaces [66]. For this well-studied equation several scaling laws are known [9, 55] that are also found in the perturbation dynamics of spatially extended dynamical systems [91, 93]. The average velocity of the saturated interface is equal to the largest Lyapunov exponent,

$$\lambda = c + \varepsilon \lim_{t \rightarrow \infty} \langle [\nabla h(x,t)]^2 \rangle_x.$$

Using this equivalence, finite-time and finite-size scaling relations for the Lyapunov exponent have been derived [93].

In Ch. 5 we study the synchronization transition of coupled spatially extended dynamical systems. There a nonlinear saturating term will be added to the stochastic PDE (2.17) to limit the magnitude of the synchronization error $w(x,t)$. Nonlinear spatially extended multiplicative noise equations have been studied extensively during the last years in a variety of contexts [105, 36, 12, 108, 51, 81, 107, 82, 40]. Some of the results that are of interest for the synchronization transition are reported in Ch. 5. We just mention that in contrast to the zero-dimensional case the transition parameter between stable ($w \rightarrow 0$) and unstable (w finite) solutions can depend on the noise amplitude [36, 12]. Furthermore, the applicability of stochastic models of chaotic spatially extended systems can be limited in systems displaying spatio-temporal intermittency, when laminar structures play an important role in the dynamics [18].

3 Scaling of Lyapunov Exponents

In 1985 DAIDO discovered by means of numerical simulations that the Lyapunov exponents of weakly coupled chaotic maps show a very strong dependence on the strength of the coupling [26]. He was able to find an approximate logarithmic scaling relation and coined the notion “coupling sensitivity of chaos” for this behaviour. Further studies with different systems indicated that the effect is very general [27, 28, 29].

In this chapter a stochastic continuous-time model is presented that captures the essential aspects of the perturbation dynamics (the basic idea of stochastic modelling of chaotic fluctuations is explained in Sec. 2.4). It gives a general scaling relation which includes as a limiting case the logarithmic scaling found by DAIDO. The model further allows one to understand the origin of the effect and the significance of certain parameters. A perturbative method (the small noise expansion [6]) is shown to be not applicable to weakly coupled systems. Results of numerical simulations are presented that confirm the predictions of the derived scaling relation. Finally, a random walk picture is introduced that sheds light on the origin of the logarithmic singularity.

Parallel to our work, a similar stochastic model has been used by CECCONI and POLITI to estimate the Lyapunov exponent of a coupled map lattice in the limit of weak coupling [22] (see also Sec. 3.1.2). The analytical calculations in Secs. 3.2.2–3.2.5 have been carried out by RÜDIGER ZILLMER and are described in detail in his diploma thesis [112]. Some of the results of this chapter have been published in Refs. [113, 3, 114].

3.1 Coupling Sensitivity of Chaos

3.1.1 The Effect

The basic system already studied by DAIDO consists of two coupled one-dimensional maps,

$$\begin{aligned}u_1(t+1) &= f(u_1(t)) + \varepsilon g(u_2(t), u_1(t)), \\u_2(t+1) &= f(u_2(t)) + \varepsilon g(u_1(t), u_2(t)),\end{aligned}\tag{3.1}$$

where $t \in \mathbf{Z}$ is the discrete time variable, ε is the coupling parameter (i.e. the coupling strength), u_1 and u_2 are the state variables, f is the nonlinear map, and g is the coupling function. In the following we always choose $g(u_2, u_1) = f(u_2) - f(u_1)$, corresponding to

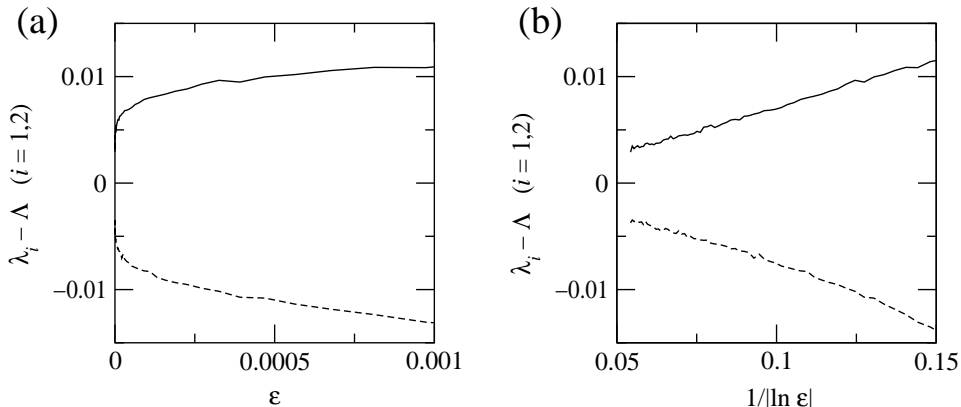


Figure 3.1: Coupled skew Bernoulli maps, Eq. (3.3). (a) The Lyapunov exponents $\lambda_1 - \Lambda$ (solid line) and $\lambda_2 - \Lambda$ (dashed line) versus ϵ for $a = 1/3$. (b) The same data in scaled coordinates.

diffusive coupling.¹ We emphasize, however, that the effects described in this chapter are also found for other coupling functions.

Since the system under study is two-dimensional, we can calculate two Lyapunov exponents by studying the dynamics of the linearized system

$$\begin{aligned} w_1(t+1) &= (1-\epsilon)f'(u_1(t))w_1(t) + \epsilon f'(u_2(t))w_2(t), \\ w_2(t+1) &= (1-\epsilon)f'(u_2(t))w_2(t) + \epsilon f'(u_1(t))w_1(t), \end{aligned} \quad (3.2)$$

where f' denotes the derivative of f . Without coupling, $\epsilon = 0$, we have two identical systems with the same Lyapunov exponents Λ . When coupling is introduced, the Lyapunov exponents are in general different. Furthermore, their values depend on the coupling parameter ϵ . We thus have the two Lyapunov exponents $\lambda_1(\epsilon)$ and $\lambda_2(\epsilon)$.

The observation of DAIDO was that for small values of the coupling parameter, $\epsilon \ll 1$, the Lyapunov exponents diverge from each other and from the zero coupling value Λ according to

$$\lambda_1 - \lambda_2 \sim -\frac{1}{\ln \epsilon} = \frac{1}{|\ln \epsilon|}, \quad \lambda_{1,2} - \Lambda \sim \frac{1}{|\ln \epsilon|}.$$

He found this to be a common behaviour of different maps f and different coupling functions g [26].

As a first example we study the dependence of two coupled skew Bernoulli maps on the coupling parameter. The skew Bernoulli map is defined as (see also Sec. 2.1.3)

$$f: [0, 1] \rightarrow [0, 1], \quad u \mapsto \begin{cases} u/a & \text{if } u \leq a, \\ (u-a)/(1-a) & \text{if } u > a, \end{cases} \quad (3.3)$$

¹Naively choosing $g(u_2, u_1) = u_2 - u_1$ would give rise to the possibility that the $u_{1,2}(t+1)$ lie outside of the interval that the map f is acting on (see also Sec. 2.2).

where $a \in (0, 1)$ is a parameter. The Lyapunov exponents of the system (3.1) of coupled maps are calculated by standard numerical methods (cf. App. A.1). In Fig. 3.1 the differences of the Lyapunov exponents $\lambda_{1,2}$ from the single map value Λ are shown as functions of the coupling parameter ε . From Fig. 3.1(b) it can be seen that for small values of ε these differences scale according to

$$\lambda_i - \Lambda \sim \frac{1}{|\ln \varepsilon|}, \quad i = 1, 2.$$

3.1.2 Previous Theoretical Results

There have been different theoretical approaches to understand the origin of the coupling sensitivity of chaos. They have in common that they started from discrete-time dynamics, i. e., coupled maps.

DAIDO used an expansion of the local Lyapunov exponents of coupled maps and was able to reproduce the $1/|\ln \varepsilon|$ dependence [27]. He pointed out the importance of fluctuations of the local expansion rates and stressed that this prerequisite distinguishes the coupling sensitivity from the usual sensitive dependence on initial conditions. He later introduced a discrete-time stochastic model that shows the logarithmic singularity, but not the quantitative dependence on the magnitude of fluctuations of the local expansion rate [29].

The following theoretical results have been obtained for the largest Lyapunov exponent of coupled map lattices with weak coupling. In that context, which corresponds to the limit of infinitely many (instead of just two) coupled systems, a similar logarithmic singularity (with different prefactors) is observed.

LIVI et al. found an analogy to the problem of directed polymers in random media. They used a mean field approach and a tree approximation to estimate the dependence of the Lyapunov exponent on the coupling strength [75]. While their model approximately shows the $1/|\ln \varepsilon|$ dependence, it wrongly predicts a phase transition at a critical coupling strength.

CECCONI and POLITI were able to improve the previous approach by using an n -tree approximation [21]. They found that the critical coupling strength of the spurious phase transition shifts to higher values of ε with increasing tree depth n .

Finally, CECCONI and POLITI used a continuous-time approximation of a discrete-time model [22]. Parallel to our work, they found a relation similar to our result (3.11) (including the quantitative dependence on the magnitude of fluctuations of the local expansion rate), but with different prefactors because of the high dimensionality. Furthermore, they were able to find an approximate result for coupled maps which have derivatives with fluctuating signs.

Our own approach does not start from coupled maps, but uses a simple continuous-time stochastic model of the perturbation dynamics with the key ingredients of exponential growth, finite-time fluctuations, and coupling. It further allows for different Lyapunov ex-

ponents of the coupled systems, which is needed to understand the phenomenon of avoided crossing of Lyapunov exponents (see Ch. 4).

3.2 Analytical Approach

3.2.1 Stochastic Model

The universality of the effect of coupling sensitivity of chaos indicates that there exists an underlying mechanism not connected with any special system. Furthermore, the effect has been found for both two- and higher-dimensional systems. The basic ingredients common to all studied systems are temporal fluctuations (due to the chaotic nature of the dynamics) and weak coupling. Since we are interested in the Lyapunov exponents, we look for a model for the perturbation dynamics, Eq. (3.2). We replace the fluctuating derivatives f' of the chaotic function by stochastic processes. In order to be able to derive a Fokker-Planck equation, we use Gaussian distributed processes. Their means and variances are connected with the chaotic systems as will be explained below. To include the more general case of coupled nonidentical systems, we allow these parameters to be different for the coupled systems.

Since the effect of coupling sensitivity is already found in two-dimensional systems, a two-dimensional model can be expected to be sufficient. For higher-dimensional systems, our model describes the dynamics in the directions corresponding to the largest Lyapunov exponents of the individual systems. Summarizing, we propose the two-dimensional system of Langevin equations

$$\begin{aligned}\frac{dw_1(t)}{dt} &= [\Lambda_1 + \chi_1(t)]w_1(t) + \varepsilon[w_2(t) - w_1(t)], \\ \frac{dw_2(t)}{dt} &= [\Lambda_2 + \chi_2(t)]w_2(t) + \varepsilon[w_1(t) - w_2(t)]\end{aligned}\tag{3.4}$$

as a continuous-time model for the linearized equations of the coupled chaotic systems. These equations have to be interpreted in the Stratonovich sense. The choices of multiplicative noise processes and the Stratonovich interpretation are explained in Sec. 2.4.1. The Gaussian stochastic processes χ_1 and χ_2 are independent and distributed according to

$$\langle \chi_i(t) \rangle = 0, \quad \langle \chi_i(t) \chi_j(t') \rangle = 2\sigma_i^2 \delta_{ij} \delta(t - t'), \quad i, j \in \{1, 2\},$$

where the averages are over different realizations. Three groups of parameters describe three important ingredients of the dynamics:

1. The *Lyapunov exponents* of the uncoupled systems are described by the constants $\Lambda_{1,2}$.
2. The *fluctuations of local expansion rates* of the uncoupled systems are characterized by the parameters $\sigma_{1,2}^2$. They are closely related to the distribution of local (finite-time)

Lyapunov exponents $\lambda(t)$, see Sec. 2.1.2. For the stochastic model (3.4) the local Lyapunov exponents are finite-time averages of the Gaussian δ -correlated processes, so that their distribution is also Gaussian with mean Λ and variance $2\sigma^2/t$ [25],

$$\text{Prob}(\lambda(t)) \sim \exp\left(-\frac{t[\lambda(t) - \Lambda]^2}{(2\sigma)^2}\right).$$

An approximate value of σ^2 can thus be calculated from the variance of local Lyapunov exponents of a given chaotic system. In connection with the numerical simulations in Sec. 3.4, the parameters σ^2 will be calculated for different systems.

3. The *coupling* is described by the coupling parameter ε . For a while a symmetrical coupling is assumed, the case of asymmetrical coupling is considered below.

It has to be stressed that we assume the statistical properties of the individual systems (characterized by the distributions of the stochastic processes $\chi_{1,2}$) to be independent of the coupling. This assumption can be justified by means of results from a perturbation analysis of weakly coupled maps [20] indicating that the invariant measure depends on the coupling strength in a nonsingular way. Nevertheless, our model will certainly fail for strongly coupled systems.

Without fluctuations, $\sigma_1^2 = \sigma_2^2 = 0$, and equal Lyapunov exponents of the uncoupled systems, $\Lambda_1 = \Lambda_2 = \Lambda$, we have a two-dimensional system of linear differential equations,

$$\frac{d}{dt} \begin{pmatrix} w_1 \\ w_2 \end{pmatrix} = \begin{pmatrix} \Lambda - \varepsilon & \varepsilon \\ \varepsilon & \Lambda - \varepsilon \end{pmatrix} \begin{pmatrix} w_1 \\ w_2 \end{pmatrix}.$$

The Lyapunov exponents are simply the eigenvalues of the time-independent real symmetric matrix (see Sec. 2.1.2). We thus obtain

$$\lambda_1 = \Lambda, \quad \lambda_2 = \Lambda - 2\varepsilon$$

for the Lyapunov exponents of the coupled systems. This means that without fluctuations of the local expansion rates we have no coupling sensitivity of chaos, a result that was already observed by DAIDO [26].

3.2.2 Fokker-Planck Treatment

To obtain the value of the largest Lyapunov exponent of the stochastic model, we now calculate the stationary probability density of the associated Fokker-Planck equation. The analytical calculations are described in detail in Ref. [112], here only an overview of the procedure is given.

First we perform a transformation to new variables. For large times and positive coupling ε both variables $w_{1,2}$ have the same sign. It is easy to see that the regions $w_1, w_2 > 0$

3 Scaling of Lyapunov Exponents

and $w_1, w_2 < 0$ are absorbing ones because for $w_1 = 0$ we have $\dot{w}_1 = \varepsilon w_2$ and for $w_2 = 0$ we have $\dot{w}_2 = \varepsilon w_1$. Thus eventually one observes the state with $w_1 w_2 > 0$ independently of initial conditions. So the transformation

$$v_1 = \ln(w_1/w_2), \quad v_2 = \ln(w_1 w_2),$$

can be performed, leading to the equations

$$\frac{dv_1}{dt} = \xi_1 - 2\varepsilon \sinh v_1 + \Lambda_1 - \Lambda_2, \quad (3.5)$$

$$\frac{dv_2}{dt} = \xi_2 + 2\varepsilon \cosh v_1 + \Lambda_1 + \Lambda_2 - 2\varepsilon, \quad (3.6)$$

where $\xi_1 = \chi_1 - \chi_2$ and $\xi_2 = \chi_1 + \chi_2$. By means of the transformation of variables we have simplified the equations in two ways. First, the multiplicative noise processes have been transformed to additive ones. Second, Eq. (3.5) for v_1 is independent of Eq. (3.6) for v_2 . Thus, although the stochastic processes $\xi_{1,2}$ are no more statistically independent, we can write the Fokker-Planck equation for the probability density $\rho(v_1, t)$ [100] (see App. A.2),

$$\frac{\partial \rho(v_1, t)}{\partial t} = \left[2\varepsilon \cosh v_1 + 2\varepsilon \sinh v_1 \frac{\partial}{\partial v_1} - (\Lambda_1 - \Lambda_2) \frac{\partial}{\partial v_1} + 2\sigma^2 \frac{\partial^2}{\partial v_1^2} \right] \rho(v_1, t), \quad (3.7)$$

where $\sigma^2 = (\sigma_1^2 + \sigma_2^2)/2$. The stationary solution of (3.7) is given by [112]

$$\rho_{\text{stat}}(v_1) = N \exp\left(lv_1 - \frac{\varepsilon}{\sigma^2} \cosh v_1\right), \quad (3.8)$$

where $l = (\Lambda_1 - \Lambda_2)/(2\sigma^2)$ and N is a normalization constant.

Basing on the solution (3.8) we now calculate the largest Lyapunov exponent of the coupled system, defined by

$$\lambda_1 = \lim_{t \rightarrow \infty} \frac{1}{t} \left\langle \ln \sqrt{w_1^2 + w_2^2} \right\rangle = \lim_{t \rightarrow \infty} \frac{1}{2t} \left\langle \ln(w_1^2 + w_2^2) \right\rangle,$$

where the averages are over different realizations of the noise processes. The logarithm can be expressed in terms of v_1 and v_2 as

$$\ln(w_1^2 + w_2^2) = \ln\left(w_1 w_2 \left(\frac{w_1}{w_2} + \frac{w_2}{w_1}\right)\right) = v_2 + \ln(2 \cosh v_1).$$

Since one is interested in the long-time limit, the stationary distribution (3.8) of v_1 may be used, leading to

$$\lambda_1 = \lim_{t \rightarrow \infty} \left\{ \frac{1}{2t} \langle v_2 \rangle_{\rho_{\text{stat}}} + \frac{1}{2t} \langle \ln(2 \cosh v_1) \rangle_{\rho_{\text{stat}}} \right\}.$$

In the following, all averages are meant with respect to the stationary distribution. Because $\langle \ln(2 \cosh v_1) \rangle$ is finite and time-independent, the second term vanishes for $t \rightarrow \infty$. In the first term, $\langle v_2/t \rangle$ can be replaced by $\langle \dot{v}_2 \rangle$. Thus the Lyapunov exponent can be calculated by averaging the r. h. s. of Eq. (3.6),

$$\lambda_1 = \frac{1}{2} \langle \dot{v}_2 \rangle = \varepsilon \langle \cosh v_1 \rangle + \frac{1}{2} (\Lambda_1 + \Lambda_2 - 2\varepsilon). \quad (3.9)$$

The averaging with the stationary distribution $\rho_{\text{stat}}(v_1)$ yields (see Ref. [112] for details)

$$\langle \cosh v_1 \rangle = \frac{K_{1-|l|}(\varepsilon/\sigma^2) + K_{1+|l|}(\varepsilon/\sigma^2)}{2K_{|l|}(\varepsilon/\sigma^2)},$$

where the K_l are modified Bessel functions (Macdonald functions) [1]. Substituting this in Eq. (3.9) we obtain a final analytical formula for the largest Lyapunov exponent. We write it in scaling form,

$$\frac{\lambda_1 - (\Lambda_1 + \Lambda_2 - 2\varepsilon)/2}{\sigma^2} = \frac{\varepsilon}{\sigma^2} \frac{K_{1-|l|}(\varepsilon/\sigma^2) + K_{1+|l|}(\varepsilon/\sigma^2)}{2K_{|l|}(\varepsilon/\sigma^2)}. \quad (3.10)$$

This form demonstrates that the essential parameters of the problem are the coupling parameter and the Lyapunov exponents' mismatch normalized to the fluctuation of the exponents,

$$\frac{\varepsilon}{\sigma^2} \quad \text{and} \quad l = \frac{\Lambda_1 - \Lambda_2}{2\sigma^2},$$

respectively. If the Lyapunov exponents of the two interacting systems are equal, $\Lambda_1 = \Lambda_2 = \Lambda$, the parameter l vanishes and we obtain (cf. [22])

$$\lambda_1 - \Lambda = \varepsilon \frac{K_1(\varepsilon/\sigma^2)}{K_0(\varepsilon/\sigma^2)} - \varepsilon. \quad (3.11)$$

We gain further insight into the scaling behaviour by approximating the modified Bessel functions. Simplified expressions can be obtained in the following limiting cases:

Small coupling, equal Lyapunov exponents. For small coupling ε/σ^2 , the leading term in ε is singular as it follows from the expansions of K_1 and K_0 [1] in Eq. (3.11),

$$\lambda_1 - \Lambda \approx \frac{\sigma^2}{|\ln(\varepsilon/\sigma^2)|}. \quad (3.12)$$

This formula corresponds to DAIDO's singular dependence of the Lyapunov exponent on the coupling parameter [26, 27, 28] and will be checked by means of numerical simulations in Sec. 3.4. It is valid in all cases when identical chaotic systems are coupled symmetrically, provided that the Lyapunov exponents in these systems fluctuate ($\sigma^2 > 0$). Moreover, even for different systems having, however, equal Lyapunov exponents (but not necessarily equal fluctuations of the exponents) we get the same singularity as for identical systems. DAIDO arrived at a similar result in his analytical treatment of coupled one-dimensional maps, cf. Eq. (19) of Ref. [29].

No fluctuations, equal Lyapunov exponents. With vanishing fluctuations, $\sigma^2 \rightarrow 0$, and fixed coupling parameter, we have $\varepsilon/\sigma^2 \rightarrow \infty$. In this case the fraction in Eq. (3.11) becomes unity, $K_1(\varepsilon/\sigma^2)/K_0(\varepsilon/\sigma^2) \rightarrow 1$, and we obtain

$$\lambda_1 = \Lambda.$$

This is consistent with the result one directly gets from the model without fluctuations, see Sec. 3.2.1.

Small coupling, different Lyapunov exponents. The expansion (3.12) remains valid for small values of mismatch $|l|$, if $(\varepsilon/\sigma^2)^{|l|}$ is close to 1. For larger mismatch, when

$$\left(\frac{\varepsilon}{\sigma^2}\right)^{|l|} \ll 1,$$

the largest Lyapunov exponent is

$$\lambda_1 \approx 2\sigma^2 |l| \frac{\Gamma(1-|l|)}{\Gamma(1+|l|)} \left(\frac{\varepsilon}{2\sigma^2}\right)^{2|l|} + \frac{1}{2} \underbrace{(|\Lambda_1 - \Lambda_2| + \Lambda_1 + \Lambda_2)}_{\max\{\Lambda_1, \Lambda_2\}}. \quad (3.13)$$

The singularity is now of the power-law type, with the power depending on the system's mismatch. Note that this is the correction to the largest of the Lyapunov exponents of the uncoupled systems. The dependence of

$$\delta\lambda = \frac{\lambda_1 - (\Lambda_1 + \Lambda_2 - 2\varepsilon)/2}{\sigma^2} \quad (3.14)$$

on $|l|$ is shown in Fig. 3.2 for the coupling parameter $\varepsilon/\sigma^2 = 10^{-5}$. Plotted are Eq. (3.10) and the appropriate form of the approximation (3.13),

$$\delta\lambda \approx |l| \left[1 + 2 \frac{\Gamma(1-|l|)}{\Gamma(1+|l|)} \left(\frac{\varepsilon}{2\sigma^2}\right)^{2|l|} \right].$$

With increasing difference $|l|$ the influence of the coupling on λ_1 decreases. For large $|l|$ we thus have $\lambda_1 \approx \max\Lambda_{1,2}$, such that Eq. (3.14) becomes (for $\varepsilon/\sigma^2 \ll |l|$)

$$\delta\lambda \approx \frac{|\Lambda_1 - \Lambda_2|/2 + \varepsilon}{\sigma^2} \approx |l|,$$

which can also be seen in Fig. 3.2.

Large coupling. For $\varepsilon/\sigma^2 \gg 1$ the expansion of (3.10) gives

$$\lambda_1 \approx \frac{\sigma^2}{2} - \frac{(1+3l^2)\sigma^4}{8\varepsilon} + \frac{1}{2}(\Lambda_1 + \Lambda_2). \quad (3.15)$$

It has to be kept in mind, however, that for large coupling the Langevin equations (3.4) cannot be expected to be a reliable model of coupled chaotic systems. Therefore Eq. (3.15) should be seen as a result which is only valid for the model itself.

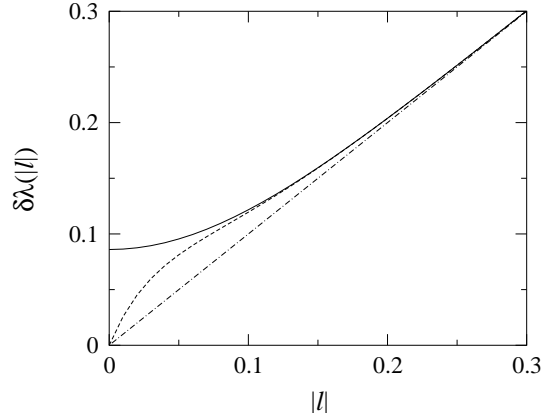


Figure 3.2: The dependence of $\delta\lambda$ (see Eq. (3.14)) on the difference $|I|$. Shown are the exact result (3.10) (solid line), the approximation (3.13) (dashed line), and the asymptotic behaviour $\delta\lambda = |I|$ (dash-dotted line).

3.2.3 The Second Lyapunov Exponent

The sum of Lyapunov exponents can be calculated from the divergence of the phase space volume using Eqs. (3.4),

$$\lambda_1 + \lambda_2 = \left\langle \frac{\partial \dot{w}_1}{\partial w_1} + \frac{\partial \dot{w}_2}{\partial w_2} \right\rangle = \Lambda_1 + \Lambda_2 - 2\varepsilon.$$

This enables us to find an expression for the second Lyapunov exponent,

$$\lambda_2 - \Lambda_2 = -(\lambda_1 - \Lambda_1) - 2\varepsilon. \quad (3.16)$$

The singularity is the same as for the first Lyapunov exponent, it just has the opposite sign. The linear decrease corresponds to the synchronization effect, leading to a negative λ_2 for coupling strengths larger than some critical ε_c .

3.2.4 Generalized Lyapunov Exponents

By means of the Furutsu-Novikov relation (see App. A.2) it is further possible to obtain results for some of the generalized Lyapunov exponents [25]

$$L(q) = \lim_{t \rightarrow \infty} \frac{1}{t} \ln \left\langle (w_1^2 + w_2^2)^{q/2} \right\rangle,$$

where the average is over different realizations of the noise processes. Details can be found in Refs. [112, 113]. Here we only give the results (for $\Lambda_1 = \Lambda_2 = \Lambda$) [113]

$$L(1) = \Lambda + \sigma^2, \quad (3.17)$$

$$L(2) = 2\Lambda + 3\sigma^2 - 2\varepsilon + \sqrt{\sigma^4 + 4\varepsilon^2}. \quad (3.18)$$

Together with the trivial general result $L(0) = 0$ we can approximate $L(q)$ with the parabola [113]

$$L(q) = \alpha q + \beta q^2$$

with the parameters

$$\alpha = 2L(1) - \frac{L(2)}{2} \quad \text{and} \quad \beta = -L(1) + \frac{L(2)}{2},$$

giving

$$L(q) = q \left(\Lambda + \frac{\sigma^2}{2} + \varepsilon - \frac{1}{2} \sqrt{\sigma^4 + 4\varepsilon^2} \right) + q^2 \left(\frac{\sigma^2}{2} - \varepsilon + \frac{1}{2} \sqrt{\sigma^4 + 4\varepsilon^2} \right). \quad (3.19)$$

In the two limiting cases of weak and strong coupling, the square root in Eq. (3.19) can be expanded. In first order we obtain for weak coupling ($\varepsilon/\sigma^2 \ll 1$)

$$L(q) \approx q \left(\Lambda + \varepsilon - \frac{\varepsilon^2}{\sigma^2} \right) + q^2 \left(\frac{\sigma^2}{2} - \varepsilon + \frac{\varepsilon^2}{\sigma^2} \right),$$

while for strong coupling ($\varepsilon/\sigma^2 \gg 1$) we obtain

$$L(q) \approx q \left(\Lambda + \frac{\sigma^2}{2} - \frac{\sigma^4}{8\varepsilon} \right) + q^2 \left(\frac{\sigma^2}{2} + \frac{\sigma^4}{8\varepsilon} \right), \quad (3.20)$$

The latter expression will be compared with the result of the small noise expansion in Sec. 3.3 below.

3.2.5 Asymmetrical Coupling

An interesting generalization of the stochastic model is to consider asymmetrical coupling,

$$\begin{aligned} \frac{dw_1(t)}{dt} &= [\Lambda_1 + \chi_1(t)]w_1(t) + \varepsilon_1[w_2(t) - w_1(t)], \\ \frac{dw_2(t)}{dt} &= [\Lambda_2 + \chi_2(t)]w_2(t) + \varepsilon_2[w_1(t) - w_2(t)], \end{aligned}$$

which can be reduced to the symmetric case by means of the transformation

$$\tilde{w}_1 = \sqrt{\varepsilon_2}w_1, \quad \tilde{w}_2 = \sqrt{\varepsilon_1}w_2.$$

We thus obtain the result

$$\frac{\lambda_1 - (\Lambda_1 + \Lambda_2 - \varepsilon_1 - \varepsilon_2)/2}{\sigma^2} = \frac{\varepsilon}{\sigma^2} \frac{K_{1-|\lambda|}(\varepsilon/\sigma^2) + K_{1+|\lambda|}(\varepsilon/\sigma^2)}{2K_{|\lambda|}(\varepsilon/\sigma^2)},$$

with the effective coupling parameter and the effective mismatch

$$\varepsilon = \sqrt{\varepsilon_1 \varepsilon_2} \quad \text{and} \quad l = \frac{1}{2\sigma^2} [(\Lambda_1 - \varepsilon_1) - (\Lambda_2 - \varepsilon_2)],$$

respectively [113].

In the extreme case of unidirectional coupling we can calculate the Lyapunov exponents directly from the model

$$\begin{aligned} \frac{dw_1(t)}{dt} &= [\Lambda_1 + \chi_1(t)]w_1(t), \\ \frac{dw_2(t)}{dt} &= [\Lambda_2 + \chi_2(t)]w_2(t) + \varepsilon[w_1(t) - w_2(t)]. \end{aligned}$$

For the first autonomous equation we obtain $\lambda_1 = \Lambda_1$. The sum of both Lyapunov exponents can again be calculated from the divergence of the phase space volume. This gives us the value of the second Lyapunov exponent, $\lambda_2 = \Lambda_2 - \varepsilon$. For unidirectionally coupled systems we thus have no coupling sensitivity [113].

3.3 Small Noise Expansion

Expansions of the largest Lyapunov exponent as well as the generalized Lyapunov exponents of a stochastic system in terms of the noise amplitude have been found by ARNOLD et al. [6]. Relevant for our model is the white noise case with two distinct real eigenvalues of the deterministic system. The linear Stratonovich stochastic differential equation (see also App. A.2) has the form

$$d\mathbf{x} = \mathbf{A}\mathbf{x}dt + \delta \sum_{i=1}^m \mathbf{B}_i \mathbf{x} \circ dW_i(t), \quad (3.21)$$

where $\mathbf{x} \in \mathbf{R}^2$, \mathbf{B}_i and

$$\mathbf{A} = \begin{pmatrix} a_1 & 0 \\ 0 & a_2 \end{pmatrix}, \quad a_1 > a_2,$$

are real 2×2 matrices, δ is the small noise amplitude, and the $W_i(t)$ are independent Wiener processes. The largest Lyapunov exponent can then be expanded as [6]

$$\lambda_1^\delta = a_1 + \frac{\delta^2}{2} \sum_{i=1}^m b_{i,12} b_{i,21} + o(\delta^2).$$

The expansion of the generalized Lyapunov exponents is given by

$$L^\delta(q) = q \left(a_1 + \frac{\delta^2}{2} \sum_{i=1}^m b_{i,12} b_{i,21} \right) + q^2 \frac{\delta^2}{2} \sum_{i=1}^m b_{i,11}^2 + qo(\delta^2) + o(q^2).$$

In the following we assume $\Lambda_1 = \Lambda_2 = \Lambda$ and $\varepsilon/\sigma^2 \gg 1$ (small noise amplitude). Our model (3.4) can be written as

$$d\mathbf{w} = \mathbf{A}\mathbf{w}dt + \delta \sum_{i=1}^2 \mathbf{B}_i \mathbf{w} \circ dW_i(t),$$

where $\mathbf{w} = (w_1, w_2)^T$, $\delta = \sqrt{2\sigma^2}$, $dW_i(t) = \chi_i(t)dt$,

$$\mathbf{A} = \begin{pmatrix} \Lambda - \varepsilon & \varepsilon \\ \varepsilon & \Lambda - \varepsilon \end{pmatrix}, \quad \mathbf{B}_1 = \begin{pmatrix} 1 & 0 \\ 0 & 0 \end{pmatrix}, \quad \text{and} \quad \mathbf{B}_2 = \begin{pmatrix} 0 & 0 \\ 0 & 1 \end{pmatrix}.$$

The eigenvalues of \mathbf{A} are $a_1 = \Lambda$ and $a_2 = \Lambda - 2\varepsilon$. In order to bring our system to the form of Eq. (3.21), we have to diagonalize \mathbf{A} and transform the matrices \mathbf{B}_i accordingly. This is accomplished by the orthogonal matrix made up of the eigenvectors,

$$\mathbf{O} = \frac{1}{2} \begin{pmatrix} 1 & 1 \\ 1 & -1 \end{pmatrix}.$$

From the resulting matrices

$$\mathbf{O}^T \mathbf{B}_1 \mathbf{O} = \frac{1}{2} \begin{pmatrix} 1 & 1 \\ 1 & 1 \end{pmatrix} \quad \text{and} \quad \mathbf{O}^T \mathbf{B}_2 \mathbf{O} = \frac{1}{2} \begin{pmatrix} 1 & -1 \\ -1 & 1 \end{pmatrix}$$

we obtain the expansions

$$\lambda_1^\delta = \Lambda + \frac{\sigma^2}{2}$$

and

$$L^\delta(q) = q \left(\Lambda + \frac{\sigma^2}{2} \right) + q^2 \frac{\sigma^2}{2}.$$

Comparing these results with our results obtained by means of the Fokker-Planck equation (Eqs. (3.15) and (3.20) for small noise amplitude, i.e., large ε/σ^2), we find that they coincide up to order σ^2 . The ε -dependence of λ_1 and $L(q)$ occurs, however, in order σ^4 and is therefore not captured by the small noise expansion up to order σ^2 . Furthermore, the Fokker-Planck treatment gives the general result (3.10) which is also valid for small values of ε/σ^2 (large noise amplitudes). Since the stochastic model is only valid for small values of ε , the small noise expansion is not applicable in the context of weakly coupled chaotic systems.

3.4 Numerical Simulations

We now compare the results obtained for the system of continuous-time Langevin equations with numerical calculations for both continuous- and discrete-time deterministic systems. The Lyapunov exponents are calculated as described in App. A.1.

3.4.1 Discrete Maps

We first study systems of two diffusively coupled one-dimensional maps $f_{1,2}$, Eq. (3.1). To have a good correspondence to the theory, we use only mappings with a constant sign of f' below, so that the fluctuations of the local expansion rate are the only source of irregularity of the perturbation dynamics. Another source of irregularity could be irregular changes of the sign of the derivative f' (as for the logistic and the tent maps). Such an irregularity is not covered by our continuous-time approach, but also leads to a logarithmic singularity similar to Eq. (3.12), see Ref. [22].

Skew Bernoulli Maps

We first consider the skew Bernoulli map (3.3). For the uncoupled map, the Lyapunov exponent and the magnitude of fluctuations are given by (see Sec. 2.1.3)

$$\Lambda = -a \ln a - (1-a) \ln(1-a) \quad (3.22)$$

and

$$\sigma^2 = \frac{1}{2} a(1-a) \left(\ln \frac{a}{1-a} \right)^2, \quad (3.23)$$

respectively. For $a = 1/2$ we obtain the ordinary Bernoulli map. In this case, there are no fluctuations of the local multipliers ($\sigma^2 = 0$), and no coupling sensitivity of the Lyapunov exponents is observed.

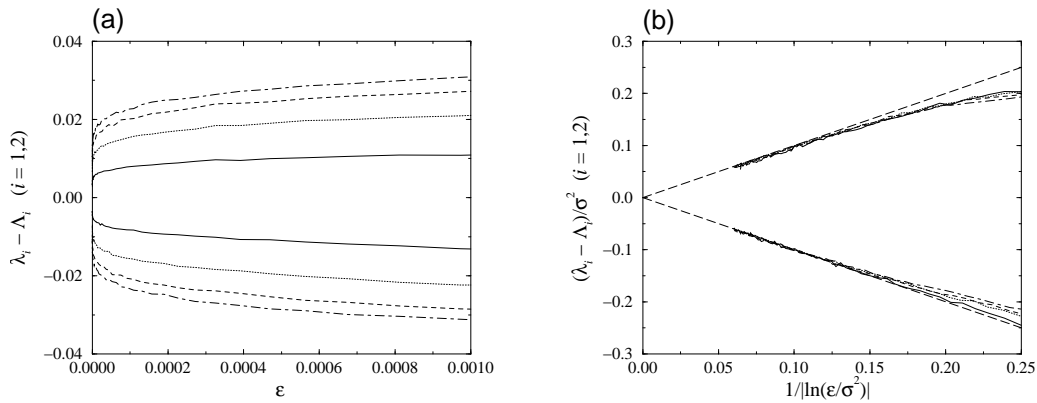


Figure 3.3: Coupled identical skew Bernoulli maps, Eq. (3.3). (a) The Lyapunov exponents $\lambda_1 - \Lambda$ and $\lambda_2 - \Lambda$ versus ϵ for $a = 1/3$ (solid lines), $a = 1/4$ (dotted lines), $a = 1/5$ (dashed lines), and $a = 1/6$ (dash-dotted lines). (b) The same graphs in scaled coordinates. The long-dashed lines show the analytical results $(\lambda_1 - \Lambda)/\sigma^2 = 1/|\ln(\epsilon/\sigma^2)|$ and $(\lambda_2 - \Lambda)/\sigma^2 = -1/|\ln(\epsilon/\sigma^2)|$, see Eqs. (3.12) and (3.16).

Figure 3.3(a) shows the differences $\lambda_{1,2} - \Lambda$ versus ε for maps with different values of $a \neq 1/2$. From Fig. 3.3(b) it can be seen that different curves collapse onto single lines for both exponents when plotted in the rescaled form according to (3.10), namely as $(\lambda_1 - \Lambda)/\sigma^2$ versus $1/|\ln(\varepsilon/\sigma^2)|$. The resulting lines are in very good agreement with the leading term of the theoretical prediction $(\lambda_1 - \Lambda)/\sigma^2 = 1/|\ln(\varepsilon/\sigma^2)|$, which is also shown.

No such good accordance between theory and numerical experiment is found in the case of generalized Lyapunov exponents. In Fig. 3.4(a,b) the results for $L(1)$ and $L(2)$ are shown for small values of ε . Also shown are the theoretical predictions from Eqs. (3.17) and (3.18), respectively. The rough correspondence is completely lost for larger values of ε , although the considerations leading to Eqs. (3.17) and (3.18) are not restricted to small ε .

Much better results are achieved if the derivatives f'_i in the linearized system (3.2) are replaced by independent and identically distributed Gaussian stochastic variables ξ_i ($i = 1, 2$). Then the system of equations reads (due to the discrete time the Lyapunov exponents and their finite-time fluctuations enter as arguments of exponentials, see Sec. 2.1.2)

$$\begin{aligned} w_1(t+1) &= (1 - \varepsilon)e^{\xi_1(t)}w_1(t) + \varepsilon e^{\xi_2(t)}w_2(t), \\ w_2(t+1) &= (1 - \varepsilon)e^{\xi_2(t)}w_2(t) + \varepsilon e^{\xi_1(t)}w_1(t), \end{aligned} \quad (3.24)$$

with

$$\langle \xi_i(t) \rangle = \Lambda, \quad \langle [\xi_i(t) - \Lambda][\xi_j(t') - \Lambda] \rangle = 2\sigma^2 \delta_{ij} \delta_{tt'}, \quad i, j \in \{1, 2\}.$$

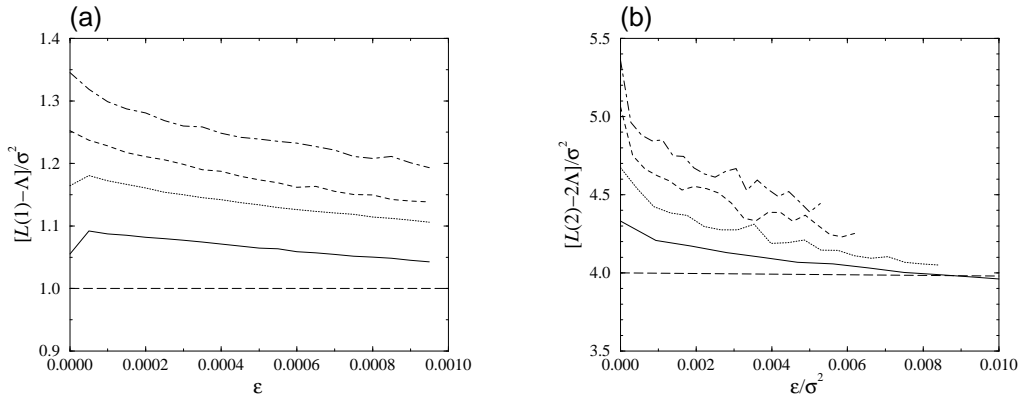


Figure 3.4: Generalized Lyapunov exponents for the skew Bernoulli maps. (a) Rescaled exponent $[L(1) - \Lambda]/\sigma^2$ versus ε for the same values of a as in Fig. 3.3. The long-dashed line shows the analytical result $[L(1) - \Lambda]/\sigma^2 = 1$, see Eq. (3.17). (b) Rescaled exponent $[L(2) - 2\Lambda]/\sigma^2$ versus ε/σ^2 for the same values of a as in Fig. 3.3. The long-dashed line shows the analytical result $[L(2) - 2\Lambda]/\sigma^2 = 3 - 2\varepsilon/\sigma^2 + \sqrt{1 + 4(\varepsilon/\sigma^2)^2}$, see Eq. (3.18).

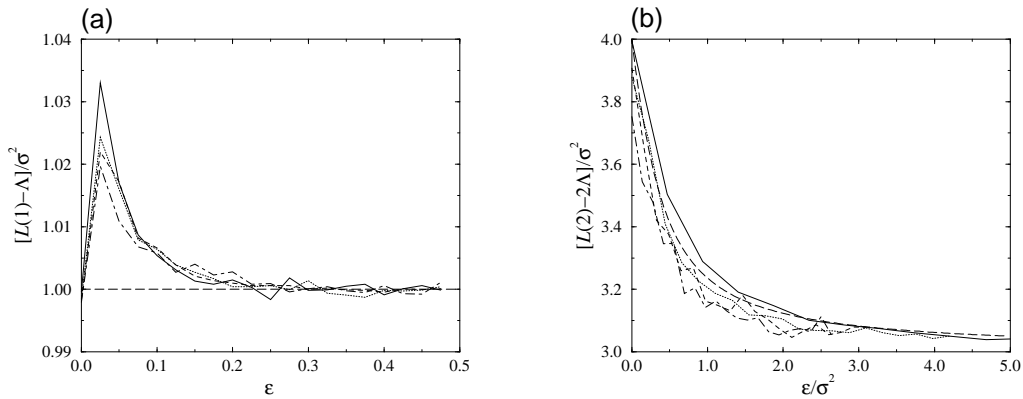


Figure 3.5: Rescaled generalized Lyapunov exponents in stochastic maps. (a) The exponent $[L(1) - \Lambda]/\sigma^2$ versus ϵ for Λ and σ^2 corresponding to the values of a used for Figs. 3.3 and 3.4. The long-dashed line shows the analytical result. Compared with Fig. 3.4(a), the relative deviation of the numerical data from the analytical result is small. (b) The exponent $[L(2) - 2\Lambda]/\sigma^2$ versus ϵ/σ^2 for Λ and σ^2 corresponding to the values of a used for Figs. 3.3 and 3.4. The long-dashed line shows the analytical result as in Fig. 3.4(b).

In Figs. 3.5(a,b) the results for $L(1)$ and $L(2)$, respectively, are shown together with the analytical curves. The values of Λ and σ^2 were calculated by means of Eqs. (3.22) and (3.23) with the values of a used above for the skew Bernoulli map.

An explanation for the discrepancy between the deterministic and stochastic results is that the distribution of $f'(u_i)$ is changed with increasing ϵ , while the distribution of the stochastic variables ξ_i remains constant. Furthermore, $f'(u_1)$ and $f'(u_2)$ are not statistically independent for larger values of ϵ . These effects have no observable influence in the case of usual Lyapunov exponents (Fig. 3.3) because of the singularity. In the case of generalized Lyapunov exponents, however, the nonsingular scaling functions are much more sensitive against changes in the distribution of multipliers.

Different Maps

One main result of the analytical approach is that the singularity does only depend on the average $\sigma^2 = (\sigma_1^2 + \sigma_2^2)/2$ of the fluctuations of local expansion rates and on the mismatch $l = (\Lambda_1 - \Lambda_2)/(2\sigma^2)$ of the Lyapunov exponents of the uncoupled systems. Although no singularity occurs if $\sigma^2 = 0$, we can expect to observe coupling sensitivity in the case of one system with fluctuations ($\sigma_1^2 > 0$) coupled to a different one without fluctuations ($\sigma_2^2 = 0$), given that the mismatch l is sufficiently small.

In order to check this prediction, we again numerically iterate the systems (3.1) and (3.2), now choosing two different maps. The first map is again the skew Bernoulli

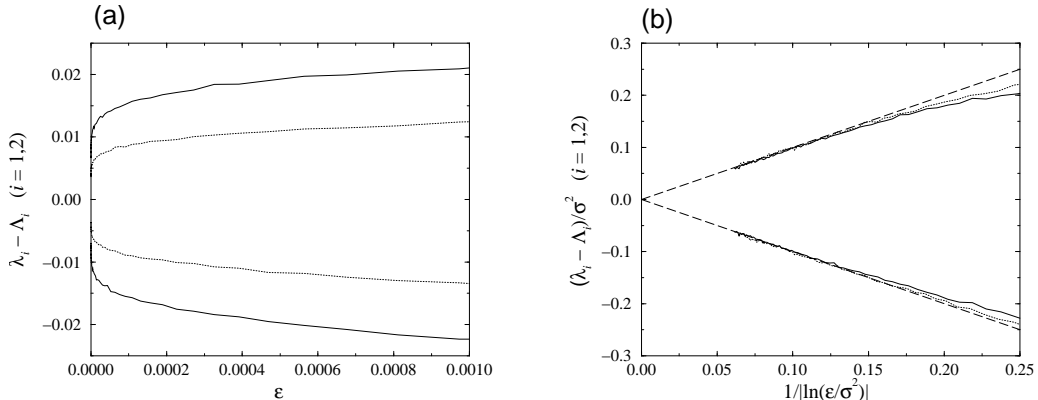


Figure 3.6: Different maps. (a) $\lambda_1 - \Lambda$ and $\lambda_2 - \Lambda$ versus ε for two coupled skew Bernoulli maps with $a = 1/4$ (solid lines) as well as one skew Bernoulli map with $a = 1/4$ coupled with the different map (3.25) (dotted lines). (b) $(\lambda_1 - \Lambda)/\sigma^2$ and $(\lambda_2 - \Lambda)/\sigma^2$ versus $1/|\ln(\varepsilon/\sigma^2)|$ for the same examples as in Fig. 3.6(a). The long-dashed lines show the analytical results as in Fig. 3.3(b).

map ($f_1(u) = f(u)$ as in Eq. (3.3)), while the second map is defined as

$$f_2(u) = e^\Lambda u \pmod{1}, \quad (3.25)$$

where Λ is the Lyapunov exponent of the skew Bernoulli map $f(u)$ (see Eq. (3.22)). With this choice we have the parameters $\sigma_1^2 > 0$, $\sigma_2^2 = 0$, and $l = 0$ (because $\Lambda_1 = \Lambda_2 = \Lambda$).

In Fig. 3.6 the result is compared with the previous result for two coupled identical skew Bernoulli maps ($a = 1/4$ in either case). As expected, the logarithmic singularity is observed in both cases, although the deviation $|\lambda_i - \Lambda_i|$ is smaller if $\sigma_2^2 = 0$. When rescaled with the average σ^2 , however, the curves collapse onto single lines for the first and second Lyapunov exponents, as can be seen in Fig. 3.6(b).

Strange Nonchaotic Attractors

DAIDO found out that for coupled logistic maps $f(u) = 4u(1 - u)$ the Lyapunov exponents exhibit power-law instead of logarithmic singular behaviour due to anomalous fluctuations of the finite-time Lyapunov exponents [29]. Here we report a similar observation in the case of coupled strange nonchaotic attractors.

Fluctuations of finite-time Lyapunov exponents is a typical feature of chaotic systems, but in some nonchaotic systems the Lyapunov exponents fluctuate as well. To this class belong strange nonchaotic attractors (SNAs) that have a negative maximal Lyapunov exponent, but a complex fractal structure in the phase space (see, e. g., Ref. [92]). The fluctuations of finite-time Lyapunov exponents are present in SNAs [92], but they are much more correlated than in chaotic systems. We demonstrate below that this leads to a weaker singularity in the Lyapunov exponents' dependence on the coupling.

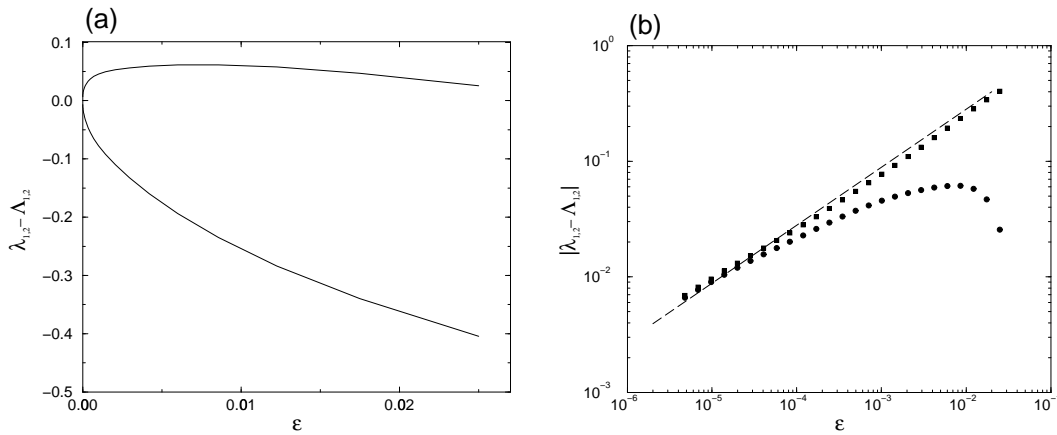


Figure 3.7: The Lyapunov exponents in coupled strange nonchaotic attractors in natural coordinates (a) and in a log-log representation (b). The dashed line in (b) has a slope 1/2.

We numerically studied two coupled quasiperiodically forced maps having strange nonchaotic attractors, using

$$f(u) = 2.5 \tanh(u) |\sin(\omega t + \phi)|, \quad (3.26)$$

where $\omega = (\sqrt{5} - 1)/2$ is the frequency of the quasiperiodic driving. The model (3.26) has been studied rigorously in Ref. [50, 67]. The results are presented in Fig. 3.7. The dependence of the Lyapunov exponents on the coupling has a singularity, but this singularity contrary to Eq. (3.12) is a power law, with a power close to 1/2. A detailed theory needs a correct account of nontrivial correlation properties of the SNA.

3.4.2 Delay Differential Equations

Our theory suggests that the effect of coupling sensitivity of chaos results from the coupling of fluctuating systems alone. It seems therefore natural to expect that the logarithmic singularity can also be found for coupled continuous-time systems. Furthermore, DAIDO observed the effect of coupling sensitivity of chaos not only for coupled one-dimensional maps, but also for two-dimensional discrete-time maps [28]. Here we give numerical evidence that the logarithmic singularity is also observed in infinite-dimensional and continuous-time systems. As an example we study a system of two coupled one-dimensional delay differential equations. A delay differential equation has an infinite number of Lyapunov exponents, and for large delays usually a finite number of exponents is positive. The

3 Scaling of Lyapunov Exponents

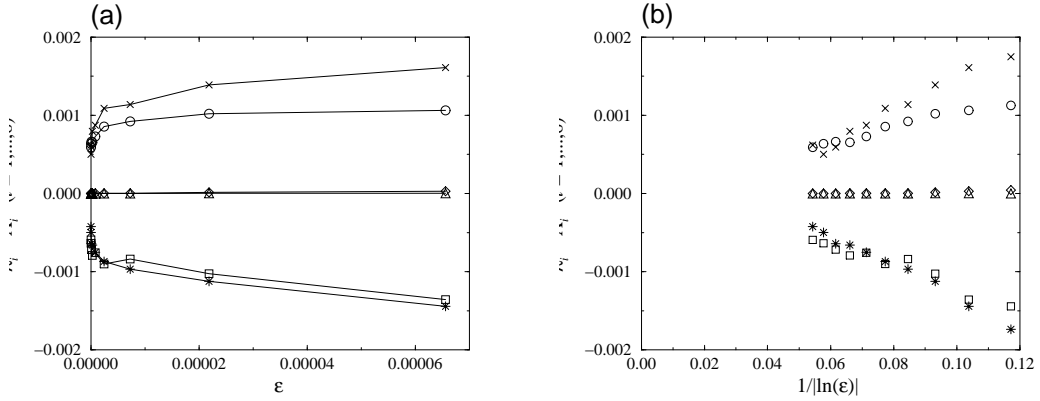


Figure 3.8: The Lyapunov exponents in the coupled Ikeda equations, in natural (a) and scaled (b) coordinates. Open circles and open squares: the splitting of the positive Lyapunov exponent; open triangles and open rhombs: the splitting of the zero exponent; crosses and stars: the splitting of the closest to zero negative exponent.

system we study reads

$$\begin{aligned}\frac{du_1(t)}{dt} &= f(u_1(t), u_1(t - \tau)) + \varepsilon[u_2(t) - u_1(t)], \\ \frac{du_2(t)}{dt} &= f(u_2(t), u_2(t - \tau)) + \varepsilon[u_1(t) - u_2(t)],\end{aligned}$$

where

$$f(u(t), u(t - \tau)) = -u(t) + a \sin u(t - \tau)$$

corresponds to the Ikeda equation, describing an optical resonator system [60]. The parameter values were chosen to be $a = 3.0$ and $\tau = 5.0$. We integrated the coupled Ikeda equations together with the linearized equations, using the fourth order Runge-Kutta routine.

The results are presented in Figs. 3.8(a,b). For the chosen parameters, the uncoupled Ikeda system has one positive and one zero (due to invariance to time shifts) Lyapunov exponent, all other exponents are negative. In the coupled system the two former zero exponents (the third and the fourth ones) are not affected by the coupling sensitivity: one exponent remains exactly zero, changes of the other one are hardly seen for small couplings. We attribute this to the fact that the zero Lyapunov exponent in an autonomous system does not fluctuate. The other Lyapunov exponents (the positive and the first negative ones), however, show the logarithmic singularity.

Further numerical simulations revealed that the Lyapunov exponents of coupled Lorenz systems (see Sec. 2.3.2) of ordinary differential equations also show the logarithmic singularity. Together, our simulations corroborate the conjecture that the coupling sensitivity of chaos is a general phenomenon of coupled fluctuating systems.

3.5 Random Walk Picture

The origin of the logarithmic singularity can be understood by a qualitative consideration [113, 3]. For simplicity we assume $\Lambda_1 = \Lambda_2 = 0$ and $\sigma_1^2 = \sigma_2^2 = \sigma^2 \gg \varepsilon$, leading to the (Stratonovich) model

$$\begin{aligned}\frac{dw_1(t)}{dt} &= \sigma \tilde{\chi}_1(t) w_1(t) + \varepsilon [w_2(t) - w_1(t)], \\ \frac{dw_2(t)}{dt} &= \sigma \tilde{\chi}_2(t) w_2(t) + \varepsilon [w_1(t) - w_2(t)]\end{aligned}$$

with

$$\langle \tilde{\chi}_i(t) \rangle = 0, \quad \langle \tilde{\chi}_i(t) \tilde{\chi}_j(t') \rangle = 2\delta_{ij} \delta(t-t'), \quad i, j \in \{1, 2\}.$$

When rescaling $t \rightarrow t/\sigma^2$, we have to rescale $\tilde{\chi} \rightarrow \sigma \tilde{\chi}$ because of the δ -correlation. Dividing by σ^2 we obtain

$$\begin{aligned}\frac{dw_1(t)}{dt} &= \tilde{\chi}_1(t) w_1(t) + \frac{\varepsilon}{\sigma^2} [w_2(t) - w_1(t)], \\ \frac{dw_2(t)}{dt} &= \tilde{\chi}_2(t) w_2(t) + \frac{\varepsilon}{\sigma^2} [w_1(t) - w_2(t)].\end{aligned}\tag{3.27}$$

Since the amplitudes of the noise processes $\tilde{\chi}_{1,2}$ are of order one and $\varepsilon/\sigma^2 \ll 1$, the coupling in the first equation of (3.27) only influences the dynamics of w_1 if $w_2 \sim \sigma^2 w_1/\varepsilon \gg w_1$. In this case the influence of the coupling on the dynamics of w_2 in the second equation of (3.4) is small. The opposite situation occurs if $w_1 \sim \sigma^2 w_2/\varepsilon \gg w_2$. Thus the coupling leads to effective equalization of w_1 and w_2 only if the system reaches the lines $w_2 = \sigma^2 w_1/\varepsilon$ and $w_1 = \sigma^2 w_2/\varepsilon$ in phase space, as illustrated in Fig. 3.9(a).

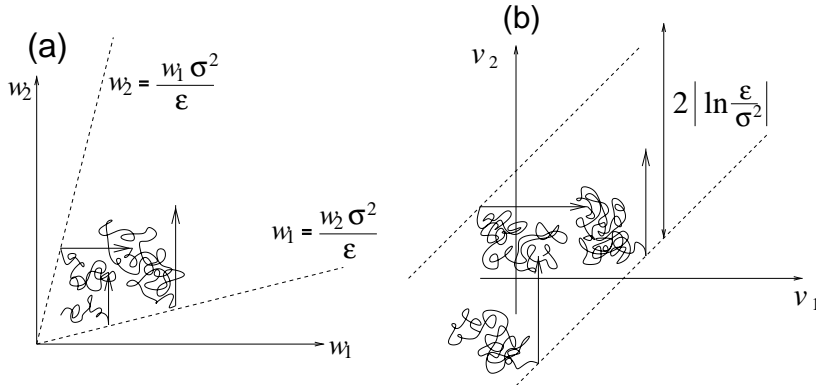


Figure 3.9: A sketch of the perturbation dynamics in coupled systems. Curly lines show the random walk not influenced by coupling; straight arrows demonstrate the effect of coupling.

For logarithmic variables $v_{1,2} = \ln w_{1,2}$ the model (3.27) is transformed to

$$\begin{aligned}\frac{dv_1(t)}{dt} &= \tilde{\chi}_1(t) + \frac{\varepsilon}{\sigma^2} \left(e^{v_2(t)-v_1(t)} - 1 \right), \\ \frac{dv_2(t)}{dt} &= \tilde{\chi}_2(t) + \frac{\varepsilon}{\sigma^2} \left(e^{v_1(t)-v_2(t)} - 1 \right).\end{aligned}\tag{3.28}$$

Now the coupling in the first equation only influences the dynamics of v_1 if $v_2 \sim v_1 + |\ln(\varepsilon/\sigma^2)|$, and vice versa. Thus the dynamics of the system is restricted to a strip of vertical and horizontal width $2|\ln(\varepsilon/\sigma^2)|$, see Fig. 3.9(b). Due to the additive noise processes in model (3.28), the dynamics between the reflections correspond to a two-dimensional random walk. The average time to reach the boundary from the middle diagonal is $[\ln(\varepsilon/\sigma^2)]^2/\sigma^2$ [38]. The reflections introduce a drift in the direction of growing $v_{1,2}$, the contribution of each reflection to the way travelled due to this drift is $|\ln(\varepsilon/\sigma^2)|$. Thus the mean drift velocity (corresponding to the largest Lyapunov exponent λ_1) is $\sigma^2/|\ln(\varepsilon/\sigma^2)|$, which is in perfect agreement with our theoretical result, Eq. (3.12).

3.6 Summary and Perspectives

In this chapter we used the Langevin approach to obtain statistical properties of the Lyapunov exponents of weakly coupled dynamical systems. For the simplest system of two coupled stochastic equations it is possible to obtain an analytical expression for the largest Lyapunov exponent, for different values of parameters (coupling, Lyapunov exponents of uncoupled systems, fluctuations of finite-time Lyapunov exponents). The logarithmic singularity, first discovered by DAIDO, is shown to exist even if rather different systems are coupled, provided their Lyapunov exponents coincide. We also gave a qualitative explanation of the effect, based on the interpretation of the perturbations' dynamics as coupled random walks.

Numerical simulations of a system with weaker stochastic properties (strange non-chaotic attractor) showed the limits of the Langevin approach. We found a power-law singularity, possibly due to existence of long correlations in the dynamics of perturbations.

An extension of the stochastic model to three coupled identical systems as well as numerical simulations led to the asymptotic result [113]

$$\lambda_1 - \Lambda \sim \frac{4}{3} \frac{\sigma^2}{|\ln(\varepsilon/\sigma^2)|} \quad \text{for} \quad \frac{\varepsilon}{\sigma^2} \rightarrow 0.$$

Together with the results for the Largest Lyapunov exponent of weakly coupled CMLs [75, 22], it can be summarized that the coupling sensitivity of chaos is a general phenomenon of coupled fluctuating systems.

An interesting consequence of the coupling sensitivity of chaos is found in the context of Anderson localization in disordered systems. The localization length is given by the inverse

of the smallest positive Lyapunov exponent (see, e. g., Ref. [25]). The site-by-site coupling of two chains of Anderson maps leads to a $1/|\ln \varepsilon|$ dependence of the Lyapunov exponents that is in first order also found for the localization length. Coupling two disordered solids thus leads to a substantial increase of the localization length [115].

Lyapunov exponents are very hard to estimate from experimental time series. It is therefore difficult to directly observe the rather small effect of coupling sensitivity in experiments. The coupling dependence of the localization length, however, may be observable via its influence on transport coefficients like the electrical conductivity.

4 Avoided Crossing of Lyapunov Exponents

This chapter deals with an effect that follows from the coupling sensitivity of chaos studied in the previous chapter. Consider several subsystems (e. g., maps or systems of ordinary differential equations) depending on one or more parameters. If the parameters of the subsystems are randomly chosen, the Lyapunov exponents of the uncoupled subsystems will in general be different. It may be, however, that some subsystems have nearly equal Lyapunov exponents. If we now introduce weak coupling between the subsystems, the coupling sensitivity sets in such that the spacing between Lyapunov exponents that are close to each other without coupling increases dramatically.

It will be shown by means of numerical simulations that this effect leads to phenomena which are qualitatively similar to, but quantitatively different from the well-known effect of energy level repulsion in quantum systems. Basing on the results of the previous chapter, an approximate formula for the distribution of spacings between Lyapunov exponents will be derived. Some of the results of this chapter have been published in Ref. [4].

4.1 Lyapunov Exponents and Energy Levels

4.1.1 Numerical Evidence for Avoided Crossing

Our starting model is a system of N symplectically coupled standard maps which are, in general, different:

$$\begin{aligned} I_i(t+1) &= I_i(t) + K_i \sin \theta_i(t) + \frac{\varepsilon}{\mathcal{N}\{j\}} \sum_{\{j\}} \sin(\theta_i(t) - \theta_j(t)), \\ \theta_i(t+1) &= \theta_i(t) + I_i(t+1), \quad i \in \{1, \dots, N\}. \end{aligned} \tag{4.1}$$

Here $I_i(t)$ and $\theta_i(t)$ are the 2π -periodic state variables at site i and time t , and ε serves as the coupling parameter. The coupling can be global if the sum on the r. h. s. is over all elements in the ensemble; in this case $\mathcal{N}\{j\} = N - 1$. In the case of local coupling in a one-dimensional periodic lattice, the sum is over nearest neighbours and $\mathcal{N}\{j\} = 2$. The parameters K_i of all systems are, in general, different from each other, their random distribution defines disorder in the model. Below we take all parameters K_i in the region of strong chaos, $K_i > 7$. The standard map used in (4.1) is the basic model of Hamiltonian chaos [73], it describes, in particular, a periodically kicked rotator.

The Lyapunov exponents are calculated with standard methods (see App. A.1) as the logarithms of the eigenvalues of the limiting matrix

$$\lim_{t \rightarrow \infty} [\mathbf{P}(t)^T \mathbf{P}(t)]^{1/(2t)}, \quad \mathbf{P}(t) = \prod_{\tau=0}^{t-1} \mathbf{J}(\tau), \quad (4.2)$$

where $\mathbf{J}(t)$ is the Jacobian of the mapping (4.1) (see Sec. 2.1.2). Due to its symplecticity, a single standard map has (for chaotic trajectories) one positive and one negative Lyapunov exponent of the same absolute value which depends on the parameter K .

To demonstrate the avoided crossing of Lyapunov exponents, the maps in Eq. (4.1) are now considered as depending on a common parameter $\eta \in [0, 1]$ according to

$$K_i = K_i(\eta) = K_i(0) + \eta[K_i(1) - K_i(0)].$$

The parameters $K_i(0)$ and $K_i(1)$ are random numbers uniformly distributed in the interval $7 \leq K_i \leq 10$. We present in Fig. 4.1 the results of numerical calculations of the Lyapunov exponents of a particular realization of a system (4.1) of six nearest-neighbour-coupled standard maps. In Fig. 4.1(a), the six positive Lyapunov exponents λ_i ($i = 1, \dots, 6$) are shown as functions of the common parameter η for the case $\varepsilon = 0$, i. e. without coupling. As can be expected for independent Lyapunov exponents, many crossings are observed. This is no longer the case when a weak nearest-neighbour coupling ($\varepsilon = 10^{-8}$) is introduced, as can be seen from Fig. 4.1(b): the crossings are avoided, a behaviour which is well-known for energy levels of quantum-mechanical systems. Note, however, a quantitative difference:

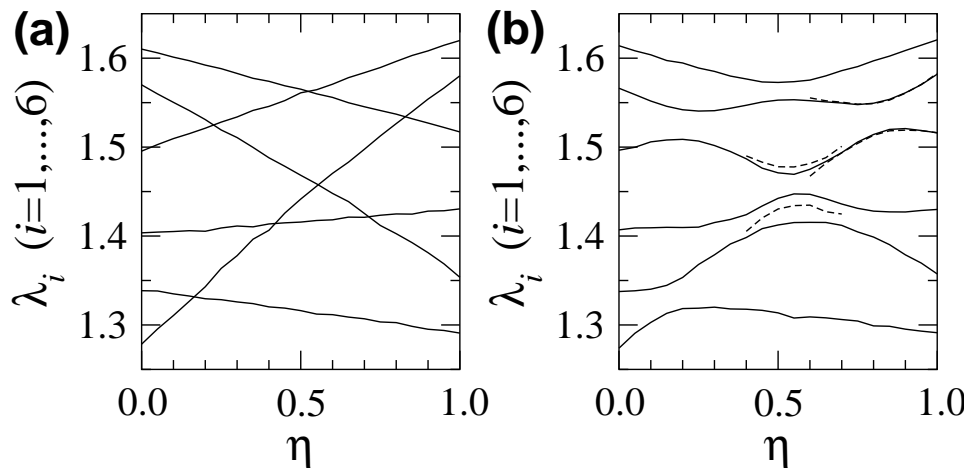


Figure 4.1: Lyapunov exponents λ_i ($i = 1, \dots, 6$) versus parameter η (see text) for six standard maps with parameters $K_i(\eta)$. (a) Without coupling crossings of Lyapunov exponents are possible. (b) Crossings are avoided when nearest-neighbour coupling with coupling parameter $\varepsilon = 10^{-8}$ is applied. The dashed lines correspond to avoided crossings of only two coupled maps, see text.

since the Lyapunov exponents are calculated from the eigenvalues of a product of random matrices, the avoided crossing is already observed for extremely small (in absolute value) off-diagonal elements of the single matrices.

A theoretical explanation for this strong repulsion of Lyapunov exponents will be discussed below, here we want to describe further numerical experiments showing that the picture above is quite universal. A qualitatively similar pattern of avoided crossings has also been obtained for a lattice of standard maps with global coupling. We have observed it also for dissipative systems, e.g., for N globally coupled skew Bernoulli maps f_i with parameters $a_i \in (0, 1)$ defining the location of the discontinuity (see Eq. (2.4)),

$$u_i(t+1) = f_i(u_i(t)) + \frac{\varepsilon}{N-1} \sum_{j=1}^N [f_j(u_j(t)) - f_i(u_i(t))], \quad i \in \{1, \dots, N\}. \quad (4.3)$$

Another dissipative system we studied is the Ikeda map for a complex amplitude E (not to be confused with the Ikeda delay differential equation studied in Sec. 3.4.2),

$$E(t+1) = a + bE(t) \exp\left(ic - \frac{id}{1 + |E(t)|^2} \right), \quad i = \sqrt{-1}.$$

which describes a chaotic regime of light propagation in a ring cavity with a nonlinear element [59]. Coupling such systems can be achieved by overlapping the light fields (see, e.g., the experiments in Ref. [102]). Below we describe the Lyapunov exponents in coupled Ikeda maps, where the disorder is due to different values for the parameters d_i of the different maps, whereas the other parameters are kept constant ($a = 1$, $b = 0.9$, $c = 0.4$). The Ikeda map with these parameters has one positive and one negative Lyapunov exponent; we follow only the statistics of the positive Lyapunov exponents.

4.1.2 Energy Levels in Quantum Systems

At this point a very brief review of the energy level statistics in quantum systems (e.g., large atomic nuclei) is necessary to understand our line of approach. For details the reader is referred to Refs. [53, 54, 77, 99].

The historical starting point is the observation of an avoidance of small spacings between adjacent energy levels in complex quantum systems. It was the idea of WIGNER to approximate the matrix elements of the Hamiltonian by random numbers, such that the energy levels correspond to the eigenvalues of large random matrices

$$\mathbf{H} = \begin{pmatrix} h_{11} & \cdots & h_{1N} \\ \vdots & \ddots & \vdots \\ h_{N1} & \cdots & h_{NN} \end{pmatrix},$$

where the h_{ij} are Gaussian distributed, and the symmetry properties of \mathbf{H} depend on certain symmetries of the quantum system. The main interest focuses on the distribution of the

level (or eigenvalue) spacings δE , or their normalized versions $s = \delta E / \langle \delta E \rangle$. For randomly chosen energy levels (or diagonal random matrices) the normalized spacings are distributed according to the Poisson distribution, which has the probability density

$$\rho(s) = e^{-s}. \quad (4.4)$$

For nonintegrable quantum systems (or nondiagonal random matrices), however, the spacings are distributed according to the so-called Wigner distribution, whose exact form depends on the symmetries of the system. For time reversal invariant systems with integer total spin (or real symmetric random matrices) the Gaussian orthogonal ensemble applies. In this case the probability density has the form

$$\rho(s) = \frac{\pi}{2} s e^{-\pi s^2/4}. \quad (4.5)$$

While small spacings are possible in the Poisson distribution, they are avoided in the Wigner distribution. In the last two decades it has been discovered that the avoidance of small energy level spacings is a manifestation of quantum chaos (see, e. g., Refs. [54, 99]).

Estimating the probability density from a given set of samples is no easy task. Especially when the number of samples is small, it is much easier to estimate the cumulative distribution function (CDF)

$$\Phi_s(z) = \text{Prob}(s \leq z) = \int_0^z \rho(s) ds.$$

The CDF of the Poisson distribution can easily be calculated from the probability density (4.4),

$$\Phi_s(z) = 1 - e^{-z},$$

and for the Wigner distribution (Gaussian orthogonal ensemble) we calculate from the density (4.5)

$$\Phi_s(z) = 1 - e^{-\pi z^2/4}.$$

For very small z we can expand the exponentials and obtain in first order $\Phi_s(z) \sim z$ for the Poisson distribution and $\Phi_s(z) \sim z^2$ for the Wigner distribution. The simplest way to estimate $\Phi_s(z)$ from a set of samples $\{z_n\}$, $n \in \{1, \dots, N\}$, is to sort the samples by increasing magnitude ($z_1 \leq z_2 \leq \dots \leq z_N$) and to use $\Phi_s(z_n) = n/(N+1)$ as the desired estimate, possibly in connection with interpolation (see, e. g., Ref. [41]). This method is used throughout this chapter.

4.1.3 Distribution of Lyapunov Exponent Spacings

Now we demonstrate that the consequence of the Lyapunov exponent repulsion is a particular statistics of Lyapunov exponent spacings in disordered systems of the type (4.1) or (4.3). We performed the numerical experiment with different kinds of coupled maps as follows. First, we fixed the system size N and the expectation value ε_0 of the coupling constant. Then, for each randomly chosen set of parameters (we used uniformly distributed parameters $K_i \in [7, 10]$ for the standard maps, $a_i \in [0.2, 0.3]$ for the skew Bernoulli maps, and $d_i \in [7.5, 8.5]$ for the Ikeda maps) and coupling constant ε (exponentially distributed according to the probability density $\rho(\varepsilon) = \exp(-\varepsilon/\varepsilon_0)/\varepsilon_0$ with expectation value $\varepsilon_0 = 10^{-5}$ for the standard and skew Bernoulli maps, $\varepsilon_0 = 10^{-4}$ for the Ikeda maps), we determined N Lyapunov exponents, which corresponds to $N - 1$ spacings $\Delta_i = \lambda_i - \lambda_{i+1}$. These spacings are considered as $N - 1$ samples of a random distribution (for the standard and Ikeda maps only the positive Lyapunov exponents are considered). Performing calculations for many sets of parameters K_i (or a_i , or d_i) and ε , we obtain a representative statistics for the Lyapunov exponent spacings, see Fig. 4.2 where the distribution function $\Phi_{\Delta}(z) = \text{Prob}(\Delta \leq z)$ is shown.

Examining Fig. 4.2 we see that the distribution of spacings of coupled maps has a very strong depletion for small z , not only compared to the Poisson distribution $\Phi \sim z$ (which occurs in the absence of coupling), but also compared to the Wigner distribution for the Gaussian orthogonal ensemble of random matrices, for which $\Phi \sim z^2$ (see Sec. 4.1.2).

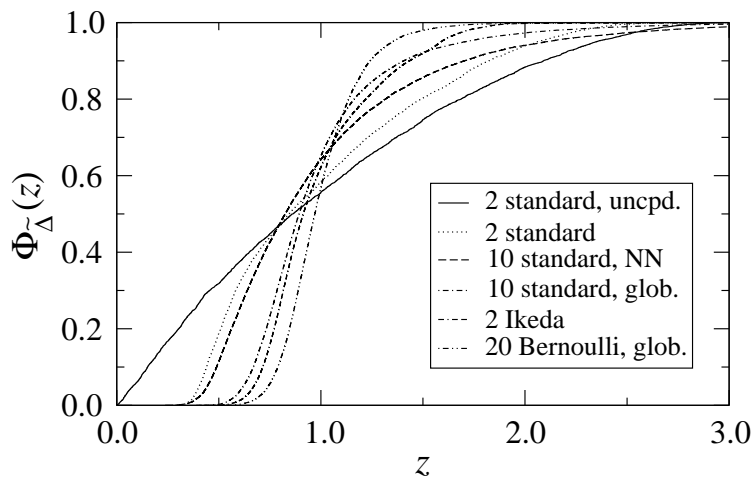


Figure 4.2: Numerically estimated cumulative distribution functions $\Phi_{\tilde{\Delta}}(z)$ for the normalized (in such a way that the mean spacing is 1) Lyapunov exponent spacings $\tilde{\Delta}$ of different systems (Standard and Bernoulli maps with average coupling parameter $\varepsilon_0 = 10^{-5}$, Ikeda maps with $\varepsilon_0 = 10^{-4}$) with different types of coupling (uncpd.: uncoupled, NN: nearest neighbour coupling, glob.: global coupling).

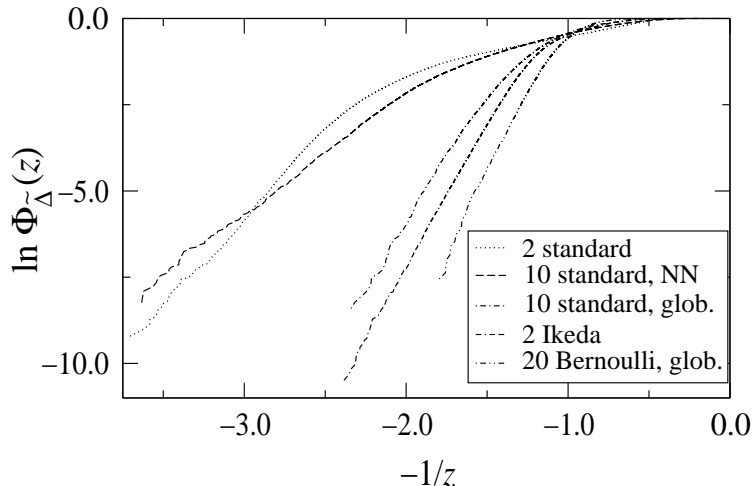


Figure 4.3: Cumulative distribution functions of Fig. 4.2 in scaled coordinates, cf. Eq. (4.8).

To resolve this strong depletion we present the same data in Fig. 4.3 in scaled coordinates. The scaling is motivated by our theory (see Sec. 4.2 below) and it shows that the distribution function is exponentially small for small spacings: $\Phi_{\Delta}(z) \sim \exp(-1/z)$. Note also that although the distribution functions are qualitatively similar for different systems, they do not collapse onto a single curve. This is an indication for the nonuniversality of the Lyapunov exponent spacing distribution.

4.1.4 Relation to Random Matrix Theory

As is clear from Eq. (4.2), the problem we consider can be formulated as a problem of random matrix theory (with the usual modelling of chaotic fluctuations with random ones, see Sec. 2.4). Namely, we are interested in the eigenvalues of infinite products of random matrices, having both quenched (time-independent) disorder and dynamic (time-dependent) noise. The quenched randomness comes from the distribution of the parameters in the disordered ensemble, e. g., from the distribution of parameters K_i of the standard maps. The dynamic noise comes from fluctuations due to the chaotic evolution (e. g., in the standard map the local Jacobian $\mathbf{J}(t)$ depends on the chaotic variables I and θ).

To be more specific, we consider a system of N globally coupled one-dimensional maps as given by Eq. (4.3). If we replace the local derivatives $f'_i(u_i(t))$ by stochastic variables $\exp(\Lambda_i + \xi_i(t))$, where Λ_i is the Lyapunov exponent of the single map f_i and $\xi_i(t)$ accounts for the fluctuations of the local expansion rates, the Lyapunov exponents of the system of

coupled maps are related to the eigenvalues of the matrix product

$$\prod_{\tau=0}^{t-1} \begin{pmatrix} (1-\varepsilon)e^{\Lambda_1+\xi_1(t)} & \frac{\varepsilon}{N-1}e^{\Lambda_2+\xi_2(t)} & \dots & \frac{\varepsilon}{N-1}e^{\Lambda_N+\xi_N(t)} \\ \frac{\varepsilon}{N-1}e^{\Lambda_1+\xi_1(t)} & (1-\varepsilon)e^{\Lambda_2+\xi_2(t)} & \dots & \frac{\varepsilon}{N-1}e^{\Lambda_N+\xi_N(t)} \\ \vdots & \vdots & \ddots & \vdots \\ \frac{\varepsilon}{N-1}e^{\Lambda_1+\xi_1(t)} & \frac{\varepsilon}{N-1}e^{\Lambda_2+\xi_2(t)} & \dots & (1-\varepsilon)e^{\Lambda_N+\xi_N(t)} \end{pmatrix}.$$

Here, the parameters ε , Λ_i , and the properties of the stochastic variables ξ_i represent the quenched disorder, whereas the dynamic noise is given by the time-dependent values of the stochastic variables $\xi_i(t)$. We again stress that the eigenvalues of the matrix product are already influenced by very small absolute values of the off-diagonal elements (i. e., very small values of ε), which is not the case for the eigenvalues of a single matrix.

The two limiting cases, when our problem can be reduced to standard ones, are clear. In the case when the quenched disorder is absent (or if we consider just one realization of parameters of the interacting chaotic systems), we have a standard problem of the calculation of Lyapunov exponents for a product of random matrices [25]. Another well-known situation appears if the dynamic noise is absent ($\xi(t) = 0$): in this case all the matrices of the product are equal and the problem reduces to the calculation of the eigenvalues of this one matrix (see Sec. 2.1.2). This problem has been widely discussed, recently mainly in the context of quantum chaos (see, e. g., Ref. [53]). For chaotic systems the fluctuations can vanish only in exceptional cases (e. g., for the skew Bernoulli map this happens for the symmetric situation $a_i = 1/2$ only; for the standard map in the chaotic state and for the Ikeda map the fluctuations are always finite). Another limiting case is that of uncoupled systems ($\varepsilon = 0$): here we have a product of diagonal matrices with both quenched and dynamic randomness, and the Lyapunov exponents simply follow the statistics of the quenched disorder.

4.2 Theoretical Approach

4.2.1 Hyperbolic Approximation of Coupling Sensitivity

Similar to the case of quantum-mechanical systems (see, e. g., Ref. [99]), the essential qualitative and quantitative characteristics of the Lyapunov exponent repulsion can be acquired from the consideration of two coupled dissipative chaotic systems. We demonstrate this with the following numerical experiment: we calculate the Lyapunov exponents for two coupled maps of Fig. 4.1, switching off the interaction with other systems. The results for two crossings are shown as dashed lines in Fig. 4.1. One can see that the behaviour of the Lyapunov exponents remains at least qualitatively the same.

Daido [26] has first shown that two coupled identical chaotic systems experience a singular repulsion of the Lyapunov exponents: $\Delta \sim |\ln \varepsilon|^{-1}$, where Δ is the difference between the Lyapunov exponents and ε is the coupling parameter (coupling sensitivity of chaos). In Ch. 3 a general expression for the coupling dependence of the first and second Lyapunov

exponents of two coupled systems has been derived by means of a stochastic model. From Eqs. (3.10) and (3.16) we obtain the following expression for the difference Δ between the Lyapunov exponents of two coupled systems,

$$\Delta(|l|, \varepsilon, \sigma) = \varepsilon \frac{K_{1-|l|}(\varepsilon/\sigma^2) + K_{1+|l|}(\varepsilon/\sigma^2)}{K_{|l|}(\varepsilon/\sigma^2)}, \quad (4.6)$$

where σ^2 is the variance of the finite-time Lyapunov exponent, $l = \delta\Lambda/2\sigma^2$ is proportional to the difference $\delta\Lambda = \Lambda_1 - \Lambda_2$ of the “bare” (i. e., without coupling) Lyapunov exponents of the interacting systems, and K are the modified Bessel functions [1]. Although Eq. (4.6) was obtained in the continuous-time Langevin approximation where the fluctuations of the Lyapunov exponents are modelled by Gaussian white noise processes (thus discarding all temporal correlations), it very well describes the coupled standard maps (Fig. 4.4) as well as other chaotic systems [113]. Because expression (4.6) is rather inconvenient for further analysis, we use a hyperbolic approximation for it,

$$\Delta^2 \approx (\delta\Lambda)^2 + \left(\frac{2\sigma^2}{\ln(\varepsilon/\sigma^2)} \right)^2. \quad (4.7)$$

The first term on the r. h. s. corresponds to the limit $\delta\Lambda \rightarrow \infty$, while the second term is based on an expansion of Eq. (4.6) for $\delta\Lambda = 0$ and small ε/σ^2 (see Eq. (3.12)). From Fig. 4.4 one can see that this approximation is rather good.

Using (4.7) we can show that in a disordered system the probability to observe tiny values of Δ is exponentially small. It is clear that only small values of $\delta\Lambda$ and ε can give small spacings Δ . If we assume that $\delta\Lambda$ and ε are independent random numbers with constant densities near zero, then the distribution function $\Phi_\Delta(z) = \text{Prob}(\Delta \leq z)$ can be approximated by the integral over the area $A(z) = \{(\delta\Lambda, \varepsilon) : (\delta\Lambda)^2 + [2\sigma^2/\ln(\varepsilon/\sigma^2)]^2 \leq z^2\}$, leading to

$$\begin{aligned} \Phi_\Delta(z) &\sim \iint_{A(z)} d(\delta\Lambda) d\varepsilon \\ &= 2\sigma^2 \int_{-z}^z \exp\left(-\frac{2\sigma^2}{\sqrt{z^2 - (\delta\Lambda)^2}}\right) d(\delta\Lambda) \\ &= 2\sigma^2 z \int_{-\pi/2}^{\pi/2} \exp\left(-\frac{2\sigma^2}{z \cos \alpha}\right) \cos \alpha d\alpha, \end{aligned}$$

where we have substituted $\delta\Lambda = z \sin \alpha$ in the last step. For $2\sigma^2/z \gg 1$ only the region around $\alpha = 0$ contributes, such that we can use the approximations $1/\cos \alpha \approx 1 + \alpha^2/2$ in the exponent and $\cos \alpha \approx 1$ in the integrand. Integrating over $(-\infty, \infty)$ (the contribution of

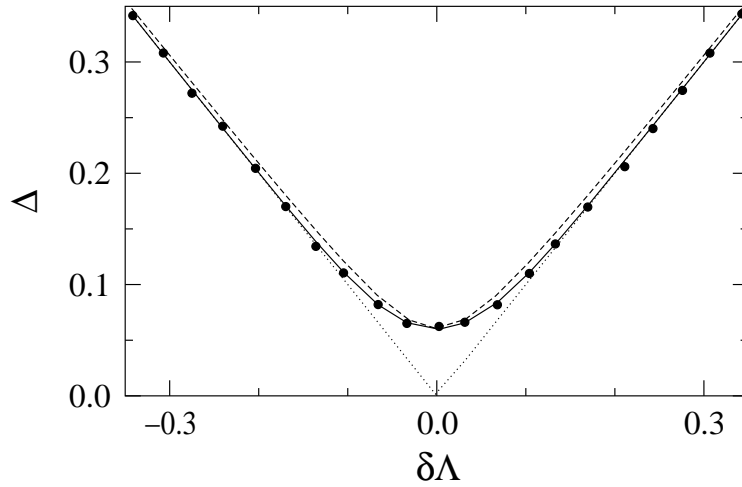


Figure 4.4: Dependence of the Lyapunov exponent difference Δ on the difference $\delta\Lambda$ between the “bare” Lyapunov exponents for two coupled standard maps with coupling parameter $\varepsilon = 10^{-5}$: comparison of numerical results (circles) with the analytical expression (Eq. (4.6) with numerically calculated values for σ^2 , solid line) and the hyperbolic approximation (Eq. (4.7), dashed line). The dotted line depicts the Lyapunov exponent difference without coupling, $\Delta = |\delta\Lambda|$.

the tails is negligible) gives the exponential depletion at small spacings,

$$\begin{aligned}\Phi_{\Delta}(z) &\sim 2\sigma^2 z \exp\left(-\frac{2\sigma^2}{z}\right) \int_{-\infty}^{\infty} \exp\left(-\frac{2\sigma^2 \alpha^2}{z}\right) d\alpha \\ &\sim 2\sqrt{\pi} z^{3/2} \exp\left(-\frac{2\sigma^2}{z}\right).\end{aligned}\quad (4.8)$$

The numerically calculated cumulative distribution functions are in conformity with this result, as can be seen from Fig. 4.3.

The theoretical analysis above is, strictly speaking, restricted to the case of two interacting chaotic systems. Nevertheless, we expect that it works at least qualitatively for large ensembles as well, because we have seen that the Lyapunov exponent repulsion is a “local” event, where only the two chaotic subsystems whose Lyapunov exponents are close to each other are involved (recall the dashed lines in Fig. 4.1).

4.2.2 Distribution Functions for Special Cases

For just two coupled systems and given distributions of the parameters the exact form of the CDF can be calculated for certain limiting cases. First we consider two uncoupled systems ($\varepsilon = 0$) with Lyapunov exponents $\Lambda_{1,2}$ independently chosen from the uniform distribution on a real interval of length L . The Lyapunov exponent spacing is simply

$\Delta = |\delta\Lambda| = |\Lambda_1 - \Lambda_2|$, and we can calculate the CDF by direct integration,

$$\Phi_{\Delta}^0(z) = \frac{2z}{L} \left[1 - \frac{z}{2L} \right]. \quad (4.9)$$

For small z we have in first order $\Phi_{\Delta}^0(z) \sim z$, a linear increase as for the Poisson distribution.

Now we couple the two systems with a fixed coupling parameter ε and choose the Lyapunov exponents $\Lambda_{1,2}$ from the same uniform distribution as before. We assume that the variance σ^2 does not vary much, such that we can consider it as a constant parameter. We can calculate the new CDF from Eq. (4.9) by replacing z by the inverse function $|\delta\Lambda|(\Delta)$ of the hyperbolic approximation (4.7),

$$\Phi_{\Delta}^1(z) = \frac{2\sqrt{z^2 - [2\sigma^2/|\ln(\varepsilon/\sigma^2)|]^2}}{L} - \frac{z^2 - [2\sigma^2/|\ln(\varepsilon/\sigma^2)|]^2}{L^2}. \quad (4.10)$$

For large z we have $\Phi_{\Delta}^1(z) \approx \Phi_{\Delta}^0(z)$.

In the other limit we now consider $\delta\Lambda = 0$ and ε distributed according to the exponential distribution with expectation value ε_0 . If we again assume that the variance σ^2 can be considered as constant, we can calculate the CDF by substituting the inverse function $\varepsilon(\Delta)$ of the hyperbolic approximation (4.7) (with $\delta\Lambda = 0$) in the CDF $\Phi_{\varepsilon}(z) = 1 - \exp(-z/\varepsilon_0)$ of

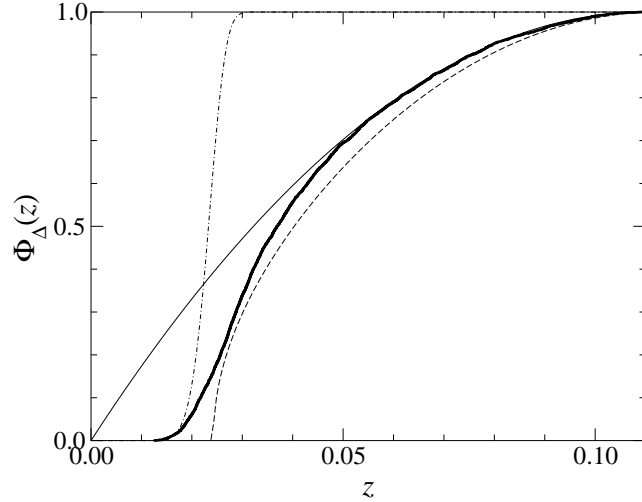


Figure 4.5: Cumulative distribution functions (see text) $\Phi_{\Delta}^0(z)$ (thin solid line), $\Phi_{\Delta}^1(z)$ (dashed line), and $\Phi_{\Delta}^2(z)$ (dot-dashed line) for parameter values $L = 0.11$, $\sigma^2 = 0.113$, and $\varepsilon_0 = 10^{-5}$. Also shown is the numerically estimated CDF for two coupled skew Bernoulli maps with parameters a_i randomly chosen from a uniform distribution in $[0.2, 0.3]$ and ε randomly chosen from an exponential distribution with expectation value $\varepsilon_0 = 10^{-5}$ (5000 spacings). Note that the spacings Δ are not normalized (in contrast to Fig. 4.2).

the exponential distribution,

$$\Phi_{\Delta}^2(z) = 1 - \exp\left(-\frac{\sigma^2}{\varepsilon_0} \exp\left(-\frac{2\sigma^2}{z}\right)\right). \quad (4.11)$$

For $2\sigma^2/z \gg 1$ the second exponential is small. Expanding the first exponential, we obtain in first order the exponential depletion (see Eq. (4.8))

$$\Phi_{\Delta}^2(z) \approx \frac{\sigma^2}{\varepsilon_0} \exp\left(-\frac{2\sigma^2}{z}\right).$$

In Fig. 4.5 the CDFs $\Phi_{\Delta}^{0,1,2}(z)$ are shown for parameter values that apply to skew Bernoulli maps with $a_i \in [0.2, 0.3]$ (see Sec. 2.1.3). The comparison with the numerically estimated CDF for two coupled skew Bernoulli maps shows that $\Phi_{\Delta}^1(z)$ and $\Phi_{\Delta}^2(z)$ give reasonable approximations for large and small values of z , respectively. The numerically estimated CDF for uncoupled ($\varepsilon = 0$) skew Bernoulli maps perfectly follows the approximation $\Phi_{\Delta}^0(z)$.

4.3 Summary and Perspectives

Concluding, we have characterized numerically and theoretically the statistics of the Lyapunov exponents in disordered chaotic systems. Its main feature is the exponential depletion of the distribution function at small spacings between the exponents. This follows directly from the effect of coupling sensitivity of chaos, according to which the repulsion between the Lyapunov exponents is extremely strong. This repulsion manifests itself also in the avoided crossing of Lyapunov exponents, considered as dependent on a parameter. We have demonstrated that the effects of level repulsion and avoided crossing are observed for chaotic systems of different nature: Hamiltonian and dissipative ones. Also the coupling can be of different form; in particular, qualitatively similar patterns of avoided Lyapunov exponent crossings and of the Lyapunov exponent spacing distribution function are observed for global and nearest-neighbour couplings in a lattice.

Our framework of consideration was motivated by the analogy to the problem of level statistics in quantum chaos and complex quantum systems [54, 99, 53]. Qualitatively, the behaviour of Lyapunov exponents is quite similar to that of energy levels in quantum chaos. The main difference is that for disordered chaotic dynamical systems we have two sources of randomness: one quenched due to the disorder and one dynamic due to the chaotic fluctuations. Thus, in contrast to the problem of the distribution of the eigenvalues of a single random matrix, we face the problem of the distribution of the eigenvalues of a product of random matrices. There are two limiting cases when these two problems are equivalent. One is the case without coupling, where the Lyapunov exponents remain independent random

numbers and obey the Poisson distribution. The other one is the case of vanishing fluctuations of the local Lyapunov exponents (no dynamic randomness); here we have one random matrix whose eigenvalues give the Lyapunov exponents.

The problem we studied here should not be confused with the dependence of the Lyapunov exponents of integrable Hamiltonian systems on a small perturbation that destroys integrability. For those systems, which can also be related to products of random matrices, a power-law behaviour of the Lyapunov exponents has been found [13, 85]. In our case, however, the subsystems are already nonintegrable without coupling ($\varepsilon = 0$).

Concerning an experimental verification of our results, the same problems as for the coupling sensitivity of chaos are encountered, i. e., it is very difficult to measure the Lyapunov exponents of an experimental system directly. Therefore one has to look for indirect effects on measurable quantities. A possible candidate is the electrical conductivity in quasi-one-dimensional disordered solids, which depends on the Lyapunov exponents in a nontrivial way via the Landauer formula [70]. Further research, however, is needed to understand possible consequences of the avoided crossing of Lyapunov exponents on the conductivity in such systems.

5 Synchronization of Extended Systems

Spatially extended dynamical systems have been introduced in Ch. 2. They typically exhibit local nonlinear dynamics as well as spatial coupling. The latter often consists of local diffusive coupling, but long-range or global couplings are also possible. In this chapter, however, we will limit ourselves to local coupling.

Here we consider two spatially extended systems that are additionally coupled to each other in a bidirectional way as schematically shown in Fig. 5.1. Two different coupling parameters apply. The local coupling within a single extended system is described by the parameter ε . For continuous-space systems (partial differential equations) this is typically the diffusion constant. The coupling between the two extended systems is described by the parameter γ . Synchronization between the two extended systems occurs in dependence on γ for a fixed value of ε .

There are several works showing the possibility of synchronization of specific spatially extended systems with different coupling schemes [5, 69, 86, 62, 16, 63, 37]. This chapter, however, is concerned with the general nature of the transition to synchronization, i. e., the dependence of the synchronization error on the coupling strength.

After an overview of the general framework and our stochastic model, first numerical results for the synchronization of coupled map lattices are presented that indicate the existence of two different types of the synchronization transition. These two types of transition are then studied in detail by means of numerical simulations. Finally, the introduction of a discrete growth model allows an approximate numerical determination of the critical exponents.

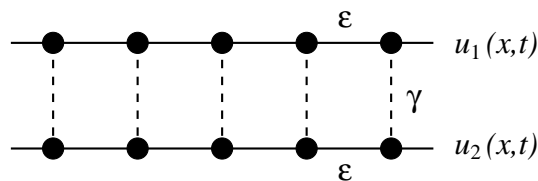


Figure 5.1: A sketch of two coupled spatially extended systems, e. g. coupled map lattices. Besides the local dynamics at each lattice site, there is interaction between neighbouring sites within one system (coupling parameter ε) as well as interaction between corresponding sites of the two systems (coupling parameter γ).

5.1 General Framework

5.1.1 Coupled Spatially Extended Systems

A spatially extended system is typically given either as a coupled map lattice (CML) or as a partial differential equation (PDE), see Sec. 2.2. Although our numerical simulations are limited to CMLs, the general synchronization mechanism is the same for PDEs.

A typical model for bidirectionally coupled PDEs is given by

$$\begin{aligned}\frac{\partial \mathbf{u}_1(x,t)}{\partial t} &= \mathbf{f}(\mathbf{u}_1(x,t)) + \varepsilon \Delta \mathbf{u}_1(x,t) + \gamma \mathbf{C}[\mathbf{u}_2(x,t) - \mathbf{u}_1(x,t)], \\ \frac{\partial \mathbf{u}_2(x,t)}{\partial t} &= \mathbf{f}(\mathbf{u}_2(x,t)) + \varepsilon \Delta \mathbf{u}_2(x,t) + \gamma \mathbf{C}[\mathbf{u}_1(x,t) - \mathbf{u}_2(x,t)],\end{aligned}\tag{5.1}$$

where $\mathbf{u}_{1,2} = (u_{1,2}^{(1)}, \dots, u_{1,2}^{(d)})^T \in \mathbf{R}^d$ are the state vectors, $t \in \mathbf{R}$ is the continuous time variable, $x \in [0, L)$ is the continuous space variable, $L \in \mathbf{R}^+$ is the system length, ε is the diffusion constant (the Laplacian Δ acts componentwise), γ is the coupling parameter, and $\mathbf{C} \in \mathbf{R}^{d \times d}$ is the coupling matrix (see also Secs. 2.2 and 2.3). Periodic boundary conditions $\mathbf{u}_i(x,t) = \mathbf{u}_i(x+L,t)$ are assumed.

For studying synchronization, the difference

$$\mathbf{w}(x,t) = \mathbf{u}_1(x,t) - \mathbf{u}_2(x,t)$$

plays a crucial role. We use the linear expansion of $\mathbf{f}(\mathbf{u}_2)$ around \mathbf{u}_1 to obtain (with the Jacobian \mathbf{J} of \mathbf{f})

$$\mathbf{f}(\mathbf{u}_1) - \mathbf{f}(\mathbf{u}_2) = \mathbf{J}(\mathbf{u}_1)(\mathbf{u}_1 - \mathbf{u}_2) + O(\|\mathbf{u}_1 - \mathbf{u}_2\|^2).$$

For a small perturbation $\mathbf{w}(x,t)$ of the synchronized state we then obtain in first order

$$\frac{\partial \mathbf{w}(x,t)}{\partial t} = [\mathbf{J}(\mathbf{u}_1(x,t)) - 2\gamma \mathbf{C}] \mathbf{w}(x,t) + \varepsilon \Delta \mathbf{w}(x,t).\tag{5.2}$$

Note that \mathbf{w} is used for the actual difference $\mathbf{u}_1 - \mathbf{u}_2$ (that can be of the order of the $\mathbf{u}_{1,2}$) as well as for a small perturbation of the synchronized state in approximate models of the perturbation dynamics.

In the case of CMLs, the spatial variable $x \in \{0, \dots, L-1\}$, the system length $L \in \mathbf{N}$, and the time $t \in \mathbf{Z}$ are discretized. The discrete Laplacian in one spatial dimension reads

$$\Delta \mathbf{u}(x,t) = \mathbf{u}(x-1,t) - 2\mathbf{u}(x,t) + \mathbf{u}(x+1,t).$$

For simplicity, we use the same symbols x, t, Δ for both continuous and discrete systems.

The typical model for scalar state variables $u_{1,2}(x,t)$ is given by

$$\begin{aligned}
 \tilde{u}_1(x,t) &= f(u_1(x,t)) + \varepsilon \Delta f(u_1(x,t)), \\
 u_1(x,t+1) &= \tilde{u}_1(x,t) + \gamma[\tilde{u}_2(x,t) - \tilde{u}_1(x,t)], \\
 \tilde{u}_2(x,t) &= f(u_2(x,t)) + \varepsilon \Delta f(u_2(x,t)), \\
 u_2(x,t+1) &= \tilde{u}_2(x,t) + \gamma[\tilde{u}_1(x,t) - \tilde{u}_2(x,t)],
 \end{aligned} \tag{5.3}$$

where again ε is the diffusion constant, γ is the coupling parameter, and periodic boundary conditions $u_i(x,t) = u_i(x+L,t)$ are assumed. The discrete Laplacian acts on the $f(u_i)$ to ensure that the variables u_i are mapped to the interval which the map is acting on (see Sec. 2.2). For the same reason the coupling between the two CMLs is applied to the intermediate state variables \tilde{u}_i . For a small perturbation $w(x,t)$ of the synchronized state we now obtain in first order

$$\begin{aligned}
 \tilde{w}(x,t) &= f'(u_1(x,t))w(x,t) + \varepsilon \Delta[f'(u_1(x,t))w(x,t)], \\
 w(x,t+1) &= (1 - 2\gamma)\tilde{w}(x,t),
 \end{aligned} \tag{5.4}$$

where the second equation is exact.

Similar considerations can be made in the case of unidirectional coupling, i.e., an autonomous system $u_1(x,t)$ driving a response system $u_2(x,t)$ (see Sec. 2.3). For coupled PDEs we then obtain

$$\frac{\partial \mathbf{w}(x,t)}{\partial t} = [\mathbf{J}(u_1(x,t)) - \gamma \mathbf{C}] \mathbf{w}(x,t) + \varepsilon \Delta \mathbf{w}(x,t),$$

whereas for coupled CMLs we find

$$\begin{aligned}
 \tilde{w}(x,t) &= f'(u_1(x,t))w(x,t) + \varepsilon \Delta[f'(u_1(x,t))w(x,t)], \\
 w(x,t+1) &= (1 - \gamma)\tilde{w}(x,t).
 \end{aligned}$$

Comparing these results with Eqs. (5.2) and (5.4), we see that only the prefactor of γ changes, which is confirmed by numerical simulations. In the following we will only consider bidirectionally coupled systems. One should keep in mind, however, that the general framework of the synchronization transition also applies to unidirectionally coupled systems.

5.1.2 Stochastic Model

We now introduce a stochastic PDE model for the synchronization error of both continuous and discrete spatially extended systems (i.e., for both PDEs and CMLs). To this end, we model the dynamics of the difference $w(x,t)$ by adding a cubic nonlinearity to the linear terms in Eq. (5.2) and replacing the chaotic derivatives of $f(u_1(x,t))$ by a stochastic process

$\xi(x, t)$ (see also Sec. 2.4). Furthermore, we only follow the perturbation in the direction of largest growth and therefore use a scalar variable $w(x, t)$ (in contrast to the perturbation vector in Eq. (5.2)). We then end up with the stochastic PDE [91, 93]

$$\frac{\partial w(x, t)}{\partial t} = \left\{ c(\gamma) + \xi(x, t) - p|w(x, t)|^2 \right\} w(x, t) + \varepsilon \Delta w(x, t), \quad (5.5)$$

which is the multiplicative noise equation (2.17) with an additional nonlinear term $-p|w|^2 w$ that ensures saturation of $|w|$ if $p > 0$. This accounts for the restriction that the synchronization error $|w|$ must stay of the order of the state variables $u_{1,2}$. The function $c(\gamma)$ is connected with the transverse Lyapunov exponent (see Eq. (5.7) below). In analogy with the situation for coupled low-dimensional systems (see Sec. 2.3) we write

$$c(\gamma) = c_0 + \ln(1 - 2\gamma)$$

in the case of coupled CMLs and

$$c(\gamma) = c_0 - 2\gamma$$

in the case of coupled PDEs. The constant c_0 is connected with the Lyapunov exponent of a single (uncoupled) extended system (see Eq. (5.8) below). The Gaussian random process $\xi(x, t)$ satisfies

$$\langle \xi(x, t) \rangle = 0, \quad \langle \xi(x, t) \xi(x', t') \rangle = 2\sigma^2 \delta(x - x') \delta(t - t').$$

The variance $2\sigma^2$ is connected with the magnitude of the fluctuations of local multipliers of the single map. The field $w(x, t)$ stays positive for $t > 0$ if $w(x, 0) > 0$ for all x . We shall consider Eq. (5.5) as our general model although we will see below that it is not valid for certain CMLs, in particular those consisting of discontinuous maps. By means of the Hopf-Cole transformation $h(x, t) = \ln|w(x, t)|$, Eq. (5.5) is transformed into (see also Sec. 2.4.2)

$$\frac{\partial h(x, t)}{\partial t} = c(\gamma) + \varepsilon \Delta h(x, t) + \varepsilon [\nabla h(x, t)]^2 - p e^{2h(x, t)} + \xi(x, t), \quad (5.6)$$

which is the Kardar-Parisi-Zhang (KPZ) equation [66] for a growing and roughening interface with an additional exponential term which (for $p > 0$) prevents $h(x, t)$ from growing towards infinity (thus playing the role of a soft upper wall in the context of a growing interface).

In Fig. 5.2(a) a snapshot of the synchronization error $w = u_1 - u_2$ of coupled tent map CMLs at a fixed time is shown. Since $\gamma < \gamma_c$, no overall synchronization is observed. It is obvious, however, that the synchronization error is highly localized. Plotting $|w|$ in logarithmic coordinates reveals the connection with the roughening interface described by the KPZ equation, see Fig. 5.2(b). Similar observations have been made for the Lyapunov vectors of spatially extended systems [91, 93]. It should be noted, however, that Fig. 5.2 shows the behaviour of the actual synchronization error, not its linear approximation.

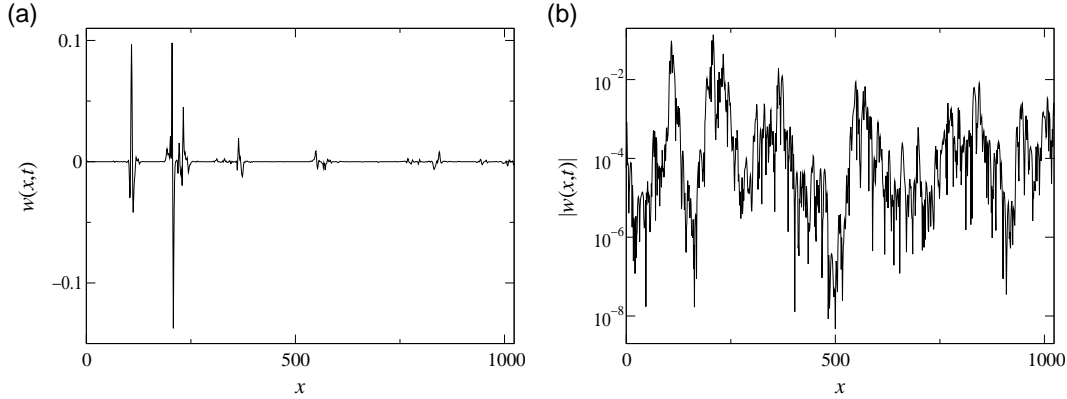


Figure 5.2: (a) Snapshot of the synchronization error $w = u_1 - u_2$ for coupled tent map CMLs ($L = 1024$) with a coupling parameter $\gamma = 0.175$ slightly below the critical γ_c . (b) Plotting $|w|$ in logarithmic coordinates gives the profile corresponding to the roughening interface. The spatial profiles of the state variables $u_{1,2}$ look qualitatively the same as the profile of a single tent map CML shown in Fig. 2.2.

Synchronization is observed if $\langle |w| \rangle_x(t) \rightarrow 0$, which is equivalent to $\langle h \rangle_x(t) \rightarrow -\infty$. In this case the saturating exponential term in Eq. (5.6) can be neglected and we end up with the usual KPZ equation. The average interface velocity gives the transverse Lyapunov exponent [93],

$$\lambda_{\perp} = c(\gamma) + \varepsilon \langle [\nabla h(x,t)]^2 \rangle_{x,t}, \quad (5.7)$$

where the average is over space and time after some transient phase. In the uncoupled case, $\gamma = 0$, we obtain the Lyapunov exponent of the extended system, Λ_{ext} (which in general cannot be calculated from the Lyapunov exponent Λ of the local dynamical system f and thus has to be estimated numerically). Therefore we can write Eq. (5.7) as

$$\lambda_{\perp} = \Lambda_{\text{ext}} + \ln(1 - 2\gamma)$$

in the case of coupled CMLs and

$$\lambda_{\perp} = \Lambda_{\text{ext}} - 2\gamma$$

in the case of coupled PDEs. These equations determine the constant c_0 introduced above,

$$c_0 = \Lambda_{\text{ext}} + \varepsilon \langle [\nabla h(x,t)]^2 \rangle_{x,t}. \quad (5.8)$$

Setting $\lambda_{\perp} = 0$, we obtain the linear critical coupling parameter

$$\gamma_{c,\text{lin}} = \frac{1}{2} (1 - e^{-\Lambda_{\text{ext}}}) \quad (5.9)$$

in the case of coupled CMLs and

$$\gamma_{c,\text{lin}} = \frac{1}{2} \Lambda_{\text{ext}} \quad (5.10)$$

in the case of coupled PDEs.

At this point a remark on finite-size effects is necessary. In Ref. [93] it has been shown that for long enough averaging the finite-size dependence of the Lyapunov exponent of an extended system is

$$\Lambda_{\text{ext}}(L) - \Lambda_{\text{ext}}(\infty) \sim L^{-1}. \quad (5.11)$$

This allows one to obtain an estimate of the thermodynamic limit value $\Lambda(\infty)$ by extrapolation. Eq. (5.11) corresponds to the finite-size scaling of the average surface velocity of the KPZ equation [71]. There are also scaling laws for the finite-time dependence of the Lyapunov exponent prior to saturation [93, 71].

From the finite-size dependence of Λ_{ext} it follows that also λ_{\perp} and $\gamma_{c,\text{lin}}$ are subject to finite-size effects. Using the relation (5.11) for $\Lambda_{\text{ext}}(L)$ in the synchronization condition (5.9) for coupled CMLs, we obtain (with a constant b)

$$\begin{aligned} \gamma_{c,\text{lin}}(L) &\approx \frac{1}{2} \left[1 - e^{-\Lambda_{\text{ext}}(\infty) - b/L} \right] \\ &\approx \frac{1}{2} \left[1 - (1 - b/L)e^{-\Lambda_{\text{ext}}(\infty)} \right] \\ &\approx \gamma_{c,\text{lin}}(\infty) + \frac{b}{2L} e^{-\Lambda_{\text{ext}}(\infty)}. \end{aligned}$$

For the finite-size dependence of the critical coupling parameter it follows

$$\gamma_{c,\text{lin}}(L) - \gamma_{c,\text{lin}}(\infty) \sim L^{-1}, \quad (5.12)$$

which is also obtained from the synchronization condition (5.10) for coupled PDEs. The validity of the results (5.9), (5.11), and (5.12) for coupled CMLs is checked in Secs. 5.2.1 and 5.3.1 below by means of numerical simulations.

5.1.3 Critical Exponents and Universality Classes

In the following, we are interested in the synchronization transition of chaotic extended systems. We will show that it resembles a continuous phase transition (see, e. g., Ref. [14]), where the coupling strength γ and the averaged absolute difference $\langle |w| \rangle_{x,t}$ (averaged over space and time after some transient phase) play the roles of the control and the order parameter, respectively. Without coupling ($\gamma = 0$) we have two individual systems. Starting from different initial conditions, we have $\langle |w| \rangle_{x,t} > 0$. In the case of coupled CMLs we immediately see from Eqs. (5.3) that for $\gamma = 1/2$ the systems synchronize ($u_1(x,t) = u_2(x,t)$) after one time step.

Our tasks will be to find the critical coupling strength γ_c such that

$$\langle |w| \rangle_{x,t} \begin{cases} > 0 & \text{if } \gamma < \gamma_c, \\ = 0 & \text{if } \gamma > \gamma_c, \end{cases}$$

and to characterize the transition for different systems, i. e. to find the appropriate universality classes (see, e. g., Ref. [14]). For the latter task, the standard way to proceed is to compute some of the critical exponents. Of interest in our case are¹

$$\begin{aligned} \langle |w| \rangle_{x,t} &\sim (\gamma_c - \gamma)^\beta && \text{for } \gamma \lesssim \gamma_c, \\ L_c &\sim (\gamma_c - \gamma)^{v_\perp} && \text{for } \gamma \lesssim \gamma_c, \\ T_c &\sim (\gamma_c - \gamma)^{v_\parallel} && \text{for } \gamma \lesssim \gamma_c, \\ \langle |w| \rangle_x(t) &\sim t^{-\delta} && \text{for } \gamma = \gamma_c, \end{aligned}$$

where L_c and T_c are the correlation length and time, respectively. For the computation of the exponents β , v_\perp , and v_\parallel an accurate knowledge of the critical coupling parameter γ_c is required. Therefore, we will make use of the last relation to determine γ_c as the value of γ which the best power-law scaling is obtained for.

In Sec. 5.2.2 below it will be argued that the synchronization transition is in the directed percolation (DP) universality class for CMLs consisting of discontinuous maps. In that context it will be useful to consider the density ρ of unsynchronized sites (corresponding to the density of active sites in DP), which in the spatially discrete case is defined as

$$\rho(t) = \frac{\text{card}\{x : |w(x,t)| > w_{\text{th}}\}}{L}$$

with some (small) threshold w_{th} . The scaling relations then read [49]

$$\begin{aligned} \langle \rho \rangle_t &\sim (\gamma_c - \gamma)^\beta && \text{for } \gamma \lesssim \gamma_c, \\ \rho(t) &\sim t^{-\delta} && \text{for } \gamma = \gamma_c. \end{aligned}$$

It is not a priori clear that the exponents are the same for $|w|$ and ρ ; arguments will be given in Sec. 5.4.2 below. A further scaling variable in the context of DP is the first passage time τ , defined as the first time $\langle |w| \rangle_x(t)$ (or alternatively $\rho(t)$) becomes smaller than some threshold. At criticality, τ scales with the system size L according to [101]

$$\tau \sim L^z \quad \text{for } \gamma = \gamma_c,$$

giving another way to estimate γ_c . This scaling relation is not useful for systems with γ_c depending on the system size L (as CMLs consisting of continuous maps, see below).

The critical exponents are not independent of each other. In particular, the scaling relations $\delta = \beta/v_\parallel$ and $v_\parallel = z v_\perp$ hold [61]. The values of the critical exponents of a given system can be used to decide which universality class it belongs to. In view of the following results, we mention two universality classes.

¹We denote the critical exponents by the symbols that are typically used in the context of directed percolation, see, e. g., Ref. [61]

Multiplicative Noise Equation

The first model (that applies to CMLs consisting of continuous maps, see Sec. 5.2.1 below) is the multiplicative noise equation (5.5). It can be transformed into the Kardar-Parisi-Zhang (KPZ) equation plus a nonlinear term, Eq. (5.6); we will therefore denote this type of transition as “KPZ-like”. While the critical exponents [9]

$$v_{\perp} = 1, \quad z = 3/2$$

of the original KPZ equation in one spatial dimension are known exactly, this is not the case for the additional critical exponents $(\beta, v_{\parallel}, \delta)$ of the multiplicative noise equation. Recent estimates obtained by TU et al. from a direct numerical integration of the multiplicative noise equation in one spatial dimension are [107]

$$\beta = 1.70 \pm 0.05, \quad v_{\perp} = 1.03 \pm 0.05, \quad \delta = 1.10 \pm 0.05, \quad z = 1.53 \pm 0.07.$$

The results for z and v_{\perp} are consistent with the exact values of the KPZ equation. By scaling arguments the relation $v_{\perp} = 1/(2z - 2)$ has been shown [107]. Although MUÑOZ and HWA reported a value $\beta = 1.50 \pm 0.15$ in a later work [82] (see also Ref. [40]), the estimate of TU et al. seems to rely on more accurate data and is reproduced by our simulations in Sec. 5.3.1 below.

Directed Percolation

The second model (that applies to CMLs consisting of discontinuous maps) is directed percolation (DP, see, e. g., Ref. [48]). We give a brief description of site DP. In $1 + 1$ (one spatial and one temporal) dimensions consider a square lattice that is rotated by 45° . In the following, the vertical (horizontal) direction represents space (time). Each site of the lattice can either be active or passive. We start with a few active sites that are randomly placed along a vertical line (corresponding to a spatial pattern at time $t = 0$). At every time step, each of the upper and lower right neighbouring sites of an active site is activated with a probability p that plays the role of the control parameter. There exists a critical value p_c such that the process dies out for $p < p_c$ and survives for $p > p_c$. A continuous phase transition is found if the fraction of active sites is used as the order parameter. Directed percolation is considered to be a general model for fluctuating extended systems with absorbing states. The passive state is absorbing in the sense that a site cannot be activated if both its upper and lower left neighbouring sites are passive.

Although the critical exponents are not known exactly even in one spatial dimension, there exist very accurate estimates [61],

$$\begin{aligned} \beta &= 0.276486 \pm 0.000008, & v_{\perp} &= 1.096854 \pm 0.000004, \\ \delta &= 0.159464 \pm 0.000006, & z &= 1.580745 \pm 0.000010. \end{aligned}$$

At the critical point a finite-size scaling relation is known [101] that in the language of the synchronization transition reads

$$\langle |w| \rangle_x(t) \sim L^{-\beta/\nu_\perp} g(t/L^z). \quad (5.13)$$

There also exists a field-theoretic description of DP similar to the multiplicative noise equation (5.5) introduced above (with $w > 0$), but with a quadratic nonlinearity and a multiplicative noise term proportional to \sqrt{w} instead of w [48]. Applications of DP include models of epidemics and chemical reactions [48].

5.1.4 Previous Results

The stochastic model for the synchronization error and its connection with the KPZ equation was suggested by PIKOVSKY and KURTHS [91]. They did not, however, include a nonlinear saturating term.

GRASSBERGER showed by means of numerical simulations and heuristic arguments that the synchronization transition of stochastically coupled cellular automata (i. e., systems with discrete state variables) is in the DP universality class [49]. He further argued that the synchronization of extended systems with continuous state variables (such as CMLs) generically corresponds to the KPZ equation with a nonlinear saturating term (see also Ref. [48]).

BAGNOLI et al. studied unidirectionally coupled CMLs with an all-or-nothing type of coupling [8]: at each time step, pairs of state variables $u_1(x, t)$ and $u_2(x, t)$ are equalized with a probability p . With p as the control parameter, a DP transition of the synchronization error is found.

Finally BARONI et al. studied CMLs that are not directly coupled to each other, but driven by the same realization of an additive noise process $\xi(x, t)$ [10, 11]. From the results of numerical simulations they concluded that the transition is KPZ-like for CMLs consisting of continuous maps (such as tent or logistic maps), but DP-like for CMLs consisting of discontinuous maps (such as Bernoulli maps). The DP-like transition was also found in the case of continuous maps with a very strong nonlinearity.

5.2 Two Types of Synchronization Transition

5.2.1 Continuous and Discontinuous Maps

At this point we present first numerical results for different CMLs of moderate length ($L = 1024$) to illustrate that there are two different kinds of the synchronization transition. More exact numerical results and estimates of the critical exponents can be found in Sec. 5.3 below. We study CMLs consisting of skew Bernoulli maps (see also Sec. 2.1.3),

$$f : [0, 1] \rightarrow [0, 1], \quad u \mapsto \begin{cases} u/a & \text{if } u \leq a, \\ (u-a)/(1-a) & \text{if } u > a, \end{cases} \quad (5.14)$$

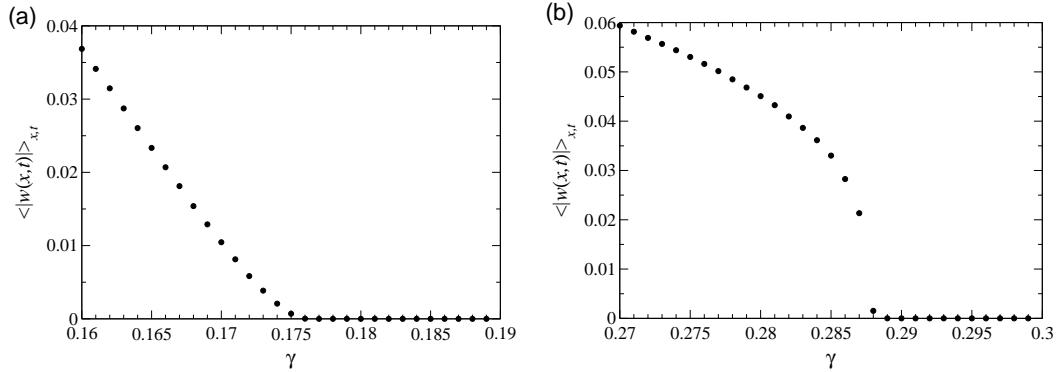


Figure 5.3: Synchronization transition for CMLs consisting of $L = 1024$ tent (a) and Bernoulli (b) maps, respectively, with parameter $a = 1/2$. The results shown are averages over 10 different initial conditions and 50000 iterations (after a transient of 50000 iterations).

skew tent maps,

$$f : [0, 1] \rightarrow [0, 1], \quad u \mapsto \begin{cases} u/a & \text{if } u \leq a, \\ (1-u)/(1-a) & \text{if } u > a. \end{cases} \quad (5.15)$$

and logistic maps,

$$f : [0, 1] \rightarrow [0, 1], \quad u \mapsto au(1-u). \quad (5.16)$$

The skew tent and Bernoulli maps depend on a parameter $a \in (0, 1)$; for $a = 1/2$ we obtain the usual tent map and Bernoulli shift, respectively. The Lyapunov exponent of the single map can be calculated analytically (see Sec. 2.1.3),

$$\Lambda = -a \ln a - (1-a) \ln(1-a).$$

For the logistic map, $a \in (0, 4]$. For $a = 4$, the map can be transformed into the tent map with $a = 1/2$; the Lyapunov exponent is therefore given by $\Lambda = \ln 2$.

In Fig. 5.3 the averaged absolute difference $\langle |w| \rangle_{x,t}$ is plotted as a function of the coupling parameter γ for CMLs consisting of $L = 1024$ tent and Bernoulli maps, respectively. All the maps of a CML have the same parameter value $a = 1/2$. Throughout this chapter, “democratic” coupling ($\epsilon = 1/3$) is applied if not stated otherwise. Obviously, the transition is of different form for the two examples, with exponents $\beta > 1$ for the tent map CMLs and $\beta < 1$ for the Bernoulli map CMLs. A transition of the type shown in Fig. 5.3(a) is also found for skew tent ($a \neq 1/2$) and logistic maps, while a transition of the type shown in Fig. 5.3(b) is also found for skew Bernoulli ($a \neq 1/2$) maps.

In Tab. 5.1 results for the Lyapunov exponents and critical coupling parameters for CMLs consisting of the maps described above are shown. Apart from the values for the single-map Lyapunov exponent Λ , these results are based on numerical simulations. Recall

Map	a	Λ	Λ_{ext}	$\gamma_{c,\text{lin}}$	γ_c
Tent	1/2	$\ln 2 \approx 0.6931$	0.4340	0.1760	0.17605 ± 0.00005
	1/3	$\ln 3 - (2/3)\ln 2 \approx 0.6365$	0.3644	0.1527	0.1527 ± 0.0003
Logistic	4	$\ln 2 \approx 0.6931$	0.3809	0.1584	0.1584 ± 0.0001
Bernoulli	1/2	$\ln 2 \approx 0.6931$	0.6931	0.250	0.2875 ± 0.0001
	1/3	$\ln 3 - (2/3)\ln 2 \approx 0.6365$	0.6670	0.2430	0.280 ± 0.0005

Table 5.1: Results for example maps with parameters a : single-map Lyapunov exponent Λ (analytical), Lyapunov exponent of the CML Λ_{ext} (numerical), linear critical coupling parameter $\gamma_{c,\text{lin}}$ (Eq. (5.9)), actual critical coupling parameter γ_c (numerical), all for system length $L = 1024$.

that they will in general depend on the system length L (see Sec. 5.1.2). The values for the actual critical coupling parameter γ_c are not obtained from the data shown in Fig. 5.3. Instead, those values of γ are chosen which the best scaling $\langle |w| \rangle_x(t) \sim t^{-\delta}$ is found for (see also Figs. 5.6 and 5.8 below).

It is obvious that $\gamma_c = \gamma_{c,\text{lin}}$ for the continuous skew tent and logistic maps, while $\gamma_c > \gamma_{c,\text{lin}}$ for the discontinuous skew Bernoulli maps. This is in accordance with observations by BARONI et al. for the synchronization of CMLs driven by the same realization of an additive noise process [10, 11]. In particular, it has been shown in Ref. [10] that for stochastic synchronization of CMLs consisting of discontinuous maps the critical value γ_c coincides with the value of γ at which the velocity v_F of nonlinear information propagation becomes zero (see Sec. 2.2 for a definition of v_F). This is reproduced by our calculations for coupled Bernoulli map CMLs as can be seen in Fig. 5.4(b). For tent CMLs, v_F as well as λ_{\perp} become zero at $\gamma = \gamma_{c,\text{lin}}$ (see Fig. 5.4(a)). In Fig. 5.4(a) it is also obvious that the transverse Lyapunov exponent λ_{\perp} is proportional to $\gamma_c - \gamma$ in the vicinity of γ_c .

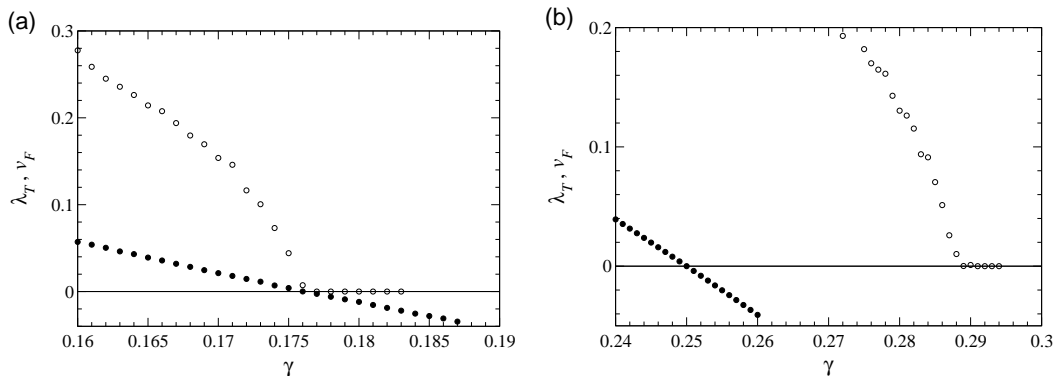


Figure 5.4: The transverse Lyapunov exponent λ_{\perp} (denoted by λ_T in the figures, filled circles) and velocity of nonlinear information propagation v_F (open circles) versus the coupling parameter γ for CMLs consisting of $L = 1024$ tent (a) and Bernoulli (b) maps, respectively, with parameters $a = 1/2$.

5.2.2 Spatiotemporal Dynamics

Because of the multiplicative nature of the linear perturbation dynamics (see Eqs. (5.2), (5.4), and (5.5)), the synchronization error decreases exponentially such that the synchronization is never perfect. This means that for $\gamma \approx \gamma_c$ nearly synchronized sites can easily desynchronize due to fluctuations. In other words, the synchronized state is not absorbing in the sense of DP. While these considerations hold in the case of CMLs consisting of continuous maps, the linear approximation is not adequate for CMLs consisting of discontinuous maps. There the nonlinear mechanism of information propagation inhibits synchronization even if the transverse Lyapunov exponent λ_{\perp} is clearly negative. Since this mechanism is associated with finite perturbations of the synchronized state, however, already synchronized sites are not expected to desynchronize by themselves: small fluctuations are damped because λ_{\perp} is clearly negative.

In Fig. 5.5 the spatiotemporal evolution of the synchronization error is plotted for values of the coupling parameter γ slightly larger than the critical γ_c . As can be seen, there are desynchronization events in fully synchronized regions in the case of tent map CMLs (Fig. 5.5(a)), while this is not the case for Bernoulli map CMLs (Fig. 5.5(b)). For the latter, desynchronization of already synchronized sites is only possible due to the influence of neighbouring unsynchronized sites. From the different synchronization mechanisms we can guess the corresponding types of transition.

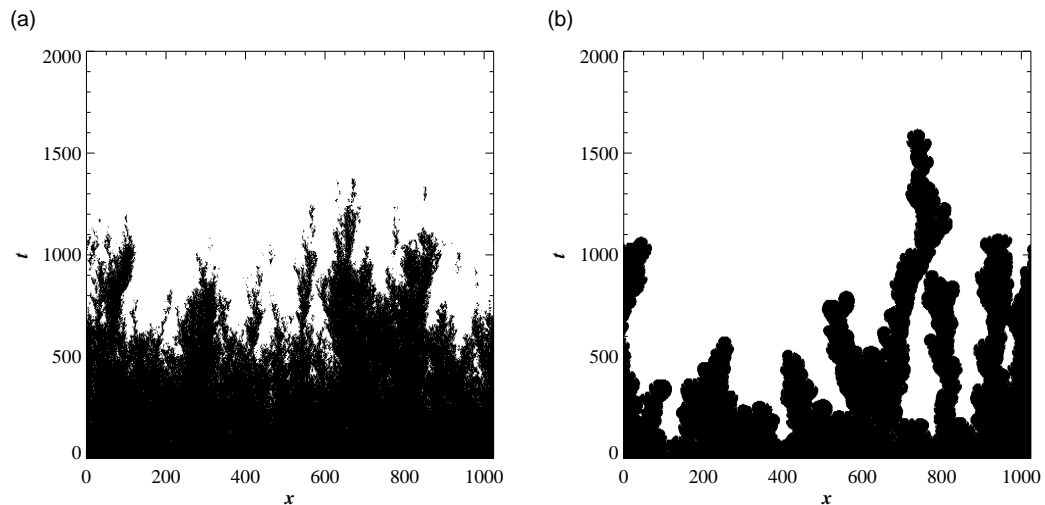


Figure 5.5: Space-time plots of the synchronization of coupled CMLs with coupling parameters γ slightly larger than the critical values γ_c . A black dot corresponds to an unsynchronized and a white dot to a synchronized site, respectively (threshold $w_{\text{th}} = 10^{-8}$). (a) Tent maps, $\gamma = 0.18$; (b) Bernoulli maps, $\gamma = 0.295$. In both cases $a = 1/2$ and $L = 1024$, random initial conditions for $u_1(x, 0)$ and $u_2(x, 0)$, coupling switched on after some transient evolution of the uncoupled CMLs.

- For CMLs consisting of continuous maps (more exactly for CMLs whose stability is determined by linear mechanisms) the transition is ruled by the linear perturbation dynamics and is therefore expected to be KPZ-like (see Sec. 5.1.2).
- For CMLs consisting of discontinuous maps (more exactly for CMLs whose stability is determined by nonlinear mechanisms, see the remarks on stable chaos in Sec. 2.2), however, $\gamma_c > \gamma_{c,\text{lin}}$ and the synchronized state is absorbing for $\gamma \approx \gamma_c$ (see also Ref. [11]): since $\lambda_\perp < 0$ for $\gamma \lesssim \gamma_c$, there are no local desynchronization events in already synchronized regions. Since the velocity v_F of nonlinear information propagation is positive, however, desynchronization can occur by means of “diffusion” of the local difference $w(x,t)$ to neighbouring, already synchronized sites. Writing “1” for an unsynchronized and “0” for a synchronized site, we can set up a simple discrete model whose dynamics are given by the rules

$$1 \xrightarrow{p_1} 0, \quad 01 \xrightarrow{p_2} 11, \quad 10 \xrightarrow{p_2} 11, \quad 000 \not\rightarrow 010,$$

with transition rates p_1 and p_2 for local synchronization and error diffusion, respectively. At the critical coupling parameter γ_c the velocity v_F vanishes. Since v_F does not depend on the system length (it describes the propagation of initially localized perturbations), γ_c also does not depend on L . Concluding, the transition is expected to be DP-like.

In the following sections we will confirm these expectations by numerical results.

5.3 Numerical Results for Coupled Map Lattices

5.3.1 Continuous Maps

We first consider CMLs consisting of continuous maps, in particular tent maps with parameter $a = 1/2$. As mentioned before, the critical coupling parameter is obtained from the scaling law $\langle |w| \rangle_x(t) \sim t^{-\delta}$. In Fig. 5.6 the time dependence of $\langle |w| \rangle_x$ is shown for several values of γ around 0.176. Best scaling is found for $\gamma_c = 0.17605$. Strong fluctuations near the critical point, long transients, and finite-size effects inhibit a direct estimation of the critical exponent. From Fig. 5.6 it can be seen, however, that the numerical results are consistent with the exponent $\delta = 1.19$ that is found for the discrete single step model introduced in Sec. 5.4.1 below.

The scaling behaviour $\langle |w| \rangle_{x,t} \sim (\gamma_c - \gamma)^\beta$ of the data from Fig. 5.3 is not good enough to allow checking the value $\beta = 1.699$ estimated in Sec. 5.4.1 below. It is well-known that the estimation of the exponent β is difficult due to long transients [49]. A larger system size, longer simulation times, and averages over a larger number of initial conditions would be needed.

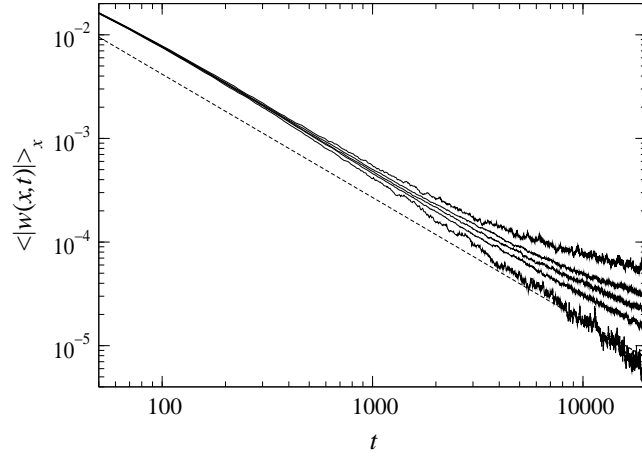


Figure 5.6: Coupled tent map CMLs ($a = 1/2$, $L = 1024$): time dependence of the space-averaged absolute difference $\langle |w(x,t)| \rangle_x(t)$ for coupling parameters $\gamma \in \{0.1759, 0.1760, 0.17605, 0.1761, 0.1762\}$ (upper to lower solid lines) in doubly-logarithmic coordinates. The best scaling $\sim t^{-\delta}$ is observed for $\gamma_c = 0.17605$. The dashed line has a slope -1.19 as found in Sec. 5.4.1. The numerical results are averages over 1000 to 10000 initial conditions. The decreasing absolute slope at large t indicates saturation due to finite-size effects.

Finally, we have checked the predictions for the finite-size dependence $\sim L^{-1}$ of the Lyapunov exponent Λ_{ext} of the extended system and the critical coupling parameter γ_c . We numerically calculated Λ_{ext} for CMLs of lengths $L \in \{32, 64, 128, 256, 512, 1024\}$ (using the 0-norm, see App. A.1). The critical coupling parameter obtained from a scaling analysis

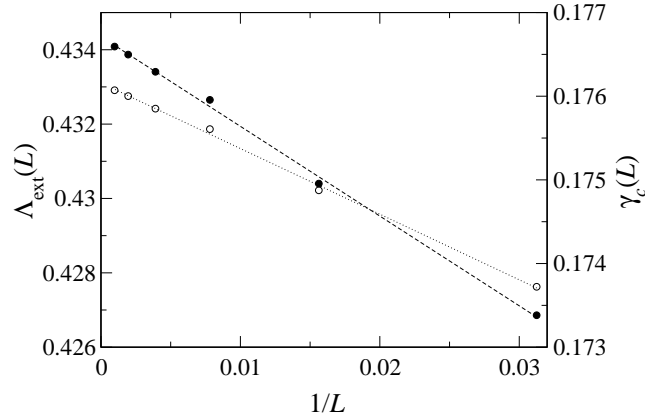


Figure 5.7: Coupled tent map CMLs ($a = 1/2$, $L \in \{32, 64, 128, 256, 512, 1024\}$): finite-size scaling of the Lyapunov exponent, $\Lambda_{\text{ext}}(L)$ (filled circles, left axis), and the critical coupling parameter, $\gamma_c(L)$ (open circles, right axis). The straight lines are linear fits.

as shown in Fig. 5.6 coincided for all L with the linear estimate $\gamma_{c,\text{lin}}$, see Eq. (5.9) and Tab. 5.1. In Fig. 5.7 the scaling $\sim L^{-1}$ is shown.

5.3.2 Discontinuous Maps

Now we consider CMLs consisting of discontinuous maps, in particular Bernoulli maps with parameter $a = 1/2$. The critical coupling parameter, which is larger than the linear prediction (5.9), is again obtained from the scaling law $\langle |w| \rangle_x(t) \sim t^{-\delta}$. From Fig. 5.8 the critical coupling parameter $\gamma_c = 0.2875$ is found for a CML of length $L = 1024$. The same value of γ_c is also found for other system lengths (see the finite-size scaling results below). We conclude that the critical coupling parameter does not depend on the system length in the case of CMLs consisting of discontinuous maps.

In Sec. 5.2.2 it was argued that the synchronization transition is in the directed percolation (DP) universality class for CMLs consisting of discontinuous maps. From Fig. 5.8 we see that the numerical results are consistent with the DP value $\delta = 0.159$ [61] for the critical exponent. Further numerical evidence for the DP nature of the synchronization transition is given by the validity of the finite-size scaling relation (5.13), which can be seen from Fig. 5.9. There the rescaling with the DP exponents $\beta/v_{\perp} = 0.252$ and $z = 1.581$ [61] results in a very good collapse of the different curves onto the single scaling function.

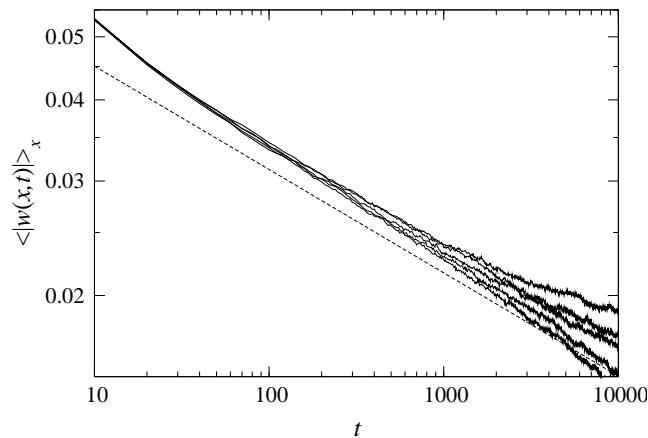


Figure 5.8: Coupled Bernoulli map CMLs ($a = 1/2$, $L = 1024$): time dependence of the space-averaged absolute difference $\langle |w| \rangle_x(t)$ for coupling parameters $\gamma \in \{0.2873, 0.2874, 0.2875, 0.2876, 0.2877\}$ (upper to lower solid lines) in doubly-logarithmic coordinates. The best scaling $\sim t^{-\delta}$ is observed for $\gamma_c = 0.2875$. The dashed line has a slope -0.159 as expected for DP. The numerical results are averages over 1000 initial conditions.

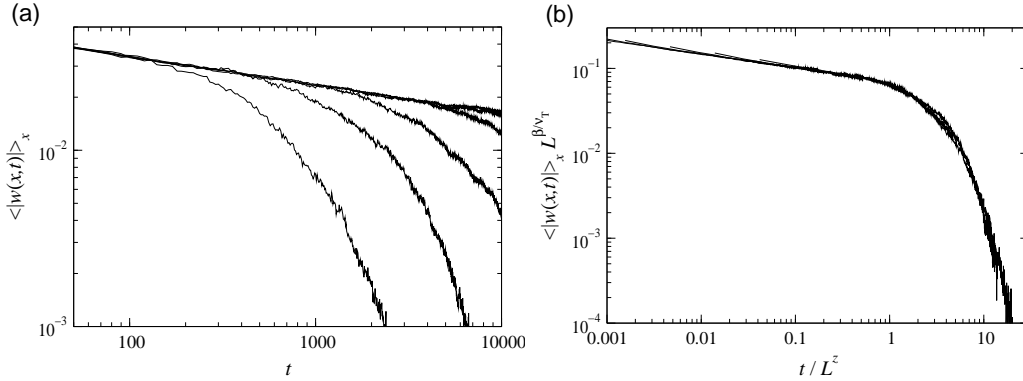


Figure 5.9: Finite-size scaling for Bernoulli map CMLs with $a = 1/2$ and coupling parameter $\gamma = 0.2875$. The time dependence of the averaged absolute difference $\langle |w| \rangle_x(t)$ is plotted in unscaled (a) and scaled (b) coordinates for system lengths $L \in \{32, 64, 128, 256, 512, 1024\}$ (lower to upper lines). The DP values $\beta/\nu_{\perp} = 0.252$ and $z = 1.581$ [61] have been used for the exponents (ν_T in the figure corresponds to ν_{\perp} in the text).

5.4 Numerical Results for Discrete Growth Models

5.4.1 Single Step Model with Lower Wall

Since the synchronization transition has been shown to fall into the universality class of the KPZ equation with a saturating term, it is promising to make use of discrete growth models that are known to belong to the KPZ universality class. The saturation can be provided by a growth-limiting wall. While a similar approach has already been used by MUÑOZ and HWA in the context of the multiplicative noise equation [82], the specific single step model we employ has the advantage that the free interface velocity (i. e., without a wall) is known exactly, even for systems of finite length. Since this velocity corresponds to the transverse Lyapunov exponent, the critical point is known exactly, which makes estimating critical exponents much easier.

The original single step model has been introduced for studying roughening interfaces. It is a restricted solid on solid (RSOS) model that has been shown to belong to the KPZ universality class [76]. It can be related to the totally asymmetric exclusion process [72]. The basic model consists of of an even number L of sites of integer height $H_I(x, t) \in \mathbf{N}_0$, $x \in \{0, \dots, L-1\}$, $t \in \mathbf{Z}$, with periodic boundary conditions, $H_I(x+L, t) = H_I(x, t)$. The initial state (flat interface) is typically given by

$$H_I(x, 0) = \begin{cases} 0 & \text{for even } x, \\ 1 & \text{for odd } x. \end{cases} \quad (5.17)$$

A timestep consists of L substeps. At each substep, a site is chosen randomly. If this site is a local minimum, its height is increased by two; otherwise nothing is done. In this way it is

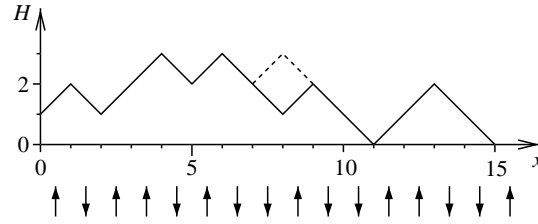


Figure 5.10: A sketch of the interface of the single step model ($L = 16$). At $x = 8$ a local minimum is found and the local height of the interface is increased by two. The arrows indicate positive and negative slopes between the sites.

ensured that the height difference between neighbouring sites is always one (see Fig. 5.10 for an illustration). If we denote a positive slope between interface sites by \uparrow and a negative slope by \downarrow , we have the simple transition rule

$$\downarrow\uparrow \rightarrow \uparrow\downarrow, \quad \uparrow\downarrow \not\rightarrow \downarrow\uparrow.$$

The velocity of the saturated interface can be calculated as follows. Due to periodic boundary conditions we always have $L/2$ slopes \downarrow and $L/2$ slopes \uparrow . After a transient phase neighbouring slopes can be assumed to be uncorrelated. The probability to randomly find a slope \downarrow at site x is $(L/2)/L$. Given this, the probability to have a slope \uparrow at the right neighbouring site $x + 1$ is $(L/2)/(L - 1)$. If such a combination is found, the average height of the interface is increased by $2/L$. Since a timestep consists of L substeps, we obtain the interface velocity [71]

$$V_I = L \frac{2}{L} \frac{L/2}{L} \frac{L/2}{L-1} = \frac{1}{2} \frac{L}{L-1}. \quad (5.18)$$

In first order we obtain a finite-size correction $V_I(L) \approx V_I(\infty) + 1/(2L)$ with $V_I(\infty) = 1/2$. The scaling $\sim L^{-1}$ is a general behaviour that can be explained by analytical arguments [71]. It corresponds to the finite-size scaling of the Lyapunov exponent of a spatially extended system, see Sec. 5.1.2. Note that a flat interface (5.17) has $L/2$ minima (instead of $\approx L/4$ after saturation) and therefore has a larger velocity than the one given by Eq. (5.18).

In Sec. 5.1.2 we have introduced a stochastic model for the dynamics of the synchronization error $w(x, t)$. For the transformed variable $h = \ln|w|$ we obtain the KPZ equation (5.6) with an additional local nonlinear term that prevents $h(x, t)$ from growing beyond order one. Synchronization in this model corresponds to an interface h moving towards $-\infty$. In our single step model, a hard wall at height $H_W(t)$ moving with a velocity V_W will play the role of the saturating nonlinearity. We will now argue that a lower wall is appropriate. In the modified KPZ equation (5.6) the $(\nabla h)^2$ term has the positive prefactor ε . From Eq. (5.7) it thus follows that the interface velocity increases with the roughness of the interface. For the single step model, however, the interface velocity is largest for a flat interface. By

changing the sign of h ($\tilde{h} = -h$) and dividing by -1 , Eq. (5.6) is transformed into

$$\frac{\partial \tilde{h}(x,t)}{\partial t} = -c(\gamma) + \varepsilon \Delta \tilde{h}(x,t) - \varepsilon [\nabla \tilde{h}(x,t)]^2 + p e^{-2\tilde{h}(x,t)} - \xi(x,t).$$

Now the prefactor of the $(\nabla \tilde{h})^2$ term is negative, in accordance with the single step model. For \tilde{h} synchronization corresponds to an interface moving towards $+\infty$, and the saturating term $+p \exp(-2\tilde{h})$ corresponds to a soft lower wall preventing \tilde{h} from becoming much less than order one.

The connection between the single step model and the synchronization error now is as follows. The variable $h(x,t) = \ln |w(x,t)|$ corresponds to the difference between the height of the wall and the height of the interface at site x ,

$$\begin{aligned} h(x,t) &\longleftrightarrow H_W(t) - H_I(x,t), \\ \langle |w(x,t)| \rangle &\longleftrightarrow \left\langle e^{H_W(t) - H_I(x,t)} \right\rangle. \end{aligned}$$

The transverse Lyapunov exponent corresponds to the difference between the velocities of the wall and the interface,

$$\lambda_{\perp} \longleftrightarrow V_W - V_I.$$

In this way, synchronization corresponds to an interface moving faster than the wall (thus escaping from the wall), whereas desynchronization corresponds to an interface moving slower than the wall.

We now give a summary of the single step model with a hard lower wall and some details of its implementation.

1. The system length L is chosen as a power of two, which allows using the logical “and” operation to ensure periodic boundary conditions.
2. One unit timestep consists of L substeps.
3. If not stated otherwise, the initial interface is flat (according to Eq. (5.17)) and attached to the wall ($H_W(0) = 0$).
4. A substep corresponds to first randomly selecting a site x and checking if it is a local minimum. If so, its height is increased by two:

$$\text{if } H_I(x-1,t) > H_I(x,t) < H_I(x+1,t) \text{ then } H_I(x,t) \mapsto H_I(x,t) + 2.$$

5. The free interface has the steady-state velocity $V_I = (1/2)L/(L-1)$ (see Eq. (5.18)). When starting with a flat interface, the initial velocity is larger.

6. The height $H_W(t)$ of the wall is increased by one after N_W substeps, which results in the wall velocity $V_W = L/N_W$. The heights of all sites that lie below the wall after this step are immediately increased by two:

$$\text{if } H_I(x,t) < H_W(t) \text{ then } H_I(x,t) \mapsto H_I(x,t) + 2.$$

7. The velocity difference $\delta V = V_W - V_I$ is equivalent to the transverse Lyapunov exponent λ_\perp and acts as the control parameter. The critical value is given by $\delta V = 0$. If δV is positive, the wall moves faster than the interface and catches it. If δV is negative, the interface moves faster than the wall and escapes, which corresponds to synchronization.
8. The velocity difference δV (i.e., the control parameter) is varied by adjusting N_W according to

$$N_W = \frac{L}{V_I + \delta V} = \frac{2(L-1)}{1 + 2\delta V(1-1/L)}.$$

We now present numerical results for a system length $L = 2^{20} = 1,048,576$ that allow estimating the critical exponents δ and β . In Fig. 5.11 the time dependence of $\langle \exp(H_W - H_I) \rangle_x$ is shown for different values of δV . A scaling $\sim t^{-\delta}$ is clearly found for $\delta V = 0$; a power law fit gives $\delta = 1.19$. In Fig. 5.12 the transition $\langle \exp(H_W - H_I) \rangle_{x,t}$

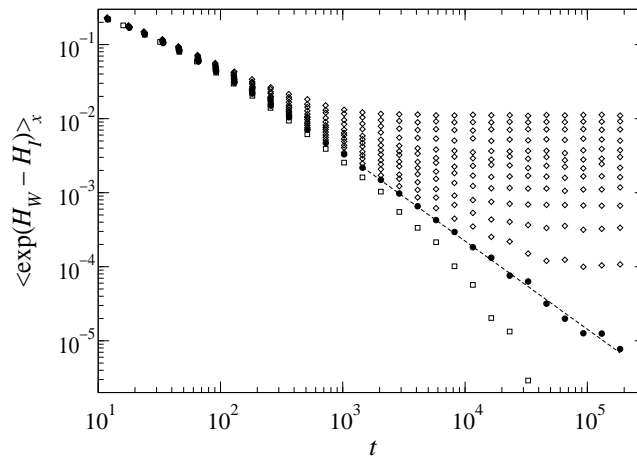


Figure 5.11: $\langle \exp(H_W - H_I) \rangle_x$ versus t for the single step model with system length $L = 1,048,576$ and $\delta V = -0.001$ (squares), $\delta V = 0$ (filled circles), $\delta V \in \{0.0005, 0.001, \dots, 0.004, 0.005, \dots, 0.008\}$ (lower to upper lines of diamonds). For $\delta V = 0$, we find $\langle \exp(H_W - H_I) \rangle_x \sim t^{-\delta}$ with $\delta = 1.19$. The shown results are averages over five different runs (with different sequences of random numbers), all starting with a flat interface attached to the wall.

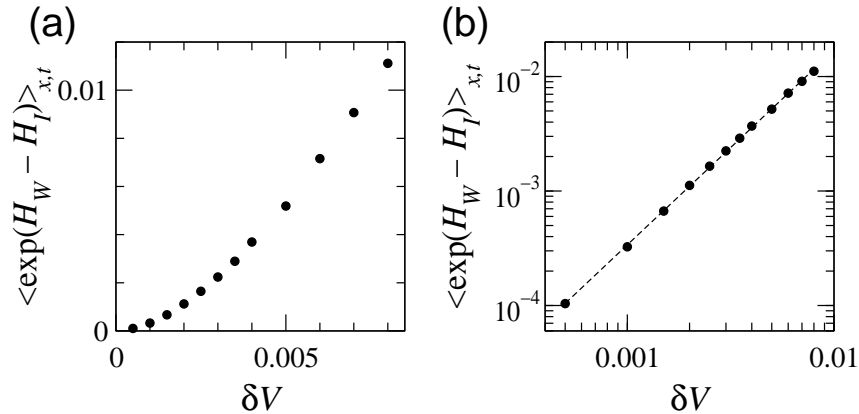


Figure 5.12: (a) The transition of $\langle \exp(H_W - H_I) \rangle_{x,t}$ versus δV for $L = 1,048,576$. The data from Fig. 5.11 have been time-averaged after saturation. (b) The same data in doubly-logarithmic coordinates. The scaling behaviour $\langle \exp(H_W - H_I) \rangle_{x,t} \sim \delta V^\beta$ is confirmed with $\beta = 1.699$.

(time-averaged after saturation) versus δV is shown for the unsynchronized phase $\delta V > 0$. A power law fit gives $\beta = 1.699$.

While our estimate for β is consistent with the result of TU et al. (see Sec. 5.1.3 and Ref. [107]), our estimate for δ is slightly different. It is, however, consistent with our numerical results for coupled tent map CMLs, as has been shown in Fig. 5.6.

5.4.2 Single Step Model with Attractive Lower Wall

We now want to modify the single step model introduced in the previous section in such a way that it describes the synchronization transition in the case of CMLs consisting of discontinuous maps (see Sec. 5.3.2). To this end, it is useful to have a look at a snapshot of the profile of the synchronization error w of Bernoulli map CMLs coupled with a parameter $\gamma_{c,\text{lin}} < \gamma < \gamma_c$. In Fig. 5.13 we observe a localization of w as in the case of coupled tent map CMLs (see Fig. 5.2). In logarithmic coordinates, however, no typical KPZ-like interface is observed. On the contrary, the interface sticks around $w \approx 10^{-2}$ in some places while it has very small values of w in between.

To include this behaviour into the single step model, we make the wall attractive. This is achieved by changing point 4 of the algorithm described in Sec. 5.4.1, which now reads

- 4'. A substep corresponds to first randomly selecting a site x and checking if it is a local minimum. If it is a minimum at the same height as the wall, its height is increased by two with probability $1 - q$; if it is a minimum at a larger height, its height is increased

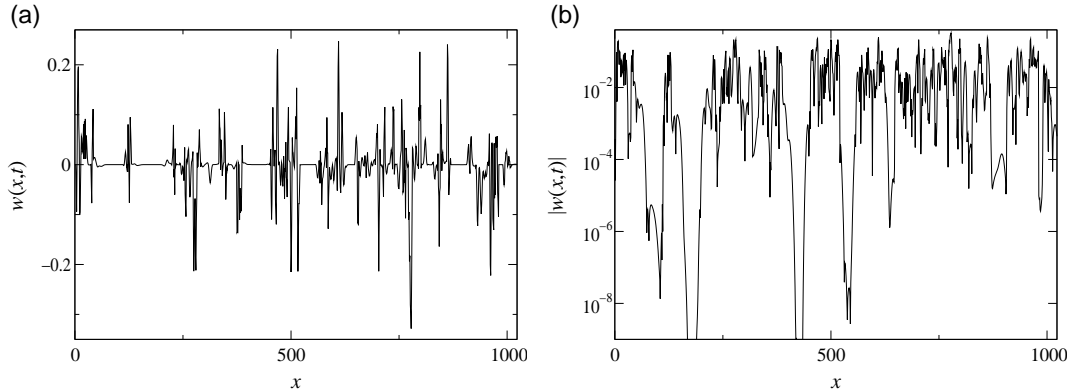


Figure 5.13: (a) Snapshot of the synchronization error $w = u_1 - u_2$ for coupled Bernoulli map CMLs ($L = 1024$) with a coupling parameter $\gamma = 0.2865$ slightly below the critical value γ_c , but above $\gamma_{c,\text{lin}}$. (b) Plotting $|w|$ in logarithmic coordinates gives the profile corresponding to the roughening interface. It does not, however, show typical KPZ-like properties (cp. Fig. 5.2).

by two with probability 1:

$$\begin{aligned} &\text{if } H_I(x-1, t) > H_I(x, t) < H_I(x+1, t) \quad \text{then} \\ &\text{if } H_I(x, t) \begin{cases} = H_W(t) & \text{then } H_I(x, t) \mapsto H_I(x, t) + 2 \quad \text{with prob. } 1 - q, \\ > H_W(t) & \text{then } H_I(x, t) \mapsto H_I(x, t) + 2 \quad \text{with prob. } 1. \end{cases} \end{aligned}$$

For large enough q we thus achieve that the interface stays attached to the wall even if the interface velocity is larger than the wall velocity ($V_I > V_W$, i. e., $\delta V < 0$). The parameter q measures the attractivity of the wall, the limiting cases are the single step model with a nonattractive wall introduced in Sec. 5.4.1 ($q = 0$) and an interface that cannot escape from the wall ($q = 1$).

As usual in the context of DP, we study the behaviour of the density of attached (or unsynchronized) sites

$$\rho(t) = \frac{\text{card}\{x : H_I(x, t) = H_W(t)\}}{L}.$$

The density $\rho(t)$ scales in the same way as $\langle |w| \rangle$: since $V_I > V_W$ (or $\lambda_\perp < 0$) the interface at a certain site stays either at the wall or moves far away from it (see also Fig. 5.13(b)). This means that the contribution to $\langle |w| \rangle$ of sites that are not attached to the wall is negligible.

In Fig. 5.14 numerical results for the temporal evolution of $\rho(t)$ for $L = 2^{20} = 1,048,576$, $q = 0.7$, and different values of δV are shown. The critical velocity difference is no longer known exactly but has to be estimated from the scaling behaviour. From Fig. 5.14 we find a value $\delta V_c = -0.07035 \pm 0.00005$ that is clearly less than zero. For $\delta V_c < \delta V < 0$ we have phase coexistence: a free (initially detached) interface moves away from the wall, whereas an initially attached interface stays attached to the wall. The scaling $\sim t^{-\delta}$ is consistent with the exponent $\delta = 0.159$ known for DP.

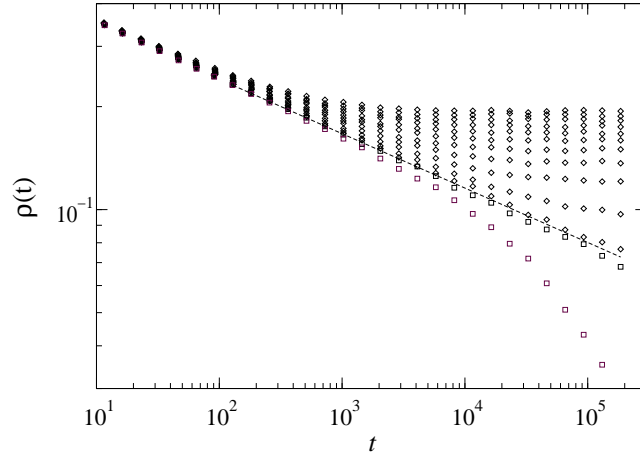


Figure 5.14: Density $\rho(t)$ of attached sites versus t for the single step model with system length $L = 1,048,576$, $q = 0.7$, and $\delta V \in \{-0.071, -0.0704\}$ (squares), $\delta V \in \{-0.0703, -0.070, -0.0695, \dots, -0.0655\}$ (lower to upper lines of diamonds). From these results we estimate the critical control parameter as $\delta V_c = -0.07035 \pm 0.00005$. The dashed line shows the scaling $\rho(t) \sim t^{-\delta}$ with $\delta = 0.159$ as expected for DP. The shown results are averages over one to five different runs (with different sequences of random numbers), all starting with a flat interface attached to the wall.

In Fig. 5.15 the scaling behaviour $\langle \rho \rangle_t \sim \delta V^\beta$ (time-averaged after saturation) is shown for $\delta V > \delta V_c$. A power law fit gives an exponent $\beta = 0.266$ which is not too different from the DP value $\beta = 0.276$. We stress that the critical velocity difference δV_c is only known

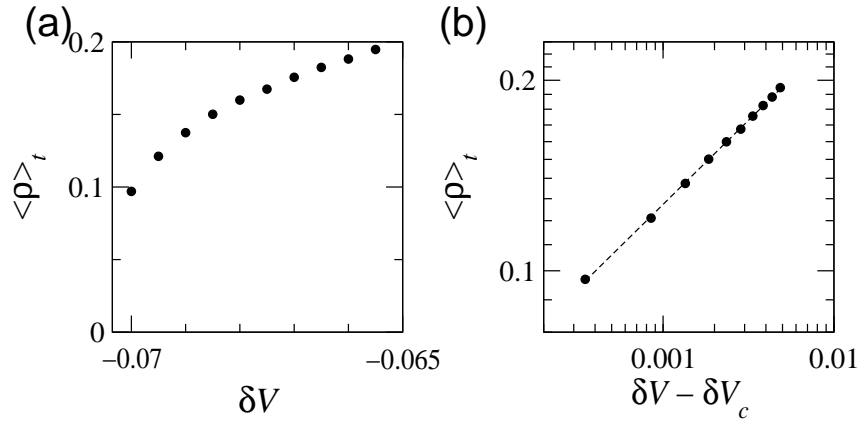


Figure 5.15: (a) The transition of $\langle \rho \rangle_t$ versus $\delta V - \delta V_c$ (with $\delta V_c = -0.07035$) for $L = 1,048,576$ and $q = 0.7$. The data from Fig. 5.14 have been time-averaged after saturation. (b) The same data in doubly-logarithmic coordinates. The scaling behaviour $\langle \rho \rangle_t \sim \delta V^\beta$ is confirmed with $\beta = 0.266$.

approximately in this case such that the estimate of β cannot be expected to be very accurate.

We finally remark that an analysis of the finite-size scaling $\tau \sim L^z$ of the first passage time (after which the interface detaches from the wall) is difficult because the control parameter δV enters the model via the discrete number $N_W \in \mathbf{N}^+$ of substeps between successive increments of the wall height (see point 8 of the algorithm in Sec. 5.4.1). For small values of the system size L , the control parameter can therefore only be changed in rather large steps. Even worse, for different L the same value of the control parameter cannot be applied. The highly fluctuating results indicate the validity of the scaling law (with the DP value $z = 1.58$) at the critical velocity difference δV_c . For large values of L , the steps between different possible values of the control parameter δV are very small and do not pose problems; the first passage time, however, becomes astronomically large.

5.5 Summary and Perspectives

In this chapter we have introduced a stochastic model for the synchronization error of coupled extended dynamical systems. The stochastic partial differential equation is known as the multiplicative noise equation and can be transformed into the Kardar-Parisi-Zhang (KPZ) equation with an additional growth-limiting term.

We have shown that the multiplicative noise equation is the correct model for coupled map lattices (CMLs) consisting of continuous maps (more exactly CMLs whose stability is determined by linear mechanisms). The critical coupling parameter for these systems can be calculated from the condition that the transverse Lyapunov exponent is zero. This critical coupling parameter shows a finite-size dependence $\sim L^{-1}$. A discrete growth model has been introduced (single step model with lower wall) which has a critical point that is known exactly and allows efficient numerical computation of the critical exponents. Accurate values for the critical exponents of the multiplicative noise equation are still missing. The single step model with a lower wall may be useful in this context. Our results for the critical exponents should only be regarded as first estimates; large-scale simulations are needed to obtain definitive values. Furthermore, the estimation of the critical exponents ν_\perp and ν_\parallel for the correlation length and time of the perturbation dynamics (see Sec. 5.1.3) remains to be done.

For CMLs consisting of discontinuous maps (more exactly CMLs whose stability is determined by nonlinear mechanisms) the multiplicative noise equation does not describe the synchronization transition. Here the critical coupling parameter is given by the condition that the velocity of nonlinear information propagation v_F becomes zero; at that point the transverse Lyapunov exponent is already clearly negative. We have shown that the synchronization transition for such systems is in the universality class of directed percolation (DP), which can be understood from the observation that the synchronized state is absorbing. For DP, the critical exponents are known with very high accuracy (although not exactly). Our numerical results agree very well with these exponents. The single step model

has been modified to describe this type of transition by making the wall attractive. This modified single step model is also interesting in the context of nonequilibrium wetting transitions [56, 57]. The connection with previous models is currently under investigation [96]. Also of interest is the nature of the phase diagram (for the two phases attached/detached interface) with the two control parameters δV and q : as q is varied between 0 and 1, the type of transition changes from KPZ-like to DP-like. The question arises if the critical exponents change continuously or discontinuously in between; also this is a point of current investigation [97].

The existence of two different mechanisms for the synchronization transition and the observed universality classes (KPZ with growth-limiting term, DP) are in accordance with results of BARONI et al. for CMLs that are not directly coupled to each other, but driven by the same realization of an additive noise process [10, 11]. Recently a finite-size Lyapunov exponent has been proposed to characterize the stability of dynamical systems with respect to finite perturbations, which might be useful for calculating the critical coupling parameter of spatially extended systems that exhibit a DP-like synchronization transition [23]. One may argue, however, that CMLs consisting of discontinuous maps can be regarded as unphysical. Although our numerical simulations have been limited to CMLs, from our theoretical description the typical synchronization transition of coupled partial differential equations can be expected to be KPZ-like (recall that so far stable chaos has not been observed in PDEs). Furthermore, our considerations have been limited to one spatial dimension. Results for the multiplicative noise equation indicate similar transitions (with different critical exponents) in two and three spatial dimensions [40]. In three spatial dimensions, however, two different types of transition are observed in dependence on the noise strength [51, 40].

The main problems for an experimental verification of our theoretical and numerical results are the requirements of long time series and an accurate measurement of the critical coupling strength. Possible coupled chaotic systems that can be considered as extended in one spatial dimension are:

- Semiconductor laser arrays [78] and broad area semiconductor lasers [32] that could be coupled by injecting light from one system into the other one.
- External cavity semiconductor lasers [80] for which the time delay can be regarded as a one-dimensional spatial extension [43, 44]. Also for these systems the coupling can be realized via light injection [79, 2]. A similar, but simpler model system consists of coupled Ikeda delay differential equations [60], see Sec. 3.4.2.
- Liquid crystals describable by the anisotropic Ginzburg-Landau equation [31]. In this PDE model, different diffusion constants apply in different spatial directions.

At least the finite-size dependence $\gamma_c \sim L^{-1}$ (where L corresponds to the delay time in the case of external cavity semiconductor lasers) should be observable in experiments.

6 Conclusion

In this work different aspects of the perturbation dynamics of coupled chaotic systems have been studied. As two central phenomena the coupling dependence of the Lyapunov exponents of weakly coupled chaotic systems and the coupling dependence of the synchronization error of strongly coupled spatially extended chaotic systems have been chosen. This choice was motivated by the observed universality, which manifests itself in scaling laws which are valid for a wide range of different systems. By replacing the chaotic fluctuations in the linearized perturbation dynamics by stochastic processes, we were able to give explanations for the observed universality and to obtain analytical or approximate results.

In the following, we discuss our main results. Finally, we report open questions and future perspectives.

6.1 Discussion of Main Results

Coupling Sensitivity of Chaos

We have introduced a stochastic continuous-time model for the perturbation dynamics of weakly coupled chaotic systems, which includes the key ingredients of exponential growth, temporal fluctuations, and coupling (Ch. 3 and Refs. [113, 3, 114]). By means of the Fokker-Planck equation we have been able to derive a general analytic expression for the coupling dependence of the largest Lyapunov exponent. In contrast to previous models [29, 75, 22] it is also valid for coupled nonidentical systems. As a special case for very small coupling and identical Lyapunov exponents of the uncoupled systems, we have obtained as an approximation the $1/\ln|\varepsilon|$ dependence of the largest Lyapunov exponent known as coupling sensitivity of chaos [26]. In agreement with previous observations [26], our results underline the necessity of fluctuations of the local multipliers (or finite-time Lyapunov exponents) for this singular behaviour of the Lyapunov exponent. Analytical or approximate expressions have also been obtained for the sum of Lyapunov exponents and for the generalized Lyapunov exponents.

A comparison with results of numerical simulations for coupled maps, but also for coupled high-dimensional delay differential equations, undermined the validity of our theoretical results, but also showed the limits of the stochastic approach. These limits are reached when the implicit assumption of coupling-independence of the local multipliers breaks down, i. e., for strong coupling and for nonsingular coupling dependence (e. g., for the generalized Lyapunov exponents), or when long temporal correlations are present (e. g.,

for strange nonchaotic attractors). Furthermore, our model is restricted to maps $f(u)$ whose first derivatives $f'(u)$ have the same sign for all u . Numerical simulations, however, give the $1/\ln|\varepsilon|$ dependence of the largest Lyapunov exponent also for general maps [26]; recently a stochastic model similar to ours has been proposed for the perturbation dynamics of weakly coupled map lattices, which includes the possibility of sign changes of the derivatives $f'(u)$ [22]. Finally we have shown that our simple stochastic model allows a qualitative understanding of the coupling sensitivity of chaos as a restricted random walk phenomenon.

Avoided Crossing of Lyapunov Exponents

As a consequence of the coupling sensitivity of chaos, we have found the new phenomenon of avoided crossing of Lyapunov exponents in weakly coupled disordered chaotic systems (Ch. 4 and Ref. [4]). Disorder in this context refers to differences between the parameters of the coupled subsystems. The repulsion between Lyapunov exponents is qualitatively similar to the energy level repulsion in nonintegrable quantum systems [54], but quantitatively much stronger. Indeed a relation to random matrix theory [77] can be drawn. In our problem, however, the eigenvalues of products of random matrices are of interest, and we have two sources of randomness: quenched disorder due to different subsystems and dynamic noise due to chaotic fluctuations. Using the results obtained in the context of the coupling sensitivity of chaos (Ch. 3), we have derived the asymptotic expression $\Phi_\Delta(z) \sim \exp(-1/z)$ for the distribution function of small spacings between the Lyapunov exponents, which agrees well with results of numerical calculations for different systems (dissipative and Hamiltonian ones) and different coupling schemes (nearest neighbour and global types).

Synchronization Transition of Spatially Extended Systems

Finally we have studied the dependence of the averaged difference between the states of two strongly coupled spatially extended chaotic systems on the coupling strength (Ch. 5). Inspired by the observation that this synchronization transition can be seen as a continuous phase transition, our investigations were based upon a multiplicative noise PDE model with a nonlinear saturation term, which has been proposed before as a model for the synchronization transition [91, 48, 49] and also studied in other contexts [12, 51, 107, 82, 40]. By means of the Hopf-Cole transformation this model can be related to the Kardar-Parisi-Zhang (KPZ) equation [9, 55]. We have shown that the critical coupling parameter γ_c can be calculated from the Lyapunov exponent Λ_{ext} of a single spatially extended system, and that γ_c inherits the finite-size scaling $\sim L^{-1}$ from Λ_{ext} [93]. Furthermore, we have added the saturation mechanism to a discrete growth model (the single step model known to belong to the KPZ universality class) by means of a hard wall pushing the interface from below. The transverse Lyapunov exponent then corresponds to the difference between the wall and interface velocities, while the synchronization error corresponds to the average height difference between the wall and the interface. This discrete model is computationally efficient,

and its critical parameter is known exactly.

Numerical simulations for different coupled map lattices (CMLs) revealed the existence of two types of the synchronization transition.

- For CMLs consisting of continuous maps, good agreement with the predictions of the stochastic model has been found. In particular, the predicted value and the finite-size scaling of the critical coupling parameter γ_c as well as the scaling $\langle |w| \rangle_x \sim t^{-\delta}$ of the space-averaged synchronization error are reproduced, the latter in consistence with the exponent $\delta = 1.19$ estimated from the discrete growth model.
- For CMLs consisting of discontinuous maps, the numerical results do not agree with the predictions of the stochastic model. Namely, the critical coupling parameter is larger than expected, and the scaling $\langle |w| \rangle_x \sim t^{-\delta}$ shows an exponent $\delta < 1$. This can be explained by the dominance of a nonlinear mechanism of information flow, leading to an instability with respect to finite perturbations of linearly stable systems [95]. Due to the linear stability, the synchronized state is absorbing and the transition is in the directed percolation (DP) universality class. This has been shown by the consistence of the numerical results with the DP exponent $\delta = 0.159$ and by a very good data collapse of results for different system lengths according to a finite-size scaling relation.

The existence of two different types of the synchronization transition is in agreement with recent results for the synchronization of CMLs which are not directly coupled, but driven by the same additive noise process [10, 11]. The lower wall in the discrete growth model can be made attractive such that the model shows the DP transition. For this modified model, however, the critical parameter is not known exactly anymore.

6.2 Open Questions and Perspectives

A main direction of further research should be the study of manifestations of our theoretical results in physical systems. Our results concerning the synchronization transition of spatially extended systems (Ch. 5) are directly applicable to coupled optical systems, such as broad area semiconductor lasers [32], semiconductor laser arrays [78], or lasers with time-delayed feedback [80], which can all be regarded as spatially one-dimensional. These systems have been shown to provide spatiotemporal chaos, and they can easily be coupled site by site via light injection. The experimentalist would have to cope with two problems. First, the accurate adjustment and measurement of the coupling strength could pose difficulties. Second, an accurate measurement of the synchronization error would be needed to estimate the critical coupling strength and the critical exponents.

To directly observe the coupling dependence of the Lyapunov exponents (Chs. 3 and 4) in experimental weakly coupled chaotic systems is expected to be difficult, although some

methods exist to estimate at least the largest Lyapunov exponent from experimental time series [65]. A more promising approach could be to look for indirect effects on measurable quantities that depend on the Lyapunov exponents. The Lyapunov exponents of disordered systems play a special role in this context, as they are connected with the localization length, the electrical conductance, and correlation functions [25, 70]. Further theoretical research is needed to investigate possible consequences of the coupling sensitivity of chaos and of the avoided crossing of Lyapunov exponents. First results exist, however, for the localization length in coupled one-dimensional disordered lattices [115].

On the theoretical side, the connection of the avoided crossing of Lyapunov exponents with random matrix theory (Ch. 4) deserves further research. A starting point could be the limit of vanishing dynamic noise (i. e., coupled maps with nonfluctuating local multipliers): in that case the problem of calculating the eigenvalues of the product of random matrices reduces to calculating the eigenvalues of a single random matrix.

Furthermore, several open questions exist in the context of the synchronization transition of spatially extended systems (Ch. 5). First, it would be interesting to check the validity of our results for coupled partial differential equations (PDEs). Second, an obvious generalization is given by coupled systems of higher spatial dimension. Studies of the multiplicative noise PDE in three spatial dimensions predict two different types of transition in dependence on the magnitude of fluctuations [51, 107, 40]. Third, accurate estimates of the critical exponents for the multiplicative noise PDE are still needed. We think that the discrete growth model (single step model with lower wall) could be a useful tool to numerically obtain these estimates, since the critical point is known exactly for this model. Fourth, the phase diagram of the modified discrete growth model (single step model with attractive lower wall) is expected to be interesting in its own right. It is given by the location and nature of the transition between an attached and a moving interface in the parameter space that is spanned up by the attractivity q of the wall and the velocity difference δV between the wall and the free interface. This phase diagram and its possible connection with a nonequilibrium wetting model [56, 57] are currently under investigation [97].

A Appendix

A.1 Numerical Calculation of Lyapunov Exponents

Lyapunov exponents are introduced in Ch. 2 as indicators for the stability properties of dynamical systems. Here we describe the methods used in this work to numerically calculate these exponents (see, e. g., Ref. [84]). A comparison of different methods for calculating Lyapunov exponents can be found in Ref. [39].

A.1.1 Discrete Maps

To calculate all N Lyapunov exponents of an N -dimensional map of the form (2.2), we have to follow the dynamics of N perturbation vectors \mathbf{w}_i , $i = 1, \dots, N$, which for $t = 0$ are linearly independent and normalized to unit length. The largest Lyapunov exponent is then given by

$$\lambda_1 = \lim_{t \rightarrow \infty} \frac{1}{t} \ln \|\mathbf{w}(t)\|, \quad (\text{A.1})$$

it does not depend on the norm. The sum of the n largest Lyapunov exponents is given by

$$\sum_{i=1}^n \lambda_i = \lim_{t \rightarrow \infty} \frac{1}{t} \ln V_n(t), \quad (\text{A.2})$$

where V_n is the volume spanned up by the perturbation vectors $\mathbf{w}_1, \dots, \mathbf{w}_n$.

At this point we face two problems. First, the norm $\|\mathbf{w}(t)\|$ grows or shrinks exponentially if λ_1 is greater or less than zero, respectively. So already for moderate values of t the norm can either not be calculated due to numerical overflow, or is zero due to limited numerical precision. In both cases, λ_1 cannot be calculated from Eq. (A.1). Second, if λ_1 is positive and some other perturbation vector \mathbf{w}_i , $i > 1$, has a component in the direction of \mathbf{w}_1 , this component grows with a larger exponential rate than the components in all other directions. In this way the different perturbation vectors rapidly align in the direction of largest growth. As a result the calculation of volumes spanned up by different vectors becomes impossible due to limited numerical precision.

The remedy for these problems is reorthonormalization of the perturbation vectors \mathbf{w}_i after not too long time intervals. The growth rate of the linear system is independent of the length of the vectors, such that renormalization of the vectors is a valid way to overcome the first problem. Reorthogonalizing the vectors ensures that \mathbf{w}_1 points in the direction of

largest growth, \mathbf{w}_2 points in the direction of second largest growth perpendicular to \mathbf{w}_1 , and so on. Furthermore, the volumes are now rectangular and we have

$$\ln V_n = \sum_{i=1}^n \ln \|\mathbf{w}_i\| .$$

So we can subtract the expressions (A.2) for different n to directly calculate λ_i ,

$$\lambda_i = \frac{1}{N_{\text{ort}} T_{\text{ort}}} \sum_{j=1}^{N_{\text{ort}}} \ln \|\mathbf{w}_i(t_j)\| ,$$

where N_{ort} and T_{ort} are the (large) number of and the (short) time interval between reorthonormalizations, and t_j is the time of the j -th reorthonormalization. The reorthonormalization method used for the numerical calculations in this work is the modified Gram-Schmidt algorithm, which is numerically more accurate than the classical Gram-Schmidt algorithm [15]. Before the calculation of the λ_i starts, a sufficiently long transient phase is necessary to ensure that the system is on its attractor. It should be kept in mind that in practice one always calculates finite-time Lyapunov exponents.

A.1.2 Differential Equations

For an N -dimensional system of ordinary differential equations of the form (2.1) the algorithm is essentially the same as for discrete maps. The numerical integration schemes used in this work (Runge-Kutta, Bulirsch-Stoer [98]) calculate $\mathbf{u}(t)$ at discrete times $t = t_n$. If adaptive stepsize methods [98] are used, the intervals between different t_n are in general of different length. Therefore also the intervals between reorthonormalizations will in general be of different length. The Lyapunov exponents are calculated according to

$$\lambda_i = \frac{1}{T} \sum_{j=1}^{N_{\text{ort}}} \ln \|\mathbf{w}_i(t_j)\| ,$$

with the (long) integration time T .

A.1.3 Spatially Extended Systems

The Lyapunov exponents of spatially extended systems are calculated in a similar way as described above. The state and perturbation vectors are usually written as $u(x, t)$ and $w(x, t)$, respectively, where x is the space and t is the time variable, which can both be either discrete or continuous. With the system length L , we have $x \in [0, L)$ in the spatially continuous and $x \in \{0, 1, \dots, L-1\}$ in the spatially discrete case, respectively. The q -norm ($q \in \mathbf{N}_0$) at time t is given by

$$\|w\|_q(t) = \left[\frac{1}{L} \int_0^L |w(x, t)|^q dx \right]^{1/q} ,$$

where the integral has to be replaced by a sum for spatially discrete systems. The limiting cases are

$$\|w\|_0(t) = \exp\left(\frac{1}{L} \int_0^L \ln |w(x,t)| dx\right)$$

and

$$\|w\|_\infty(t) = \max_x |w(x,t)|.$$

Although the Lyapunov exponents are norm-independent, the properties of the finite-time Lyapunov exponents in general depend on the norm used in the calculations. In Ref. [93] it has been shown that of the family of q -norms only the 0-norm has the self-averaging property that the magnitude of fluctuations of the finite-time Lyapunov exponents decreases with increasing system length.

A.1.4 Generalized Lyapunov Exponents

The q -th generalized Lyapunov exponent is defined as

$$L(q) = \lim_{t \rightarrow \infty} \frac{1}{t} \ln \langle \|\mathbf{w}(t)\|^q \rangle,$$

where the average is over different trajectories of the system. This average has to be carried out explicitly, which makes the numerical calculation of generalized Lyapunov exponents much more difficult than the calculation of Lyapunov exponents. The standard approach consists of first calculating $L_m(q)$ by approximating (in the discrete-time case)

$$\langle \|\mathbf{w}(t)\|^q \rangle \approx \frac{1}{m} \sum_{j=1}^m \|\mathbf{w}(t+j)\|^q$$

for different (small) values of m . The value of $L(q)$ is then calculated by considering $L_m(q)$ as a function of $1/q$ and extrapolating to $1/q \rightarrow 0$. Details can be found in Ref. [25].

A.2 Stochastic Differential Equations

We briefly review some results for stochastic differential equations that are needed in this work. The subject is treated in detail in Refs. [58, 38, 100, 109].

A.2.1 Langevin Equation

A differential equation with a stochastic driving term is called a Langevin equation. For a one-dimensional stochastic variable $x(t)$ it is given by (in Stratonovich form, see below)

$$dx(t) = f(x)dt + g(x) \circ dW(t),$$

where $W(t)$ is a Wiener process (i. e., the displacement of a Brownian particle with starting point $W(0) = 0$). It has a Gaussian distribution characterized by

$$\langle W(t) \rangle = 0, \quad \langle W(t)W(t') \rangle = \min(t, t').$$

In general, the functions f and g can also be time-dependent. In this work, we often write Langevin equations in the intuitive form

$$\frac{dx(t)}{dt} = f(x) + g(x)\xi(t),$$

where $\xi(t) = dW(t)/dt$ is a Gaussian stochastic process with zero mean, unit variance, and no temporal correlations,

$$\langle \xi(t) \rangle = 0, \quad \langle \xi(t)\xi(t') \rangle = \delta(t - t').$$

The simplest Langevin equation reads

$$dx(t) = dW(t).$$

Its solution is given by

$$x(t) = x(0) + \int_0^t dW(\tilde{t}) = x(0) + W(t),$$

This simple example demonstrates that the variable $x(t)$ depends on $W(t)$. For the solution of a multiplicative noise equation,

$$dx(t) = g(x) \circ dW(t),$$

it is thus not clear how the integral in the solution

$$x(t) = x(0) + \int_0^t g(x(\tilde{t})) \circ dW(\tilde{t})$$

shall be calculated. There is no definite answer to this question, one has to decide between different interpretations of the Langevin equation. In the Stratonovich interpretation the solution is given by

$$x(t) = x(0) + \lim_{N \rightarrow \infty} \sum_{n=0}^{N-1} g \left(\frac{x(t_{n+1}) + x(t_n)}{2} \right) [W(t_{n+1}) - W(t_n)] \quad \text{with} \quad t_n = \frac{nt}{N}.$$

For this choice the variable $x(t)$ can be transformed by the usual rules of calculus, which is not the case for other interpretations. One can also argue that the Stratonovich interpretation is closest to physical processes (which are never exactly δ -correlated).

In this work Langevin equations are used as models of chaotic processes. Since these models are constructed to match the properties of the chaotic processes, we have to choose one specific interpretation in advance. Throughout this work, the Stratonovich interpretation is used. The question of deciding between the Stratonovich and Itô interpretations in stochastic modelling is treated in detail in Sec. 5.4.2 of Ref. [58].

A.2.2 Fokker-Planck Equation

Given a Langevin equation, one is usually not interested in individual trajectories. Instead one often wants to calculate the moments $\langle x^q \rangle$, which are in general time-dependent. All information about the distribution of $x(t)$ can be obtained from the probability density function $\rho(x, t)$. The temporal evolution of $\rho(x, t)$ is described by the Fokker-Planck equation

$$\begin{aligned} \frac{\partial \rho(x, t)}{\partial t} &= -\frac{\partial}{\partial x} [f(x)\rho(x, t)] + \frac{1}{2} \frac{\partial}{\partial x} \left\{ g(x) \frac{\partial}{\partial x} [g(x)\rho(x, t)] \right\} \\ &= -\frac{\partial}{\partial x} \left\{ \left[f(x) + \frac{1}{2}g(x)g'(x) \right] \rho(x, t) \right\} + \frac{1}{2} \frac{\partial^2}{\partial x^2} [g^2(x)\rho(x, t)], \end{aligned}$$

where $g' = dg/dx$. This equation can be considered as a continuity equation for the probability density $\rho(x, t)$ and the probability flow

$$j(x, t) = \left[f(x) + \frac{1}{2}g(x)g'(x) \right] \rho(x, t) - \frac{1}{2} \frac{\partial}{\partial x} [g^2(x)\rho(x, t)].$$

Let x be defined on an interval with borders a and b ($a < b$), which can be $\pm\infty$. If there is no probability flow across these borders, the stationary probability density is given by

$$\rho_s(x) = \frac{N}{g(x)} \exp \left(2 \int_a^x \frac{f(\tilde{x})}{g^2(\tilde{x})} d\tilde{x} \right),$$

where N is a normalization constant.

A.2.3 Furutsu-Novikov Relation

At several points in this work it is necessary to calculate averages of the form $\langle \xi(t)F[\xi] \rangle$, where $F[\xi]$ is a functional of $\xi(t)$ (e. g., an integral). For a Gaussian stochastic process $\xi(t)$ with zero mean the Furutsu-Novikov relation provides a very convenient way to evaluate averages of this kind [35, 83]. In one dimension the relation reads

$$\langle \xi(t)F[\xi] \rangle = \int \langle \xi(t)\xi(t') \rangle \left\langle \frac{\delta F[\xi]}{\delta \xi(t')} \right\rangle dt',$$

where $\delta F/\delta \xi$ is the functional derivative, and the integral extends over the interval which t' is defined on.

As an example which is of particular importance for this work we study

$$w[\xi] = \exp \left(\Lambda t + \int_0^t \xi(\tilde{t}) d\tilde{t} \right)$$

with a constant Λ and a Gaussian noise process $\xi(t)$ with

$$\langle \xi(t) \rangle = 0, \quad \langle \xi(t)\xi(t') \rangle = 2\sigma^2\delta(t-t').$$

Using the chain rule, the functional derivative is calculated as

$$\frac{\delta w[\xi]}{\delta \xi(t')} = \begin{cases} w[\xi] & \text{if } t' \in [0, t], \\ 0 & \text{else.} \end{cases}$$

The Furutsu-Novikov relation thus gives

$$\langle \xi(t)w[\xi] \rangle = \int_0^t 2\sigma^2\delta(t-t') \langle w[\xi] \rangle dt' = \sigma^2 \langle w[\xi] \rangle$$

(note that only one half of the δ -distribution contributes to the integral). Applications can be found in Secs. 2.4.1 and 3.2.4.

Notation

t	time (discrete or continuous)
x	space (discrete or continuous)
\mathbf{u}	state vector with components $u^{(i)}$
\mathbf{w}	perturbation vector, synchronization error
f	nonlinear function
\mathbf{J}	Jacobian of f
\mathbf{P}	product matrix $\prod \mathbf{J}$
\mathbf{P}^T	transpose of \mathbf{P}
ε	coupling parameter (between subsystems), diffusion constant
γ	coupling parameter (between extended systems, Ch. 5)
γ_i	eigenvalues
λ_i	Lyapunov exponents
Λ_i	Lyapunov exponents of uncoupled systems
$\lambda_i(t)$	local (finite-time) Lyapunov exponents
$2\sigma^2$	variance of local Lyapunov exponent $\lambda(1)$
λ_{\perp}	transverse Lyapunov exponent
$L(q)$	generalized Lyapunov exponents
χ, ξ	stochastic processes
$2\sigma^2$	variance of stochastic process
$W(t)$	Wiener process
$\text{Prob}(X)$	probability of event X
$\rho(s)$	probability density of stochastic variable s
$\Phi_s(z)$	cumulative distribution function $\text{Prob}(s \leq z)$
ODE	ordinary differential equation
PDE	partial differential equation
CML	coupled map lattice
CDF	cumulative distribution function
KPZ	Kardar-Parisi-Zhang
DP	directed percolation

References

- [1] M. Abramowitz and I. A. Stegun, eds., *Handbook of Mathematical Functions* (GPO, Washington, DC, 1964).
- [2] V. Ahlers, U. Parlitz, and W. Lauterborn, Hyperchaotic dynamics and synchronization of external-cavity semiconductor lasers, *Phys. Rev. E* **58**(6):7208–7213 (1998).
- [3] V. Ahlers, R. Zillmer, and A. S. Pikovsky, Statistical theory for the coupling sensitivity of chaos, in D. S. Broomhead, E. A. Luchinskaya, P. V. E. McClintock, and T. Mullin, eds., *Stochastic and Chaotic Dynamics in the Lakes: STOCHAOS*, vol. 502 of *AIP Conference Proceedings*, pp. 450–455 (American Institute of Physics, Melville, NY, 2000).
- [4] V. Ahlers, R. Zillmer, and A. Pikovsky, Lyapunov exponents in disordered chaotic systems: Avoided crossing and level statistics, *Phys. Rev. E* **63**:036213 (2001).
- [5] A. Amengual, E. Hernández-García, R. Montagne, and M. S. Miguel, Synchronization of spatiotemporal chaos: The regime of coupled spatiotemporal intermittency, *Phys. Rev. Lett.* **78**(23):4379–4382 (1997).
- [6] L. Arnold, M. M. Doyle, and N. S. Namachchivaya, Small noise expansion of moment Lyapunov exponents for two-dimensional systems, *Dynamics and Stability of Systems* **12**(3):187–211 (1997).
- [7] L. Arnold, *Random Dynamical Systems* (Springer-Verlag, Berlin, 1998).
- [8] F. Bagnoli, L. Baroni, and P. Palmerini, Synchronization and directed percolation in coupled map lattices, *Phys. Rev. E* **59**(1):409–416 (1999).
- [9] A.-L. Barabási and H. E. Stanley, *Fractal Concepts in Surface Growth* (Cambridge University Press, Cambridge, 1995).
- [10] L. Baroni, R. Livi, and A. Torcini, Noise-driven synchronization in coupled map lattices, in J.-M. Gambaudo, P. Hubert, P. Tisseur, and S. Vaienti, eds., *Dynamical Systems: From Crystal to Chaos*, p. 23 (World Scientific, Singapore, 2000).
- [11] L. Baroni, R. Livi, and A. Torcini, Transition to stochastic synchronization in spatially extended systems, *Phys. Rev. E* **63**:036226 (2001).

References

- [12] A. Becker and L. Kramer, Linear stability analysis for bifurcations in spatially extended systems with fluctuating control parameter, *Phys. Rev. Lett.* **73**(7):955–958 (1994).
- [13] G. Benettin, Power-law behavior of Lyapunov exponents in some conservative dynamical systems, *Physica D* **13**(1–2):211–220 (1984).
- [14] J. J. Binney, N. J. Dowrick, A. J. Fisher, and M. E. J. Newman, *The Theory of Critical Phenomena: An Introduction to the Renormalization Group* (Oxford University Press, Oxford, 1992).
- [15] Å. Björck, Numerics of Gram-Schmidt orthogonalization, *Linear Algebra Appl.* **197/198**:297–316 (1994).
- [16] S. Boccaletti, J. Bragard, F. T. Arecchi, and H. Mancini, Synchronization in nonidentical extended systems, *Phys. Rev. Lett.* **83**(3):536–539 (1999).
- [17] T. Bohr, M. H. Jensen, G. Paladin, and A. Vulpiani, *Dynamical Systems Approach to Turbulence*, vol. 8 of *Cambridge Nonlinear Science Series* (Cambridge University Press, Cambridge, 1998).
- [18] T. Bohr, M. van Hecke, R. Mikkelsen, and M. Ipsen, On universality in transitions to spatio-temporal chaos, e-print cond-mat/0008254 (2000).
- [19] R. Bonaccini and A. Politi, Chaotic-like behaviour in chains of stable nonlinear oscillators, *Physica D* **103**(1-4):362–368 (1997).
- [20] L. A. Bunimovich and Y. G. Sinai, Spacetime chaos in coupled map lattices, *Nonlinearity* **1**(4):491–516 (1988).
- [21] F. Cecconi and A. Politi, n -tree approximation for the largest Lyapunov exponent of a coupled map lattice, *Phys. Rev. E* **56**(5):4998–5003 (1997).
- [22] F. Cecconi and A. Politi, Analytic estimate of the maximum Lyapunov exponent in products of tridiagonal random matrices, *J. Phys. A* **32**(44):7603–7622 (1999).
- [23] M. Cencini and A. Torcini, Linear and nonlinear information flow in spatially extended systems, *Phys. Rev. E* **63**:056201 (2001).
- [24] H. Chaté, Lyapunov analysis of spatiotemporal intermittency, *Europhys. Lett.* **21**(4):419–425 (1993).
- [25] A. Crisanti, G. Paladin, and A. Vulpiani, *Products of Random Matrices: in Statistical Physics*, vol. 104 of *Springer Series in Solid State Physics* (Springer-Verlag, Berlin, 1993).

-
- [26] H. Daido, Coupling sensitivity of chaos, *Prog. Theor. Phys.* **72**(4):853–856 (1984), erratum published in *Prog. Theor. Phys.* **73**(1):310 (1985).
- [27] H. Daido, Coupling sensitivity of chaos: A new universal property of chaotic dynamical systems, *Prog. Theor. Phys. Suppl.* **79**:75–95 (1984).
- [28] H. Daido, Coupling sensitivity of chaos and the Lyapunov dimension: The case of coupled two-dimensional maps, *Phys. Lett. A* **110**(1):5–9 (1985).
- [29] H. Daido, Coupling sensitivity of chaos: Theory and further numerical evidence, *Phys. Lett. A* **121**(2):60–66 (1987).
- [30] R. J. Deissler and K. Kaneko, Velocity-dependent Lyapunov exponents as a measure of chaos for open-flow systems, *Phys. Lett. A* **119**(8):397–402 (1987).
- [31] R. Faller and L. Kramer, Phase chaos in the anisotropic complex Ginzburg-Landau equation, *Phys. Rev. E* **57**(6):R6249–R6252 (1998).
- [32] I. Fischer, O. Hess, W. Elsässer, and E. Göbel, Complex spatio-temporal dynamics in the near-field of a broad-area semiconductor laser, *Europhys. Lett.* **35**(8):579–584 (1996).
- [33] H. Fujisaka and T. Yamada, Stability theory of synchronized motion in coupled-oscillator systems, *Prog. Theor. Phys.* **69**(1):32–47 (1983).
- [34] H. Fujisaka, H. Ishii, M. Inoue, and T. Yamada, Intermittency caused by chaotic modulation II: Lyapunov exponent, fractal structure and power spectrum, *Prog. Theor. Phys.* **76**(6):1198–1209 (1986).
- [35] K. Furutsu, On the statistical theory of electromagnetic waves in a fluctuating medium (I), *J. Res. Natl. Bur. Stand. D* **67**:303–323 (1963).
- [36] J. García-Ojalvo, A. Hernández-Machado, and J. M. Sancho, Effects of external noise on the Swift-Hohenberg equation, *Phys. Rev. Lett.* **71**(10):1542–1545 (1993).
- [37] J. García-Ojalvo and R. Roy, Spatiotemporal communication with synchronized optical chaos, *Phys. Rev. Lett.* **86**(22):5204–5207 (2001).
- [38] C. W. Gardiner, *Handbook of Stochastic Methods: for Physics, Chemistry and the Natural Sciences*, vol. 13 of *Springer Series in Synergetics*, 2nd edn. (Springer-Verlag, Berlin, 1985).
- [39] K. Geist, U. Parlitz, and W. Lauterborn, Comparison of different methods for computing Lyapunov exponents, *Prog. Theor. Phys.* **83**(5):875–893 (1990).

References

- [40] W. Genovese and M. A. Muñoz, Recent results on multiplicative noise, *Phys. Rev. E* **60**(1):69–78 (1999).
- [41] N. A. Gershenfeld, *The Nature of Mathematical Modeling* (Cambridge University Press, Cambridge, 1999).
- [42] G. Giacomelli and A. Politi, Spatio-temporal chaos and localization, *Europhys. Lett.* **15**(4):387–392 (1991).
- [43] G. Giacomelli, R. Meucci, A. Politi, and F. T. Arecchi, Defects and spacelike properties of delayed dynamical systems, *Phys. Rev. Lett.* **73**(8):1099–1102 (1994).
- [44] G. Giacomelli and A. Politi, Relationship between delayed and spatially extended dynamical systems, *Phys. Rev. Lett.* **76**(15):2686–2689 (1996).
- [45] F. Ginelli, R. Livi, and A. Politi, Emergence of chaotic behaviour in linearly stable systems, e-print nlin.CD/0102005 (2001).
- [46] F. Ginelli and R. Livi, private communication (2001).
- [47] R. Graham and A. Schenzle, Carleman imbedding of multiplicative stochastic processes, *Phys. Rev. A* **25**(3):1731–1754 (1982).
- [48] P. Grassberger, Directed percolation: Results and open problems, in S. Puri and S. Dattagupta, eds., *Nonlinearities in Complex Systems*, pp. 61–89 (Narosa Publishing House, New Delhi, 1997).
- [49] P. Grassberger, Synchronization of coupled systems with spatiotemporal chaos, *Phys. Rev. E* **59**(3):R2520–R2522 (1999).
- [50] C. Grebogi, E. Ott, S. Pelikan, and J. A. Yorke, Strange attractors that are not chaotic, *Physica D* **13**(1–2):261–268 (1984).
- [51] G. Grinstein, M. A. Muñoz, and Y. Tu, Phase structure of systems with multiplicative noise, *Phys. Rev. Lett.* **76**(23):4376–4379 (1996).
- [52] J. Guckenheimer and P. Holmes, *Nonlinear Oscillations, Dynamical Systems, and Bifurcations of Vector Fields*, vol. 42 of *Applied Mathematical Sciences* (Springer-Verlag, New York, 1983).
- [53] T. Guhr, A. Müller-Groeling, and H. A. Weidenmüller, Random-matrix theories in quantum physics: Common concepts, *Phys. Rep.* **299**(4–6):189–425 (1998).
- [54] F. Haake, *Quantum Signatures of Chaos*, vol. 54 of *Springer Series in Synergetics* (Springer-Verlag, Berlin, 1990).

-
- [55] T. Halpin-Healy and Y.-C. Zhang, Kinetic roughening phenomena, stochastic growth, directed polymers and all that: Aspects of multidisciplinary statistical mechanics, *Phys. Rep.* **254**(4–6):215–414 (1995).
- [56] H. Hinrichsen, R. Livi, D. Mukamel, and A. Politi, Model for nonequilibrium wetting transitions in two dimensions, *Phys. Rev. Lett.* **79**(14):2710–2713 (1997).
- [57] H. Hinrichsen, R. Livi, D. Mukamel, and A. Politi, First-order phase transition in a $(1 + 1)$ -dimensional nonequilibrium wetting process, *Phys. Rev. E* **61**(2):R1032–R1035 (2000).
- [58] W. Horsthemke and R. Lefever, *Noise-Induced Transitions: Theory and Applications in Physics, Chemistry, and Biology*, vol. 15 of *Springer Series in Synergetics* (Springer-Verlag, Berlin, 1984).
- [59] K. Ikeda, Multiple-valued stationary state and its instability of the transmitted light by a ring cavity system, *Opt. Commun.* **30**(2):257–261 (1979).
- [60] K. Ikeda and K. Matsumoto, High-dimensional chaotic behavior in systems with time-delayed feedback, *Physica D* **29**(1–2):223–235 (1987).
- [61] I. Jensen, Low-density series expansion for directed percolation I: A new efficient algorithm with applications to the square lattice, *J. Phys. A* **32**(28):5233–5249 (1999).
- [62] Y. Jiang and P. Parmananda, Synchronization of spatiotemporal chaos in asymmetrically coupled map lattices, *Phys. Rev. E* **57**(4):4135–4139 (1998).
- [63] L. Junge and U. Parlitz, Synchronization and control of coupled Ginzburg-Landau equations using local coupling, *Phys. Rev. E* **61**(4):3736–3742 (2000).
- [64] K. Kaneko, Pattern dynamics in spatiotemporal chaos, *Physica D* **34**(1–2):1–41 (1989).
- [65] H. Kantz and T. Schreiber, *Nonlinear Time Series Analysis*, vol. 7 of *Cambridge Nonlinear Science Series* (Cambridge University Press, Cambridge, 1997).
- [66] M. Kardar, G. Parisi, and Y.-C. Zhang, Dynamic scaling of growing interfaces, *Phys. Rev. Lett.* **56**(9):889–892 (1986).
- [67] G. Keller, A note on strange nonchaotic attractors, *Fundam. Math.* **151**(2):139–148 (1996).
- [68] L. Kocarev and U. Parlitz, General approach for chaotic synchronization with applications to communication, *Phys. Rev. Lett.* **74**(25):5028–5031 (1995).

- [69] L. Kocarev, Z. Tasev, and U. Parlitz, Synchronizing spatiotemporal chaos of partial differential equations, *Phys. Rev. Lett.* **79**(1):51–54 (1997).
- [70] T. Kottos, F. M. Izrailev, and A. Politi, Finite-length Lyapunov exponents and conductance for quasi-1D disordered solids, *Physica D* **131**(1–4):155–169 (1999).
- [71] J. Krug and P. Meakin, Universal finite-size effects in the rate of growth processes, *J. Phys. A* **23**(18):L987–L994 (1990).
- [72] J. Krug, Boundary-induced phase transitions in driven diffusive systems, *Phys. Rev. Lett.* **67**(14):1882–1885 (1991).
- [73] A. J. Lichtenberg and M. A. Liebermann, *Regular and Chaotic Dynamics*, vol. 38 of *Applied Mathematical Sciences*, 2nd edn. (Springer-Verlag, New York, 1992).
- [74] R. Livi, A. Politi, and S. Ruffo, Distribution of characteristic exponents in the thermodynamic limit, *J. Phys. A* **19**(11):2033–2040 (1986).
- [75] R. Livi, A. Politi, and S. Ruffo, Scaling-law for the maximal Lyapunov exponent, *J. Phys. A* **25**(18):4813–4826 (1992).
- [76] P. Meakin, P. Ramanlal, L. M. Sander, and R. C. Ball, Ballistic deposition on surfaces, *Phys. Rev. A* **34**(6):5091–5103 (1986).
- [77] M. L. Mehta, *Random Matrices*, 2nd edn. (Academic Press, San Diego, 1990).
- [78] D. Merbach, O. Hess, H. Herzel, and E. Schöll, Injection-induced bifurcations of transverse spatiotemporal patterns in semiconductor laser arrays, *Phys. Rev. E* **52**(2):1571–1578 (1995).
- [79] C. R. Mirasso, P. Colet, and P. García-Fernández, Synchronization of chaotic semiconductor lasers: Application to encoded communications, *IEEE Photon. Technol. Lett.* **8**(2):299–301 (1996).
- [80] J. Mørk, B. Tromborg, and J. Mark, Chaos in semiconductor lasers with optical feedback: Theory and experiment, *IEEE J. Quantum Electron.* **28**(1):93–108 (1992).
- [81] R. Müller, K. Lippert, A. Kühnel, and U. Behn, First-order nonequilibrium phase transition in a spatially extended system, *Phys. Rev. E* **56**(3):2658–2662 (1997).
- [82] M. A. Muñoz and T. Hwa, On nonlinear diffusion with multiplicative noise, *Europhys. Lett.* **41**(2):147–152 (1998).
- [83] E. A. Novikov, Functionals and the random-force method in turbulence theory, *Sov. Phys. JETP* **20**(5):1290–1294 (1965), originally published in *Zh. Éksp. Teor. Fiz.* **47**:1919–1926 (1964).

-
- [84] E. Ott, *Chaos in Dynamical Systems* (Cambridge University Press, Cambridge, 1993).
- [85] G. Paladin and A. Vulpiani, Scaling law and asymptotic distribution of Lyapunov exponents in conservative dynamical systems with many degrees of freedom, *J. Phys. A* **19**(10):1881–1888 (1986).
- [86] N. Parekh, V. R. Kumar, and B. D. Kulkarni, Synchronization and control of spatiotemporal chaos using time-series data from local regions, *Chaos* **8**(1):300–306 (1998).
- [87] L. M. Pecora and T. L. Carroll, Synchronization in chaotic systems, *Phys. Rev. Lett.* **64**(8):821–824 (1990).
- [88] A. S. Pikovsky, On the interaction of strange attractors, *Z. Phys. B* **55**(2):149–154 (1984).
- [89] A. S. Pikovsky and P. Grassberger, Symmetry breaking bifurcation for coupled chaotic attractors, *J. Phys. A* **24**(19):4587–4597 (1991).
- [90] A. S. Pikovsky, Local Lyapunov exponents for spatiotemporal chaos, *Chaos* **3**(2):225–232 (1993).
- [91] A. S. Pikovsky and J. Kurths, Roughening interfaces in the dynamics of perturbations of spatiotemporal chaos, *Phys. Rev. E* **49**(1):898–901 (1994).
- [92] A. Pikovsky and U. Feudel, Characterizing strange nonchaotic attractors, *Chaos* **5**(1):253–260 (1995).
- [93] A. Pikovsky and A. Politi, Dynamic localization of Lyapunov vectors in spacetime chaos, *Nonlinearity* **11**(4):1049–1062 (1998).
- [94] A. Pikovsky, M. Rosenblum, and J. Kurths, *Synchronization: A Universal Concept in Nonlinear Sciences*, vol. 12 of *Cambridge Nonlinear Science Series* (Cambridge University Press, Cambridge, 2001), to appear.
- [95] A. Politi, R. Livi, G.-L. Oppo, and R. Kapral, Unpredictable behaviour in stable systems, *Europhys. Lett.* **22**(8):571–576 (1993).
- [96] A. Politi and R. Livi, private communication (2001).
- [97] A. Politi, R. Livi, and A. Pikovsky, private communication (2001).
- [98] W. H. Press, S. A. Teukolsky, W. T. Vetterling, and B. P. Flannery, *Numerical Recipes in C: The Art of Scientific Computing*, 2nd edn. (Cambridge University Press, Cambridge, 1992).

References

- [99] L. E. Reichl, *The Transition to Chaos: in Conservative Classical Systems: Quantum Manifestations*, 2nd edn. (Springer-Verlag, New York, 1992).
- [100] H. Z. Risken, *The Fokker-Planck Equation: Methods of Solution and Applications*, vol. 18 of *Springer Series in Synergetics*, 2nd edn. (Springer-Verlag, Berlin, 1989).
- [101] J. Rolf, T. Bohr, and M. H. Jensen, Directed percolation universality in asynchronous evolution of spatiotemporal intermittency, *Phys. Rev. E* **57**(3):R2503–R2506 (1998).
- [102] R. Roy and K. S. Thornburg, Experimental synchronization of chaotic lasers, *Phys. Rev. Lett.* **72**(13):2009–2012 (1998).
- [103] M. San Miguel and R. Toral, Stochastic effects in physical systems, in E. Tirapegui, J. Martínez, and R. Tiemann, eds., *Instabilities and Nonequilibrium Structures VI*, pp. 35–130 (Kluwer Academic Publishers, Amsterdam, 1997).
- [104] A. Schenzle and H. Brand, Multiplicative stochastic processes in statistical physics, *Phys. Rev. A* **20**(4):1628–1647 (1979).
- [105] L. Schimansky-Geier and C. Zülicke, Kink propagation induced by multiplicative noise, *Z. Phys. B* **82**(1):157–162 (1991).
- [106] H.-G. Schuster, ed., *Handbook of Chaos Control* (Wiley-VCH, Weinheim, 1999).
- [107] Y. Tu, G. Grinstein, and M. A. Muñoz, Systems with multiplicative noise: Critical behavior from KPZ equation and numerics, *Phys. Rev. Lett.* **78**(2):274–277 (1997).
- [108] C. Van den Broeck, J. M. R. Parrondo, and R. Toral, Noise-induced nonequilibrium phase transition, *Phys. Rev. Lett.* **73**(25):3395–3398 (1994).
- [109] N. G. van Kampen, *Stochastic Processes in Physics and Chemistry*, 2nd edn. (Elsevier Science, Amsterdam, 1997).
- [110] T. Yamada and H. Fujisaka, Stability theory of synchronized motion in coupled-oscillator systems II, *Prog. Theor. Phys.* **70**(5):1240–1248 (1983).
- [111] T. Yamada and H. Fujisaka, Intermittency caused by chaotic modulation I: Analysis with a multiplicative noise model, *Prog. Theor. Phys.* **76**(3):582–591 (1986).
- [112] R. Zillmer, Lyapunov-Exponenten in gekoppelten und rauschgetriebenen Systemen, Diplomarbeit, Universität Potsdam (1999).
- [113] R. Zillmer, V. Ahlers, and A. Pikovsky, Scaling of Lyapunov exponents of coupled chaotic systems, *Phys. Rev. E* **61**(1):332–341 (2000).

- [114] R. Zillmer, V. Ahlers, and A. Pikovsky, Stochastic approach to Lyapunov exponents in coupled chaotic systems, in J. A. Freund and T. Pöschel, eds., *Stochastic Processes in Physics, Chemistry, and Biology*, vol. 557 of *Lecture Notes in Physics*, pp. 400–410 (Springer-Verlag, Berlin, 2000).
- [115] R. Zillmer and A. Pikovsky, Coupling sensitivity in the context of localization (2001), unpublished.

Acknowledgements

This work would not exist in its present form without the kind help of many people and some organizations. In particular I sincerely thank:

Prof. Dr. Arkady Pikovsky for giving me the opportunity to join his research group, for introducing me to new fields of science, and for sharing many valuable ideas concerning this work;

my colleagues of the statistical physics group for the cooperative atmosphere;

Ines Katzorke and Jörg-Uwe Tessmer for their advice in computational matters;

Marita Dörrwand, Birgit Nader, and Marlies Path for their organizational support;

the members of the *Sonderforschungsbereich 555* (Complex Nonlinear Processes), in particular the main organizers Prof. Dr. Werner Ebeling, Prof. Dr. Jürgen Kurths, Prof. Dr. Lutz Schimansky-Geier, and Prof. Dr. Eckehard Schöll, for establishing a stimulating scientific environment in Berlin and Potsdam;

Dr. Antonio Politi for inviting me to Firenze for two rewarding stays;

Rüdiger Zillmer for the perfect cooperation during the first half of my PhD work as well as Francesco Ginelli, Prof. Dr. Peter Grassberger, Prof. Dr. Roberto Livi, Dr. Antonio Politi, and Dr. Alessandro Torcini for the many fruitful discussions during the second half;

Dr. Markus Abel, Dr. Bernd Blasius, Dr. Massimo Cencini, Miguel A. de la Casa, Prof. Dr. Fritz Haake, Dr. Wolfram Just, Dr. Ulrich Parlitz, Dr. Oleksandr Popovych, Prof. Dr. N. Sri Namachchivaya, Dmitri Topaj, Dr. Hong-Liu Yang, and many others for enlightening discussions;

Prof. Dr. Roberto Livi, Prof. Dr. Arkady Pikovsky, and Prof. Dr. Lutz Schimansky-Geier for acting as referees of this thesis;

Prof. Dr. Peter Grassberger, Bernd Sitte, Anke Spötter, and Rüdiger Zillmer for their critical reading of parts of the manuscript;

the *Institute for Scientific Interchange* in Torino, the *Max-Planck-Institut für Physik komplexer Systeme* in Dresden, and the *Zentrum für interdisziplinäre Forschung* in Bielefeld for promoting cooperations with other scientists during well organized workshops;

the *Deutsche Forschungsgemeinschaft* for providing my salary (project SFB 555);

my parents Haide and Klaus Ahlers for their invaluable support throughout my studies;

and Anke Spötter for her patience and for making life colourful.